CHEMICAL REVIEWS

Review

Cite This: *Chem. Rev.* 2019, 119, 870−901

pubs.acs.org/CR

Radioactive Transition Metals for Imaging and Therapy

Eszter Boros*,† and Alan B. Packard*,‡,§

†Department of Chemistry, Stony Brook University, Stony Brook, New York 11794, United States

‡Division of Nuclear Medicine and Molecular Imaging, Department of Radiology, Boston Children's Hospital, Boston, Massachusetts 02115, United States

§Harvard Medical School, Boston, Massachusetts 02115, United States

ABSTRACT: Nuclear medicine is composed of two complementary areas, imaging and therapy. Positron emission tomography (PET) and single-photon imaging, including single-photon emission computed tomography (SPECT), comprise the imaging component of nuclear medicine. These areas are distinct in that they exploit different nuclear decay processes and also different imaging technologies. In PET, images are created from the 511 keV photons produced when the positron emitted by a radionuclide encounters an electron and is annihilated. In contrast, in single-photon imaging, images are created from the γ rays (and occasionally X-rays) directly emitted by the nucleus. Therapeutic nuclear medicine uses particulate radiation such as Auger or conversion electrons or β^- or α particles. All three of these technologies are linked by the requirement that the radionuclide must be attached to a suitable vector that can deliver it to its target. It is imperative that the radionuclide remain attached to the vector before it is delivered to its target as well as after it reaches its target or else the resulting image (or therapeutic outcome) will not reflect the biological process of interest. Radiochemistry is at the core of this process, and radiometals offer radiopharmaceutical chemists a tremendous range of options with which to accomplish these goals. They also offer a wide range of options in terms of radionuclide half-lives and emission properties, providing the ability to carefully match the decay properties with the desired outcome. This Review provides an overview of some of the ways this can be accomplished as well as several historical examples of some of the limitations of earlier metalloradiopharmaceuticals and the ways that new technologies, primarily related to radionuclide production, have provided solutions to these problems.

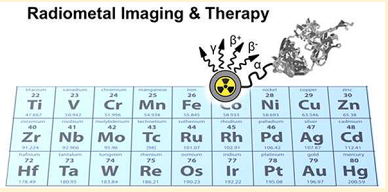

CONTENTS

Special Issue: Metals in Medicine

Received: May 8, 2018
Published: October 9, 2018

DOI: 10.1021/acs.chemrev.8b00281
Chem. Rev. 2019, 119, 870−901

1. INTRODUCTION

Simply put, nuclear medicine is a medical specialty that uses radionuclides to diagnose and treat disease. Radiopharmaceutical chemistry is the science of developing new radioactive compounds with which to accomplish these goals.

Nuclear medicine is composed of two distinct, albeit occasionally overlapping, subspecialties: imaging and therapy. While nuclear medicine imaging's goal is to obtain information about the functional status of a tissue or to detect cancer, the goal of therapy is to treat a disease. These two objectives require radionuclides with different decay properties. Imaging requires radionuclides that emit photons, either γ rays (e.g., ^{99m}Tc) or the annihilation photons that are produced by positron (β^+) decay (e.g., ^{55}Co), that interact minimally with intervening tissue, and therapy requires radionuclides that deposit their energy in the target tissue, typically a malignant tumor. Thus, therapeutic radionuclides are typically beta (β^-) or alpha (α) emitters such as ^{104}Rh or ^{223}Ra, respectively. The combination of both of these properties either in a single radionuclide (e.g., ^{188}Re) or in a "matched pair" of radionuclides gives rise to the concept of theragnostics, using an imaging radionuclide (e.g., ^{64}Cu) to identify the sites of disease and a therapeutic radionuclide (e.g., ^{67}Cu) to treat the disease.

From the imaging point of view, nuclear medicine is further subdivided into PET (positron emission tomography) and single-photon imaging, in which different nuclear decay processes are used with different detector technologies to create images. PET imaging exploits the fact that when a positron is emitted from a nucleus it travels a small, but finite, distance before it encounters an electron. When a positron encounters an electron, both are annihilated with the production of two 511 keV photons, which are emitted at approximately a 180° angle to each other. The location of the annihilation event can be determined by detecting these two 511 keV photons at the same time (coincidence) at two locations on a circular detector ring. A three-dimensional map of these events provides an image of the location of the tracer within the patient, typically with a resolution of ~5 mm. The positron energy has a significant effect on image resolution because higher-energy positrons travel a longer distance before they encounter an electron and are annihilated. For example, a positron emitted by ^{18}F ($E_{\beta+}$ = 250 keV) typically travels <1 mm before it is annihilated, while a positron emitted by ^{68}Ga ($E_{\beta+}$ = 830 keV) typically travels 3−5 mm before it is annihilated.[1−3] Consequently, the resolution of PET images obtained with ^{68}Ga is significantly lower than those obtained with ^{18}F.

In contrast, single-photon imaging makes use of the γ rays emitted by a radioactive atom. Unlike annihilation photons, γ rays are single events, so they cannot be detected using coincidence counting and provide no inherent information about the location of their source. For single-photon imaging, directional information is obtained by placing a lead collimator between the source and the detector. In most cases, these collimators contain many thousand small holes that are perpendicular to the face of the detector. Thus, any photons that impinge on the detector must have arisen from a source that is along a line perpendicular to the detector face. One important consideration is the energy of the photon that is being imaged. Low-energy photons, such as those emitted by ^{201}Tl (70 keV), are highly attenuated by tissue, which can give rise to artifacts in the resulting images. On the other hand, if the photon energy is too high, the requirement for correspondingly thick collimators becomes limiting. These two factors as well as the design of the detector systems themselves predicate photons energies on the order of 140 keV. Two-dimensional images are obtained by placing the detector perpendicular to the subject, and three-dimensional images are obtained by rotating either a single or multiple detectors around the subject. The spatial resolution of single-photon imaging is on the order of 8−10 mm, although higher resolution can be obtained with some recently developed special-purpose imaging systems.

Writing a comprehensive review of metalloradiopharmaceuticals is a formidable task, even when confined to "only" the transition metals. Radiometals have been used in diagnosis and therapy since at least the late 1950s. There is a growing wealth of literature on the topic, including several expansive review articles[4−7] in this journal. Accordingly, and to avoid duplicating previous reviews, this work is primarily confined to developments in the field since approximately 2010, although several older topics are also included to provide both a historical

DOI: 10.1021/acs.chemrev.8b00281
Chem. Rev. 2019, 119, 870−901

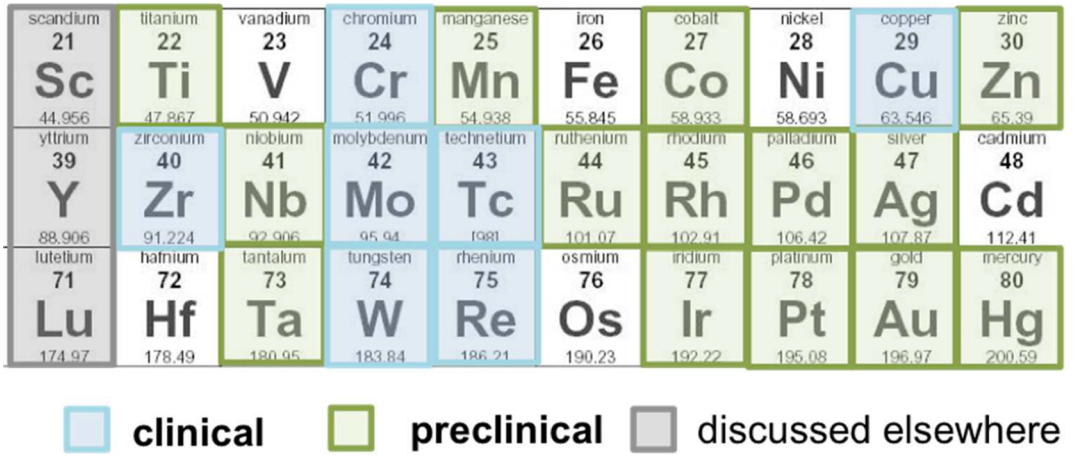

Figure 1. Transition metals discussed in this Review. The clinical designation includes use of compounds in phase 3 clinical trials.

perspective and an outlook on future directions of the field of transition metal radiochemistry.

The field has experienced several large shifts in focus over the past 2−3 decades. While gamma-emitting radiometals were of primary interest for nuclear imaging in the last century, research focus has shifted in recent years to positron-emitting radiometals. This can be explained by (i) the greater availability of PET cameras thanks to the widespread success of [^{18}F]FDG as an oncological, neurological, and inflammation tracer; (ii) improved availability of biomedical cyclotrons, which has greatly increased the number of radionuclide production sites around the globe; and (iii) an increase in the number of metal-based radiopharmaceuticals either recently approved by the FDA or in late-stage clinical trials. These include ^{68}Ga- and ^{64}Cu-labeled peptides for imaging somatostatin-receptor-positive tumors and metastatic prostate cancer as well as a ^{177}Lu-labeled octreotide derivative for treating somatostatin-receptor-positive gastroenteropancreatic neuroendocrine tumors. These developments have led to a surge in interest in exploring previously unavailable radionuclides with highly attractive properties for nuclear imaging and therapy, and the improved availability of these radionuclides has, in turn, provided close to limitless possibilities for tracer development. We highlight recent advances in newly available radionuclides such as ^{55}Co, ^{45}Ti, ^{63}Zn, and ^{90}Nb in addition to discussing selected radionuclides that have previously been explored (Figure 1, Table 1). Furthermore, this overview should be seen as a complement to the Review on radiometalloids, pseudolanthanides, lanthanides, and actinides by Kostelnik and Orvig.[8]

In addition to highlighting selected aspects of the production of these radionuclides, this Review emphasizes the radiochemistry of transition metals as it relates to the development of new radiopharmaceuticals for both imaging and therapy. To optimally harness radiometals for imaging applications, an understanding of their aqueous coordination chemistry and redox chemistry is of the utmost importance. In this context, the development of new bifunctional chelating agents (BFCs), ligands that serve the dual purposes of chelating a radiometal and attaching it to a vector, such as a peptide, is a topic of considerable current interest.

2. GENERAL CONCEPTS

In discussing metal-based radiopharmaceuticals, it is important to clarify the difference between imaging agents where the radiometal is a label and those where it is an essential part of the drug. For example, a ^{89}Zr- or ^{64}Cu-labeled antibody will bind to its antigen independent of the presence of the radiometal. In fact, a primary objective in the development of radiolabeled antibodies is that the introduction of the radiometal minimally alters the biodistribution of the protein (Figure 2). In contrast, ^{99m}Tc is not a radiolabel in the myocardial perfusion agent ^{99m}Tc-MIBI because the metal is an essential part of the drug; in the absence of the ^{99m}Tc, the ligands themselves do not accumulate in the myocardium. This was illustrated clearly by McKenzie et al., who measured the biodistribution of both ^{99m}Tc-PnAO and ^{14}C-labeled PnAO and found that, in contrast to the ^{99m}Tc complex, [^{14}C]PnAO does not enter the brain.[9] These small-molecule metalloradiopharmaceuticals are often referred to as "metal-essential radiopharmaceuticals" to distinguish them from compounds, like radiometal-labeled proteins, where the targeting vector and the radiolabel are essentially independent.

The fundamental concept underlying the development of imaging radiopharmaceuticals, whether they are based on metals or nonmetals (e.g., ^{18}F, ^{11}C), is the tracer principle. This principle, first stated by George Hevesy,[10] says that a tracer must be present at a low enough concentration so that it does not perturb the biological system that it is evaluating. In contrast, therapeutic radiopharmaceuticals are developed specifically to cause a biological effect, most often killing tumor cells. Typically, however, the biological effect of a therapeutic radiopharmaceutical derives from the emissions of the radionuclide, not from the pharmacologic action of the drug itself, which even for therapeutic radiopharmaceuticals is typically still present at concentrations several orders of magnitude lower than necessary to elicit a pharmacologic effect. Achieving this goal is usually not a significant challenge because the concentrations of the radiopharmaceuticals are still submicromolar. It is important, however, to remember that, in cases where the radiometal is used as a label, such as on a protein, a significant amount of unlabeled vector may be present, and the unlabeled vector may itself be pharmacologically active.

In discussing the development of metal-based radiopharmaceuticals, it is essential to emphasize the relevance of thermodynamics and kinetics of radiometal complex formation. The time constraints of half-life and presence of chemically/thermally/radiolytically sensitive vectors in some formulations put severe constraints on which coordination complexes can

DOI: 10.1021/acs.chemrev.8b00281
Chem. Rev. 2019, 119, 870−901

Table 1. Summary of the Decay Characteristics and Common Production Routes of Radionuclides Discussed in This Review

radionuclide	half-life	primary decay mode	primary emission energies	production route	proton energy required for production
^{44}Ti	60.0 years	EC	121 keV (EC) 199 keV (EC)	^{45}Sc(p,2n)^{44}Ti	22−40 MeV
^{45}Ti	3.1 h	β^+ (85%)	439 keV	^{45}Sc(p,n)^{45}Ti	18 MeV
		EC (15%)			
^{51}Cr	27.7 days	EC	323 keV (10%)	^{50}Cr(n,y)^{51}Cr	reactor
^{51}Mn	46.2 min	β^+ (97%)	2.21 MeV	^{50}Cr(d,n)^{51}Mn	6−10 MeV
				^{54}Fe(p,α)^{51}Mn	16 MeV
^{52}Mn	5.6 days	β^+ (29.6%)	242 keV (29%)	^{nat}Cr(p,n)$^{52/52m}$Mn	16 MeV
^{54}Mn	312.2 days	EC (100%)	834.8 keV (99.98%)	^{51}V(α,n)^{54}Mn	20 MeV
		γ			
^{55}Co	17.5 h	β^+ (77%)	1.5 MeV (77%)	^{54}Fe(d,n)^{55}Co	20 MeV
		EC (23%)		^{58}Ni(p,α)^{55}Co	16 MeV
^{57}Co	271.8 days	γ	122 keV (86%)	^{58}Ni(p,2p)^{57}Co	15−20 MeV
			136 keV (10%)		
^{58m}Co	9.1 h	EC	17.2 keV (73%)	^{58}Fe(p,n)^{58m}Co	16 MeV
			24.0 keV (24%)	^{57}Fe(d,n)^{58m}Co	
			24.8 keV (3%)		8.2 MeV
^{60}Cu	23 min	β^+ (93%)	3.92 MeV	^{60}Ni(p,n)^{60}Cu	14.7 MeV
		EC (7%)			
^{61}Cu	3.3 h	β^+ (60%)	1.22 MeV	^{61}Ni(p,n)^{61}Cu	14.7 MeV
		EC (40%)		^{60}Ni(d,n)^{61}Cu	8.1 MeV
^{62}Cu	10 min	β^+ (98%)	2.91 MeV	^{62}Ni(p,n)^{62}Cu	8−12/30 MeV
		EC (2%)		^{62}Zn (9.2 h)/^{62}Cu (generator)	(^{62}Zn: ^{63}Cu(p,2n)^{62}Zn, 26 MeV)
^{64}Cu	12.7 h	β^+ (19%)	656 keV	^{64}Ni(p,n)^{64}Cu	12 MeV
		β^- (43%)	580 keV		
		EC (38%)			
^{67}Cu	61.8 h	β^- (100%)	580 keV	^{68}Zn(p,2p)^{67}Cu	197 MeV
^{63}Zn	38.5 min	β^+ (92.7%)	990 keV	^{63}Cu(p,n)^{63}Zn	13.5 MeV
		EC (100%)			
		γ (8%)	667 keV		
		γ (7%)	962 keV		
^{89}Zr	78.4 h	β^+ (23%)	396 keV	^{89}Y(p,n)^{89}Zr	>13 MeV
		EC (77%)	γ (909 keV)		
^{90}Nb	14.6 h	β^+ (53%)	350 keV	^{90}Zr(p,n)^{90}Nb	20 MeV
^{95}Nb	35 days	γ (100%)	766 keV	^{93}Nb(2n,γ)^{95}Nb	reactor
				^{90}Zr(5n,γ)^{95}Zr→^{95}Nb	reactor
^{94m}Tc	52 min	β^+ (70.4%)	2.44 MeV	^{94} Mo(p,n)^{94m}Tc	11−12 MeV
^{99m}Tc	6.0 h	IT (γ, 89%)	140 keV	^{99}Mo/^{99m}Tc generator	^{99}Mo: fission product
^{104}Rh	35.36 h	β^- (75.0%)	566 keV	^{104}Ru(n, γ)^{105}Ru→^{105}Rh	reactor
		β^- (5.2%)	261 keV		
		β^- (19.7%)	248 keV		
		γ (20%)	319 keV		
		γ (5%)	306 keV		
^{103}Pd	17.0 days	EC (100%)	Auger and ce	^{103}Rh(p,n)^{103}Pd	7−13 MeV
^{109}Pd	13.7 h	β^- (100%)	Auger and ce	^{108}Pd(n, γ)^{109}Pd	reactor
		γ (3.67%)	88 keV		
^{178}Ta	9.3 min	EC (100%)	X-rays (54−65 keV)	^{178}W/^{178}Ta generator	reactor
^{186}Re	3.72 days	β^- (21.54%)	306.1 keV	^{186}W(p,n)^{186}Re	10 MeV
		β^- (70.99%)	359.2 keV		
		γ (9.47%)	137.16 keV		
^{188}Re	17 h	β^- (26.3%)	728.9 keV	^{188}W/^{188}Re generator	^{188}W: reactor
		β^- (70.00%)	791.4 keV		
		γ (15.61%)	155.0 keV		
^{195m}Pt	4.01 days	IT		^{194}Pt(n, γ)^{195m}Pt	reactor
		γ (3.1%)	77.83 keV		
		γ (11.7%)	98.90 keV		
		γ (2.9%)	129.79 keV		
^{197}Hg	64.1 h	EC (97%)		^{197}Au(p,n)$^{197(m)}$Hg	10 MeV
		γ (19%)	77 keV		

DOI: 10.1021/acs.chemrev.8b00281
Chem. Rev. 2019, 119, 870−901

Table 1. continued

radionuclide	half-life	primary decay mode	primary emission energies	production route	proton energy required for production
^{203}Hg	46.6 days	β^- (100%)	57.9 keV	^{202}Hg(n, γ)^{203}Hg	reactor
		γ (81.56%)	279.2 keV		

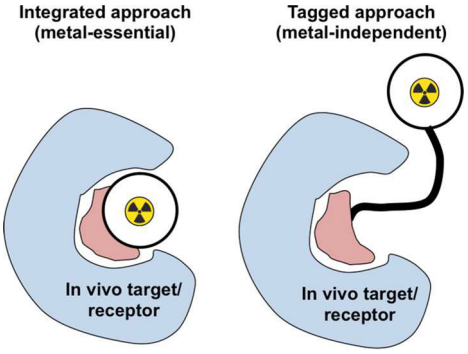

Figure 2. Schematic description illustrating the metal essential and metal-independent tracer design approach.

actually be used in nuclear medicine applications. High thermodynamic stability does not always equate with suitable radiolabeling conditions and optimal in vivo properties. Rather, it is necessary to achieve a balance between rapid complexation kinetics paired with high kinetic inertness of the product. The in vivo environment, although chemically quite mild (i.e., near neutral pH, etc.), can prove to be remarkably and rapidly destructive to radiometal complexes with very high thermodynamic stability if other factors such as kinetic and redox stability are not considered. That being said, it is the combination of all of these factors that makes research in this field so intriguing.

3. TITANIUM

3.1. Common Radionuclides and Their Properties

The primary titanium radionuclides of interest for nuclear medicine applications are ^{44}Ti and ^{45}Ti. Titanium-44 ($t_{1/2}$ = 60.0 years) decays by β^+ emission to ^{44}Sc, which is of interest for PET imaging; thus, ^{44}Ti is primarily of interest as the parent radionuclide in the long-lived ^{44}Ti/^{44}Sc generator system. Titanium-45 ($t_{1/2}$ = 3.1 h, $E_{\beta+}$ = 439 keV (85%)) is a β^+ emitter with properties that are well-suited for PET imaging.[11]

3.2. Radionuclide Production

The primary reaction to produce ^{44}Ti for use in ^{44}Ti/^{44}Sc generators is ^{45}Sc(p,2n)^{44}Ti. This reaction requires medium-energy protons (22−40 MeV) and extended target irradiation times (up to several weeks), which significantly limits the number of possible production sites.[12] This limitation has led to exploration of alternative, direct, production pathways to ^{44}Sc using lower-energy cyclotrons, which are more widely available.[13] The positron-emitting radionuclide ^{45}Ti can be synthesized using the ^{45}Sc(p,n)^{45}Ti reaction.[14] This is done by irradiating scandium discs with an 18 MeV proton beam, followed by separation and purification using a hydroxylamine resin with typical production yields of 400 MBq (11 mCi)/μAh. Alternatively, diolate resins can be used to immobilize Ti^{4+} species as precursors for organometallic Ti^{4+} complexes.[15]

3.3. Chemistry

The most common oxidation states of titanium are +3 and +4, with preference for Ti^{4+} in aqueous media under physiological conditions. The strong Lewis acidity of Ti^{4+} renders titanium aqua complexes prone to the formation of $Ti(OH)_3^+$ and $Ti(OH)_4$ at low pH and cluster formation at elevated pH. While cluster formation is less of a concern for radiochemical applications, the formation of hydroxide species accelerates decomplexation.[16] The strong Lewis acid nature of the Ti^{4+} center leads to a preference for hard, strong Lewis bases such as carboxylates, hydroxides, and phenolates and ligands such as *N,N′*-bis(2-hydroxybenzyl)ethylenediamine-*N,N′*-diacetic acid (HBED), EDTA, 2,2′-(1,2-ethanediyldiimino)bis[(2-hydroxyphenyl)acetic acid] (EHPG), and citrate, which form hexa- and heptacoordinate complexes.[17] The [^{nat}Ti(DFO)]$^+$ (DFO = *N′*-[5-(acetyl-hydroxy-amino)pentyl]-*N*-[5-[3-(5-aminopentyl-hydroxy-carbamoyl) propanoylamino]pentyl]-N-hydroxy-butane diamide complex (Figure 3) was found to have

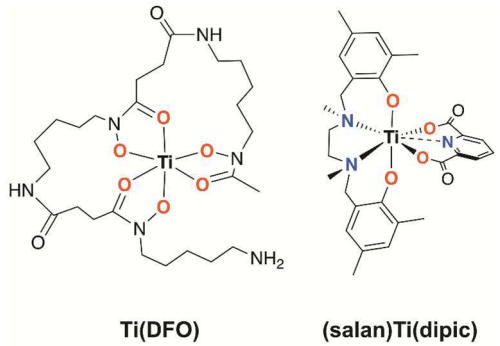

Figure 3. Structures of titanium complexes of interest in early ^{45}Ti labeling and imaging studies.

high thermodynamic stability;[18] however, radiolabeling studies with ^{45}Ti showed quantitative labeling only above pH 8 and after extended reaction times (>2 h). Thus, DFO is not an ideal chelator to produce satisfactory radiolabeling yields within a time frame consistent with the half-life of ^{45}Ti. It is possible, however, that ^{45}Ti could serve as a short-lived chemical homologue for $^{89}Zr^{4+}$.[19]

An alternative approach utilizes (salan)^{45}Ti(dipic) (salen = *N,N′*-bis(salicylidene)ethylenediamine; dipic = dipicolinic acid) complexes as an interesting way to study the in vivo behavior of a new class of titanium-based antineoplastics (Figure 3),[15] and Chen et al. used ^{45}Ti in a chelate-free approach to labeling functionalized nanoparticles.[20]

3.4. Applications

Because of its recent emergence, only a few in vivo studies using ^{45}Ti have been published. Severin et al. developed the synthesis and isolation of (salan)^{45}Ti(dipic) for tumor imaging.[15] The observed tumor uptake was low, but it is possible that this may be increased by the introduction of targeting vectors to the salan portion of the complex or by the design of more kinetically inert coordination complexes. Studies on ^{45}Ti-citrate indicate possible transchelation and entrapment of Ti^{4+} within the Fe^{3+} binding pocket of transferrin; thus, metabolic studies to assess the kinetic inertness of ^{45}Ti complexes will be important to the design of more stable ligand systems for titanium isotopes.

DOI: 10.1021/acs.chemrev.8b00281
Chem. Rev. 2019, 119, 870−901

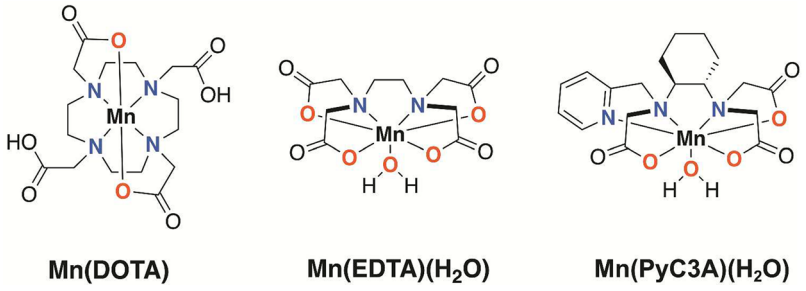

Figure 4. Mn complexes evaluated for in vivo applications in MRI and PET imaging.

4. CHROMIUM

4.1. Common Radionuclides and Their Properties

Chromium-51 is so far the only chromium radionuclide explored for nuclear medicine applications. Chromium-51 ($t_{1/2}$ = 27.7 days) decays via electron capture (EC) to ^{51}V with the emission of 323 keV γ rays (9.9%). The EC decay process causes an inner atomic shell vacancy in the ^{51}V daughter nuclide, resulting in the emission of 5.0 keV X-rays (22%) and several cytotoxic Auger electrons (10 eV to 4.38 keV).[21]

4.2. Radionuclide Production

Chromium-51 is typically produced in a reactor using the ^{50}Cr(n,γ)^{51}Cr reaction. The natural abundance of ^{50}Cr is low (4.4%), and production requires extended irradiation periods. The target typically consists of Ba^{50}CrO$_4$.[22] After irradiation, the target is processed in alkaline solution and hydrogen peroxide to reduce Cr^{6+} to Cr^{3+}. After removal of Ba^{2+} as $BaSO_4$, $NaCrO_4$ is formed when the pH is adjusted to 6−8. Alternative nuclear reactions for ^{51}Cr production involve deuteron irradiation of vanadium targets through the ^{51}V(d,2n)^{51}Cr or ^{50}V(d,n)^{51}Cr nuclear reactions.[23]

4.3. Chemistry

Typical oxidation states in aqueous media are Cr^{3+} and Cr^{6+}. Chromium-51 is isolated as Cr^{6+} in the form of perchromate (CrO_4^{2-}), which can be obtained from commercial sources in a dilute saline solution. Reduction of perchromate to the Cr^{3+} aqua complex is carried out in sodium sulfite typically followed by complexation by hexadentate ligands such as EDTA at pH 6.[24]

4.4. Applications

The use of ^{51}Cr has been primarily limited to monitoring glomerular filtration rate by measurement of the elimination of intravenously injected [^{51}Cr(EDTA)]$^-$.[24] The complex is highly hydrophilic and exhibits especially rapid blood clearance and a fast renal extraction profile. Other applications have included metabolite studies using ^{51}Cr-albumin in canines,[25] tumor imaging with ^{51}Cr-bleomycin[26] in humans, and erythrocyte tagging to monitor red cell survival in patients. Both the emission properties (medium-energy, low-abundance gamma ray) and long half-life (27.7 days) of ^{51}Cr are not ideal for targeted imaging applications, and a study of the cytotoxicity of the Auger emissions did not provide sufficiently encouraging results to justify further studies.[23]

5. MANGANESE

5.1. Common Radionuclides and Their Properties

Manganese is of increasing clinical relevance in the context of magnetic resonance imaging (MRI); the Mn^{2+} ion has ideal properties as a T_1 agent because of its 5/2 spin quantum number, rapid water-exchange rate, long electronic relaxation time (T1e), and low in vivo toxicity.[27,28] For nuclear medicine applications, three manganese isotopes are of interest: ^{52}Mn ($t_{1/2}$ = 5.6 days, $E_{\beta+}$ = 242 keV (29.6%)), ^{54}Mn ($t_{1/2}$ = 312.2 days, EC = 100%, E_γ = 834.8 keV (99.98%)), and ^{51}Mn ($t_{1/2}$ = 46.2 min, $E_{\beta+}$ = 2.21 MeV (97%)). The β^+ emission of ^{52}Mn makes it a potentially interesting option for PET imaging, but coemission of high-energy γ rays (744 keV (90.0%), 936 keV (94.5%), and 1434 keV (100%)) could cause difficulties with clinical translation, although this may be offset by the possibility of doing imaging studies at later times postinjection or use in triple-coincidence PET.[29] The application of the other two manganese radionuclides may be hampered by their half-lives: the half-life of ^{54}Mn is too long for imaging applications, and the half-life of ^{51}Mn is very short, thus requiring an on-site cyclotron for production. Despite these limitations, there is growing interest in ^{51}Mn and ^{52}Mn because advances in PET/MRI instrumentation have raised the possibility of using Mn^{2+} as a dual PET/MRI tracer.[30]

5.2. Radionuclide Production

Production of ^{51}Mn using low-energy biomedical cyclotrons has been reported via a number of nuclear reactions including the ^{50}Cr(d,n)^{51} Mn reaction with $^{50}Cr_2O_3$ powder or metallic ^{50}Cr as the target material. However, neither target material proved to be sufficiently robust to allow the beam current to be increased to >4 μA.[31] Recently, Nickles and co-workers reported use of the ^{54}Fe(p,α)^{51}Mn reaction with a metallic ^{54}Fe target that allowed irradiation with a 60 μA beam.[32] Irradiation of the ^{54}Fe target with 16 MeV protons and 30 μA beam current for 1 h produced 185−370 MBq (5−10 mCi) of ^{51}Mn after separation.[33]

The $^{52/52m}$Mn radionuclides can be obtained by irradiation of natural chromium targets with low-energy protons, but this reaction also produces ^{52m}Mn ($t_{1/2}$ = 21.2 min) and ^{54}Mn as radiocontaminants. A 1 h irradiation at 16 MeV produces ∼150 MBq (4 mCi) of ^{52}Mn contaminated with 0.1−0.4% long-lived ^{54}Mn.[34] Isolation of the product typically involves etching the target material with concentrated HCl and immobilization of Mn^{2+} on an anion-exchange column followed by removal of impurities with several EtOH−HCl washes (97:3). Mn^{2+} is eluted with 0.1 M HCl to provide $^{52}MnCl_2$ in solution.[29] These elution conditions were optimized to prevent formation of anionic manganese chloride species.

5.3. Chemistry

Under typical aqueous conditions at pH 1−9, the prevalent Mn species is aquated Mn^{2+} with a high-spin d^5 state.[35] If strong oxidants are present, uncomplexed Mn^{2+} can oxidize to form Mn_2O_3 and Mn_3O_4 species above pH 5. Typical radiolabeling conditions are pH 4−5 using acetate buffers at room

DOI: 10.1021/acs.chemrev.8b00281
Chem. Rev. 2019, 119, 870−901

temperature to 50 °C, although complexation is faster at higher pH. Mn^{2+} is high-spin d^5, has a preference for hexa- and heptadentate coordination, and exhibits rapid ligand-exchange kinetics that typically occur through interchange mechanisms. Therefore, in the context of targeted nuclear medicine applications, the coordination sphere of Mn^{2+} must be fully encumbered to prevent transchelation, which is facilitated by easy access by competing ligands. Consequently, bifunctional versions of 1,4,7-triazacyclononane-*N*,*N*′,*N*′′-triacetic acid (NOTA), diethylenetriaminepentaacetic acid (DTPA), and 1,4,7,10-tetraazacyclododecane-1,4,7,10-tetraacetic acid (DOTA) have been used as chelators for Mn^{2+} radioisotopes with considerable success, showing high in vitro and in vivo inertness. These chelators are, however, less suitable for possible dual MRI-PET tracer applications as they do not provide access to a site for water coordination.[36] This results in low, second-sphere dominated, longitudinal relaxivity for the complexes. The recent development of a Mn^{2+}-based bifunctional T_1 agent by Caravan and co-workers centered on EDTA and 1,2-cyclohexylenedinitrilotetraacetic acid (CDTA)-type hexadentate chelates that incorporate a cyclohexyl group into the EDTA backbone to impart additional kinetic inertness while allowing coordination of an inner-sphere water molecule (Figure 4).[37] The corresponding ^{52}Mn-labeled radiochemical complex exhibits sufficient in vivo inertness to suggest that it could be used with short-lived ^{51}Mn, but it also shows increased protein binding after 3 h of incubation.[38] To properly evaluate the potential of acyclic, hexadentate ^{52}Mn chelates for targeted imaging, the ^{52}Mn-labeled bifunctional analogues of these chelates conjugated with large biomolecules must be evaluated in vivo.

5.4. Applications

A number of preclinical studies have been carried out with manganese radioisotopes. $MnCl_2$ dissociates in aqueous solution of physiological pH to the Mn^{2+} aquo ion, and in vivo studies with $^{52}MnCl_2$ reveal elevated persistent uptake in the thyroid, lung, pancreas, kidneys, and liver.[32,33] Manganese(II) is hypothesized to behave like calcium biologically, allowing for free diffusion through voltage-dependent calcium channels (VDCCs). This characteristic of manganese can enable neural tract tracing and functional β-cell mass determination in the context of type 1 diabetes and neoplasias of the pancreas. As the large-scale production of ^{52}Mn has become of interest only recently, very few studies exist on targeted molecular imaging with Mn radionuclides. Severin and co-workers successfully appended *p*-SCN-DOTA to TRC105, a monoclonal antibody targeting the angiogenic marker CD105.[39] Subsequent labeling with ^{52}Mn and in vivo imaging studies in a mouse xenograft model showed satisfactory target-to-background ratios even after 120 h with low tracer uptake in typical Mn^{2+} target organs such as pancreas, thyroid, liver, and kidney. Interestingly, uptake in joints was observed with the targeted conjugate, which may indicate different pharmacokinetics of Mn^{2+} that is released slowly from the DOTA ligand over time compared with directly injected $^{52}MnCl_2$. While the authors did not elaborate, a redox-mediated transchelation mechanism producing Mn species in higher oxidation states was proposed. Indications of possible release of ^{52}Mn from DOTA is also described in recent work on liposome-packaged $[^{52}Mn(DOTA)]^{2-}$ complexes.[40] The complexation of Mn isotopes using hexa- and heptadentate chelators to form complexes with high in vivo stability (with hexadentate chelators enabling MR imaging applications) presents a relatively new challenge for the radiochemistry community.

6. COBALT

6.1. Common Radionuclides and Their Properties

Cobalt radionuclides were first synthesized >40 years ago, but there has been a resurgence of interest recently due to the development of more accessible production routes and the increased availability of low-energy cyclotrons. Cobalt-55 ($t_{1/2}$ = 17.5 h, $E_{\beta+}$ = 570 keV (77%), EC (23%))[41] is an emerging radioisotope with decay properties suitable for PET imaging with radiolabeled peptides, proteins, and antibody fragments. The positron abundance is >4 times higher than that of ^{64}Cu; however, this advantage is partially offset by the higher β^+ energy (570 vs 278 keV), which decreases image quality, and the presence of several high-energy γ rays (477 keV, 20%; 931 keV, 75%; 1409 keV, 17%), which contribute to the patient radiation dose and increase shielding requirements. The 17.5 h half-life of ^{55}Co not only enables imaging with targeting vectors with slower pharmacokinetics but also allows shipment to sites without access to on-site cyclotrons.[42] Furthermore, therapeutic applications can be explored with the Auger-emitting radionuclide ^{58m}Co ($t_{1/2}$ = 9.0 h).[43] In light of the still-limited availability of ^{55}Co, ^{57}Co ($t_{1/2}$ = 271.8 days, E_γ = 122 keV (86%), 136 keV (10%)) has been used as a surrogate for ^{55}Co-labeled tracers.[44]

6.2. Radionuclide Production

The primary production routes to high specific activity and high radionuclidic purity ^{55}Co involve deuteron and proton irradiation: ^{54}Fe(d,n)^{55}Co, ^{56}Fe(p,2n)^{55}Co, and ^{58}Ni(p,α)^{55}Co. The ^{54}Fe(d,n)^{55}Co and ^{56}Fe(p,2n)^{55}Co production routes are nonideal and suffer from the low natural abundance of the starting material (^{54}Fe) or the production of large quantities of (inseparable) long-lived byproducts such as ^{56}Co ($t_{1/2}$ = 77 days).[45] Using the ^{54}Fe(d,n)^{55}Co reaction, Dam and co-workers isolated 120−150 MBq (3.3−3.8 mCi) of ^{55}Co after a 5.5 h irradiation.[46] The ^{58}Ni(p,α)^{55}Co reaction is especially well-suited for production using low-energy (15 MeV) cyclotrons; the drawback is the production of long-lived ^{57}Co, if the proton energy increases during production, and ^{57}Ni, although this is removed during target processing. Irradiations by Lapi and co-workers produced an average of 6 MBq (0.16 mCi) ^{55}Co/μAh.[45] In all cases, postproduction separation involves anion-exchange resins where $^{55}CoCl_2$ is eluted using 4−9 M HCl, resulting in a large volume of strongly acidic solution. The volume is reduced by evaporation and reconstitution in 0.04 M HCl, providing $^{55}CoCl_2$ in a small volume.[45,46] In general, acidic conditions are preferred for radiolabeling procedures involving cobalt radionuclides. In contrast to nonredox-active metals and metalloids, where hydroxide formation may occur at elevated pH, alkaline pH promotes the oxidation of Co^{2+} to Co^{3+}.

6.3. Chemistry

The aqueous coordination chemistry of cobalt complexes has been under investigation for over a century, beginning with the pioneering work of Alfred Werner, and has played a major role in the basic understanding of coordination compounds of transition metals.[47] The commonly encountered oxidation states in aqueous media are high-spin Co^{2+} and low-spin Co^{3+}.[48,49] Cobalt(III) complexes have been explored extensively as potential chemotherapeutic agents. The slow ligand-exchange kinetics of Co^{3+} provide this metal ion with especially potent

DOI: 10.1021/acs.chemrev.8b00281
Chem. Rev. 2019, 119, 870−901

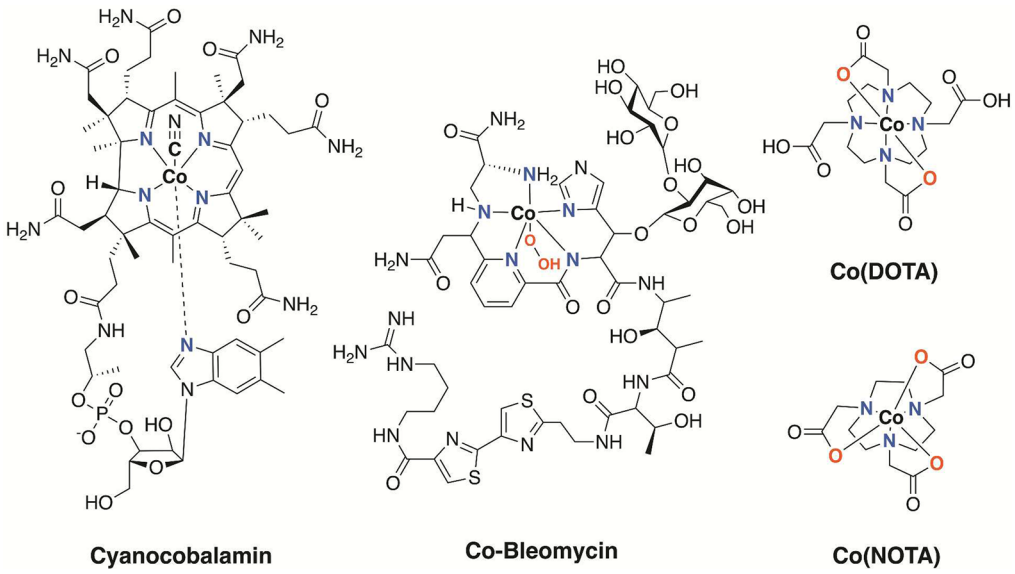

Figure 5. Structures of cyanocobalamin, Co-bleomycin, Co(DOTA), and Co(NOTA) complexes.

inhibitor properties once it attaches to metal ion binding sites of target proteins. Thus far, the only nonradioactive cobalt chemotherapeutic agent that has reached clinical trials is Doxovir, a Co^{3+} Schiff-base complex.[50] Other mechanisms of action for bioactive $Co^{2+/3+}$ complexes involve biologically triggered redox switching between Co^{3+} and Co^{2+} to alter ligand-exchange properties and accelerate target binding.[51] For radiochemical applications, the switching between oxidation states is not desirable, but instead a more kinetically inert, nonredox-active coordination complex is preferred. Maecke and co-workers extensively investigated the redox and structural features of $[Co(DOTA)]^{2-}$ and determined that the complex exhibited an overall −2 charge, was strongly paramagnetic, and had close to ideal octahedral geometry as determined by X-ray crystallography, indicating that the metal was present as high-spin Co^{2+}.[52,53] Subsequent challenge experiments proved the complex to be surprisingly kinetically inert. Typical radiolabeling conditions require a pH of 5−5.5 in 0.4 M acetate buffer at 90 °C. In addition to DOTA, NOTA has also been investigated as a bifunctional chelator for ^{55}Co; the complexation reaction occurs under milder conditions (60 °C) with the corresponding radiochemical complexes exhibiting high in vivo stability.[45]

6.4. Applications

A number of preclinical studies have been carried out with cobalt radioisotopes. Nonchelated $^{55}CoCl_2$ exhibits elevated, persistent uptake in the liver, kidney, and heart. It was hypothesized that the elevated cardiac uptake is caused by the similarity of Co^{2+} and Ca^{2+} for transmembrane internalization, followed by a trapping of the Co^{2+} by binding to cytosolic proteins.[54] In the blood, Co^{2+} is bound by serum albumin. The similarity to Ca^{2+} was explored by Korf and co-workers, where $^{55}CoCl_2$-PET was used to visualize degeneration of cerebral tissues after patients experienced a stroke.[55] The results from four patients suggested that the extent of damaged brain tissue after an ischemic stroke could, in fact, be visualized using $^{55}CoCl_2$.[56] Lameire and co-workers compared the blood and renal clearance of ^{55}Co-(EDTA) with that of ^{51}Cr(EDTA). The time−activity curves showed that ^{55}Co(EDTA) cleared quickly from blood and that the clearance rates of ^{55}Co(EDTA) and ^{51}Cr(EDTA) from the blood were not significantly different, underscoring the potential of ^{55}Co(EDTA) as a renal tracer.[57]

To date, the only clinically approved cobalt-labeled tracer is ^{57}Co-cyanocobalamin (marketed as Rubratope-57) for evaluating vitamin B_{12} absorption by monitoring ^{57}Co activity in the patient's urine as a test for pernicious anemia (vitamin B_{12} deficiency).[58] Cobalt-57-cyanocobalamin was among the first targeted tracers, followed by ^{57}Co-labeled bleomycin (Figure 5).[59] Bleomycin, an FDA-approved chemotherapeutic, was first identified as a bacterial natural product. The peptide contains structural features that enable the kinetically inert complexation of Co^{3+} by a pyrimidine, two amines, and one amide.[60] Crystal structures indicate that the resulting coordination complex is capable of binding to DNA.[61] In a small clinical study of head and neck cancer patients,[59] ^{57}Co-bleomycin clearly indicated sites of malignant lesions.[62] More extensive studies were abandoned due to the long half-life and suboptimal SPECT imaging properties of ^{57}Co, but the recent availability of ^{55}Co has led to renewed interest. Maecke and co-workers established that the cobalt complex of DOTATOC has high affinity for the somatostatin receptor and identified the corresponding ^{55}Co tracer as having high potential for targeted PET imaging of somatostatin receptor positive tumors.[53] This was later confirmed by Dam and co-workers: In both in vitro studies and in vivo studies in tumor-bearing mice, a high level of receptor-specific uptake was identified using the ^{55}Co- and ^{58m}Co-labeled DOTATOC.[46]

A report by Orvig and co-workers details the synthesis of glucose-appended hydroxypyridinone ^{55}Co complexes as possible FDG surrogates; however, no in vivo studies were reported.[63] Recent work has centered on exploiting the intermediate half-life of ^{55}Co for radiolabeling DOTA- and NOTA-conjugated peptides and smaller proteins such as affibodies. Tolmachev and co-workers evaluated ^{55}Co-labeled DOTA-$Z_{EGFR:2377}$ as a tool to image the overexpression of the human transmembrane epidermal growth factor receptor (EFGR). Imaging of EGFR using ^{55}Co was markedly superior in comparison with the ^{68}Ga-labeled equivalent.[64] Similarly, ^{55}Co-labeled peptides that target prostate-specific membrane antigen (PSMA) can be used to image prostate cancer. A study

DOI: 10.1021/acs.chemrev.8b00281
Chem. Rev. 2019, 119, 870−901

by Dam and co-workers in mice with $PSMA^+$ xenografts highlights the improved target-to-background ratios and quality of images at delayed time points (e.g., 24 h p.i.) with ^{55}Co-PSMA-617 compared to early-time-point imaging with the ^{68}Ga analogue.[65] A similar study by the same group details the imaging of $PSMA^+$ PC3 prostate cancer xenografts in mice using ^{55}Co-NOTA-AMBA, a bombesin derivative.[66]

In conclusion, new production routes for positron- and Auger-emitting cobalt radionuclides have reinvigorated interest in cobalt complexes as targeted tracers and therapeutics. The intermediate half-life, paired with low dissociation rates from DOTA and NOTA complexes in vivo, makes ^{55}Co a strong competitor to replace ^{64}Cu, where, in some cases, dissociation after extended circulation times diminishes target-to-background ratios. It also provides an alternative to ^{68}Ga when imaging at time points >4 h postinjection is advantageous.

7. COPPER

7.1. Common Radionuclides and Their Properties

The past five decades of copper radiochemistry have utilized a range of copper radionuclides: ^{60}Cu ($t_{1/2}$ = 23 min, $E_{\beta+}$ = 970 keV (93%), EC (100%)), ^{61}Cu ($t_{1/2}$ = 3.3 h, $E_{\beta+}$ = 500 keV (61%), EC (100%)), ^{62}Cu ($t_{1/2}$ = 10 min, $E_{\beta+}$ = 1319 keV (98%), EC (100%)), ^{64}Cu ($t_{1/2}$ = 12.7 h, $E_{\beta+}$ = 278 keV (19%), $E_{\beta-}$ = 190 keV (39%), EC (61%)), and ^{67}Cu ($t_{1/2}$ = 61.8 h, $E_{\beta-}$ = 141 keV (100%), $E_{\gamma1}$ = 91.3 keV (7%), $E_{\gamma2}$ = 93.3 keV (16.1%), $E_{\gamma1}$ = 184.6 keV (48.7%)).[67] Both ^{60}Cu and ^{61}Cu are short-lived and therefore depend on production at the end-user site. Copper-62 can be obtained from the ^{62}Zn ($t_{1/2}$ = 9 h)/^{62}Cu generator; however, the short half-life of ^{62}Zn results in very limited generator lifetime.[68] Over the past two decades, ^{64}Cu has dominated the field as the primary isotope of interest for nuclear medicine applications. Its 12.7-h half-life allows it to be produced in high yields on low-energy biomedical cyclotrons and shipped to end users over long distances.[69]

7.2. Radionuclide Production

Welch and co-workers described the production of short-lived ^{60}Cu and ^{61}Cu including the application of these radionuclides in imaging studies. Copper-60 and ^{61}Cu can be synthesized using a proton (14.7 MeV) or deuteron (8.1 MeV) irradiation of isotopically enriched nickel targets using the ^{60}Ni(p,n)^{60}Cu, ^{61}Ni(p,n)^{61}Cu, and ^{60}Ni(d,n)^{61}Cu nuclear reactions, producing specific activities of 3−11 GBq (80−300 mCi)/μg for ^{60}Cu and 0.7−3 GBq (20−81 mCi)/μg for ^{61}Cu.[70] Copper-62 can be produced directly using the ^{62}Ni(p,n)^{62}Cu nuclear reaction or alternatively produced by the ^{62}Zn/^{62}Cu generator. Zinc-62 can be produced with a 34−47 MeV proton beam using the ^{63}Cu(p,2n)^{62}Zn reaction.[68] Commercial ^{62}Cu generators contain 5−6 GBq (135−160 mCi) of ^{62}Cu and provide sufficient activity to image up to 20 patients over the course of 2 days.[71] Applications of ^{62}Cu are limited to perfusion studies owing to its short half-life.[72] Copper-64 is the most widely utilized copper radionuclide, and it is typically synthesized using the ^{64}Ni(p,n)^{64}Cu reaction.[73] Cyclotrons with a 12 MeV proton beam are capable of producing up to 100 MBq (3 mCi)/μAh. Alternative, now less frequently used, routes include the ^{64}Zn-(n,p)^{64}Cu reaction in a nuclear reactor, but the production of long-lived byproducts such as ^{65}Zn ($t_{1/2}$ = 245 days) makes this production route disfavored. A solution targetry method has recently been reported with nickel powder dissolved in nitric acid. This method produces 4.5 MBq (0.12 mCi)/μAh after purification, with the advantage of eliminating the need to dissolve the target postirradiation.[74] Copper-67 is the longest-lived radioisotope of copper of interest for nuclear medicine applications.[75] It requires a high-energy accelerator (193 MeV) for the ^{68}Zn(p,2p)^{67}Cu nuclear reaction[76] with reactor production routes using the ^{67}Zn(n,p)^{67}Cu nuclear reaction as a less-favorable alternative.[75,77] After irradiation, the target is dissolved in nitric acid and separated with anion-exchange column chromatography with radioactive Cu eluted in 0.1 M HCl.[78]

7.3. Chemistry

Copper is an essential metal ion for eukaryotes and plays an important role as part of the active site of enzymes crucial for electron transport, O_2 binding, and redox chemistry of various organic substrates. The biochemistry of copper remains challenging to understand and model.[79] The thus far only observed oxidation states for small-molecular complexes under physiological conditions are Cu^{2+} and Cu^+, with the two oxidation states favoring dissimilar ligand donors and coordination geometry. Biologically, sequestration of Cu^{2+} typically occurs by reduction to Cu^+ as part of the metal-ion loading process of copper transport proteins.[80] The d^9 electron configuration of Cu^{2+} leads to strong Jahn−Teller distortion of the octahedral complexes and stabilization of square-planar geometries. Extended X-ray absorption fine structure (EXAFS) studies have indicated the possibility of $[Cu(H_2O)_{5-6}]^{2+}$ existing as a 5-coordinate aquo complex that interconverts between trigonal bipyramidal and octahedral geometry.[81] The chemical hardness of Cu^{2+} dictates a preference for borderline hard Lewis base donors such as aliphatic and aromatic amines, as well as carboxylate donors;[82] however, Cu^{2+} can also accommodate softer donors such as thiolate and carbazone.[83] The kinetics of ligand exchange are rapid and favor the interchange mechanism with the axial ligands being especially labile due to the strong Jahn−Teller distortion. In contrast, Cu^+ (d^{10}) exhibits a preference for soft donors (thiol, thio-ether, and imidazole) and a tetrahedral geometry. This is exemplified by the active-site configuration of ceruloplasmin and copper transport proteins such as ATOX1, which provide histidine-rich tetrahedral binding sites.[84]

Kinetically inert complexes of copper radioisotopes must, therefore, fulfill the following criteria: access of destabilizing ligand donors to form ternary complexes must be limited, ligand systems must provide a rigid coordination environment that disfavors fluxional changes of the coordination environment, and the Cu^{2+} complex must be resistant to one-electron reduction in physiological media. The requirement for a rigid coordination environment is especially challenging as structurally rigid chelators (slow off-rate) often also exhibit very slow complexation rates or are strong proton sponges.[5] The majority of Cu^{2+} chelator development over the past two decades has focused on tri- and tetraaza macrocycle-based polyamino carboxylates. Only a few acyclic chelators have been evaluated in the context of Cu^{2+}: the noninnocent N_2S_2 bisthiosemicarbazonato ligands pyruvaldehyde bis(N_4,N_4-dimethylthiosemicarbazone) (PTSM) and 1-methyl-3-[(*E*)-[(3*E*)-3-(methylcarbamothioylhydrazinylidene)butan-2-ylidene]-amino]thiourea (ATSM) coordinate Cu^{2+} in a distorted square-planar fashion.[85] Under reducing, oxygen-deficient conditions, intracellular Cu^{2+} is reduced to Cu^+, dissociates from the protonated thiosemicarbazone ligand, and is trapped irreversibly in the cytosol. This provides a convenient small-molecule

DOI: 10.1021/acs.chemrev.8b00281
Chem. Rev. 2019, 119, 870−901

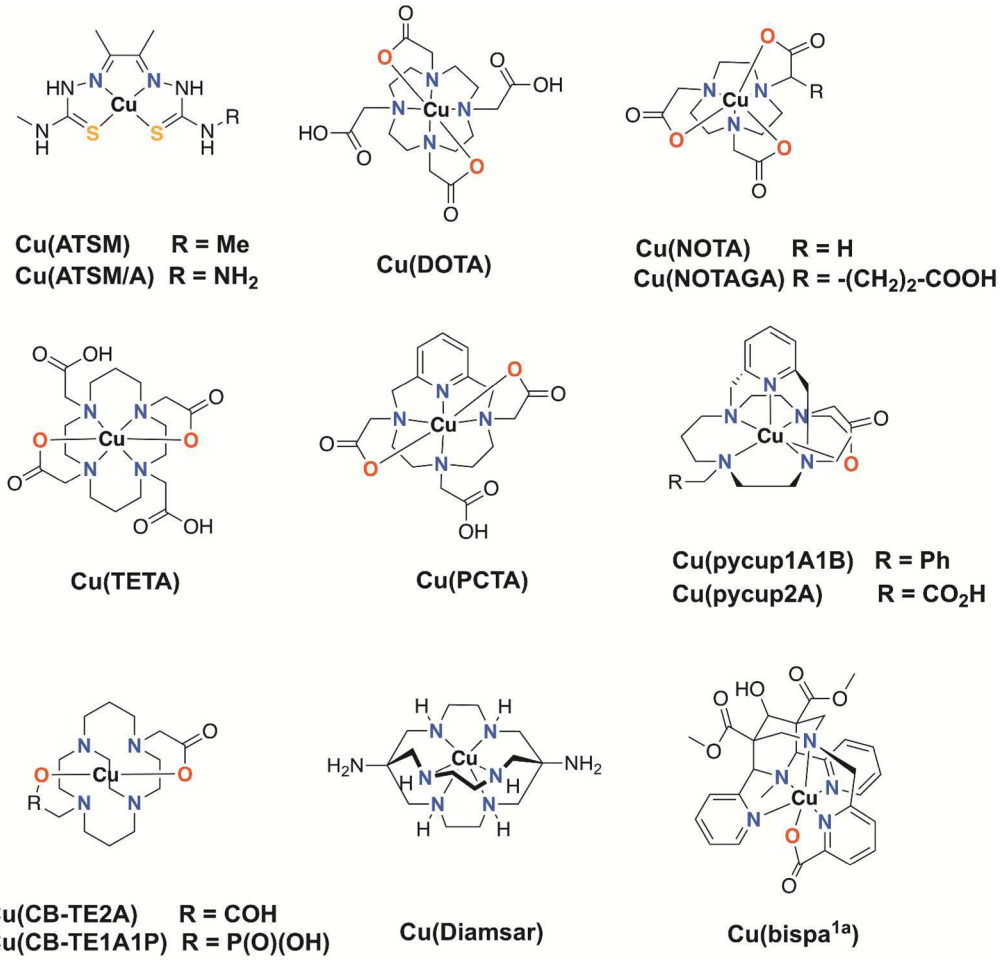

Figure 6. Copper coordination complex structures formed with common chelators.

approach to visualizing hypoxic tumors or underperfused myocardial tissue with ^{64}Cu(ATSM) complexes.[86,87] For other targeted applications, nonredox-active Cu^{2+} complexes resistant to in vivo dissociation are preferred; thus, a wide range of polyaza macrocyclic ligands have been developed for this purpose. DOTA continues to be used for targeted applications,[88] although the dissociation of the corresponding copper complex is well-documented.[89] Hancock and Martell reported the preference of Cu^{2+} for larger macrocycle cavities and the preferential formation of 6-membered metallacycles over 5-membered metallacycles.[90] Indeed, Meares and co-workers showed that cyclam-based aminocarboxylates such as triethylenetetramine (TETA) and 4,11-bis(carboxymethyl)-1,4,8,11-tetraazabicyclo[6.6.2]hexadecane (TE2A) exhibit higher thermodynamic stability and kinetic inertness than their cyclen counterparts DOTA and 1,4,7,10-tetraazacyclododecane-1,7-diacetic acid (DO2A).[91−93] To impart greater structural rigidity, the cross-bridged chelators 1,4,8,11-tetraazabicyclo[6.6.2]-hexadecane-4,11-diacetic acid (CB-TE2A) and its phosphonate analogue 1,4,8,11-tetraazacyclotetradecane-1-(methanephosphonic acid)-8-(methanecarboxylic acid) (CB-TE1A1P) were prepared by Wong, Weisman, and co-workers[94,95] and further developed by Anderson and co-workers.[96] These cross-bridged chelators are highly inert against transchelation but also require elevated temperatures for quantitative radiolabeling. Developments in recent years have focused on providing the high kinetic inertness of cross-bridged systems while also exhibiting quantitative radiolabeling under milder conditions. Other bicyclic, nitrogen-rich chelators such as bispydines (3,7-diazabicyclo[3.3.1]nonanes),[97,98] cross-bridged cyclam-appended monopicolinates,[98] and pyridyl-cross-bridged cyclam pycup derivatives[99] provide slight improvements compared with CB-TE2A but have nonideal solubility or reactivity profiles at room temperature. In this regard, sarcophagine-type copper chelators[100] have shown superior performance, including quantitative radiolabeling at room temperature and excellent in vitro and in vivo stability.[101,102] The high positive complex charge, which increases renal uptake, can be offset by including noncoordinating, anionic functional groups in the ligand backbone, as shown by Dearling et al.[101] and Donnelly and co-workers.[103]

In addition to the high kinetic inertness obtainable through structurally constrained cyclam derivatives, NOTA and NOTA-type derivatives show fast complexation at room temperature but also surprisingly high kinetic inertness in vivo.[104] The examination of possible correlations between in vivo stability and complex inertness in acidic media (1−12 M HCl) and reversibility of the Cu^{2+}/Cu^{+} redox couple did not yield results that could qualify one chelator as superior.[105] Although there has been extensive work on different permutations of copper complexes and targeting vectors, it has become clear that there is no one ideal chelator for targeted imaging with ^{64}Cu; rather, the optimal choice also depends on polarity, size, and stability of the targeting vector itself.

DOI: 10.1021/acs.chemrev.8b00281
Chem. Rev. 2019, 119, 870−901

Table 2. Most Frequently Cited ^{64}Cu Chelators (Years 2012−2018) and Their Common Radiolabeling Conditions, Thermodynamic Stability, Acid Stability, and Redox Properties

chelator	radiolabeling conditions required for >95% radiochemical yield	K_{ML}, pM	acid stability (conditions)	E_{red} (V) NHE
DOTA	5−90 °C, 30−60 min, pH 5−6	22.7 (17.6)	<3 min (5 M HCl, 90 °C)	−0.74 (irrev)
TETA	25 °C, 60 min, pH 5−7	21.9 (15.1)	<4.5 min (5 M HCl, 90 °C)	−0.980 (irrev)
CB-TE2A	95 °C, 60 min, pH 5−6	27.1	254 h (5 M HCl, 90 °C)	−0.88 (quasi-rev)
NOTA	25 °C, 30−60 min, pH 5.5	21.6 (18.4)	<3 min (5 M HCl, 90 °C)	−0.7 (irrev)
Hbispa	25 °C, <1 min, pH 5.5	18.9 (19.3)	N/A	−0.6 (quasi-rev)
DiamSar	25 °C, 5−30 min, pH 5.5	N/A	40 h (5 M HCl, 90 °C)	0.198 (irrev)

7.4. Applications

In vivo studies with Cu radionuclides have been carried out for the past three decades, with numerous tracers currently undergoing clinical trials. The first reports of clinical studies with Cu-labeled targeted agents focused on $^{60/64}$Cu(ATSM) in lung cancer patients. These early clinical results qualified Cu-ATSM as suitable to assess tumor hypoxia and patient stratification for intensity-modulated radiation therapy of more or less hypoxic regions of the tumor.[106] Copper-64-ATSM has also shown promise in assessing ischemic regions of the heart.[107] However, it is important to note that many cancer subtypes show little to no ^{64}Cu(ATSM) uptake in vivo.

In recent years, human studies have focused on the use of ^{64}Cu-labeled bioconjugates, including antibodies, antibody fragments, and small molecules. The primary challenge of using ^{64}Cu in the context of antibodies (Abs) is the dissonance between the high temperatures sometimes required to form kinetically inert Cu-complexes and the thermal instability of mAbs at temperatures above 40 °C. To circumvent thermal decomposition, strategies have included use of ligands that form less kinetically inert complexes with Cu(II) such as DOTA, BAT = 6-[*p*-(bromoacetamido)benzyl]-1,4,8,11-tetra-azacyclotetradecane-*N*, *N*′, *N*′′, *N*′′′-tetraacetic acid, and TETA.[108] BAT conjugates have been utilized with the immunoconjugate ^{64}Cu-BAT-1A3[109] to image suspected advanced primary or metastatic colorectal cancer, and ^{67}Cu-BAT-2IT-Lym-1 was evaluated for radioimmunotherapy in patients with non-Hodgkin's lymphoma. Metabolite analysis showed that <3% of the initial dose was taken up by ceruloplasmin, indicating minimal dissociation of ^{64}Cu from the antibody conjugate. Lewis and co-workers substituted BAT with TETA, which resulted in much improved in vivo properties.[108] More recent studies have utilized NOTA, SarAr (1-*N*-(4-aminobenzyl)-3,6,10,13,16,19-hexaazabicyclo-[6.6.6]eicosane-1,8-diamine), and various other cross-bridged chelators successfully in patients and preclinical studies (Figure 6).[110]

Peptide targeting vectors such as octreotide, arginyl-glycyl-aspartic acid (RGD), 2-(3-(1,3-dicarboxypropyl)ureido)-pentanedioic acid (DUPA) (for PSMA targeting), and bombesin show especially favorable performance in conjunction with cross-bridged macrocycles as thermal decomposition is less of a concern. Conversely, NOTA is better suited as a bifunctional Cu-chelator for use with antibodies, because labeling does not require heating. Work by Yoo and co-workers on in vitro and in vivo comparison of five BFC-RGD conjugates radiolabeled with ^{64}Cu shows that one shoe (chelator) does not fit all feet (vectors) and Cu bifunctional chelators should be chosen on a case-by-case basis (Table 2).[111]

8. ZINC

8.1. Common Radionuclides and Their Properties

Three zinc radionuclides have been proposed for PET imaging: ^{62}Zn ($t_{1/2}$ = 9.26 h), ^{63}Zn ($t_{1/2}$ = 38.47 min), and ^{65}Zn ($t_{1/2}$ = 243.9 days). Of these, the utility of ^{62}Zn is limited because its daughter, ^{62}Cu ($t_{1/2}$= 9.673 min), is also a positron emitter. In fact, as mentioned earlier, one proposed use of ^{62}Zn is as the parent radionuclide in the ^{62}Zn/^{62}Cu generator.[112] The utility of ^{65}Zn is limited by its very long half-life, its low positron yield (1.42%), and its high-energy gamma emission (1.11 MeV, 50.6%). In contrast, the decay properties of ^{63}Zn are well-suited to PET imaging with high β^+ yield (92.7%) and low-abundance gamma emissions (670 keV, 8%; 960 keV, 7%), although the β^+ energy (992 keV) is somewhat high.

8.2. Radionuclide Production

The first report of the production of ^{63}Zn for potential biomedical use was by the neutron irradiation of ^{nat}Zn solutions, which produced small amounts of low-specific-activity material.[113] In 2011, Guerra Gómez et al. reported the production of ^{63}Zn by irradiation of a ^{nat}Cu (^{63}Cu, 69.2%; ^{65}Cu, 30.8%) metal foil with 13.5 MeV protons.[114] The yield of ^{63}Zn prepared under these condition was 1.41 ± 0.19 GBq (38.1 ± 5.1 mCi)/μAh at the end of bombardment, but the presence of ^{65}Cu in the target results in the concomitant production of (long-lived) ^{65}Zn. The authors note, however, that this impurity could be eliminated by using isotopically enriched ^{63}Cu as the target material. An additional concern is that the specific activity of the final product is relatively low (29.4 GBq (795 mCi)/μmol at 1.5 h after EOB). The authors suggest that this is probably due to the presence of trace amounts of Zn in the Cu target and, thus, could be significantly increased by using an enriched ^{63}Cu target, because it would contain less Zn.

More recently, DeGrado et al. reported the production of ^{63}Zn using a solution target (1.7 M ^{63}Cu$(NO_3)_2$ in 0.1 N HNO_3).[115] The HNO_3 is necessary to prevent formation of insoluble Cu oxides during irradiation. A 1 h irradiation at a beam current of 20 μA produced 309 ± 17 MBq (8.35 ± 0.46 mCi)/μA with a specific activity of 108 ± 62 MBq (2.92 ± 1.68 Ci)/μg (6.86 ± 3.91 GBq (185 ± 106 mCi)/μmol), somewhat lower than that reported by Guerra Gómez et al. (29.4 GBq (795 mCi)/μmol), perhaps reflecting the effect of the larger target mass used for the solution target (1 g vs 0.27 g). The end-of-processing yield was 1.53 ± 0.10 GBq (41.4 ± 2.7 mCi), similar to the 1.4 GBq (38 mCi) reported by Guerra Gómez et al.[114]

8.3. Chemistry and Applications

Despite the less-than-optimal decay properties, Fujibayashi et al. used ^{62}Zn-EDDA (EDDA = ethylenediamine-*N*,*N*′-diacetic acid) to evaluate pancreatic function in mice.[116] These investigators reported that injection of the mice with cholecystokinin (CCK-PZ) increased Zn secretion by the

DOI: 10.1021/acs.chemrev.8b00281
Chem. Rev. 2019, 119, 870−901

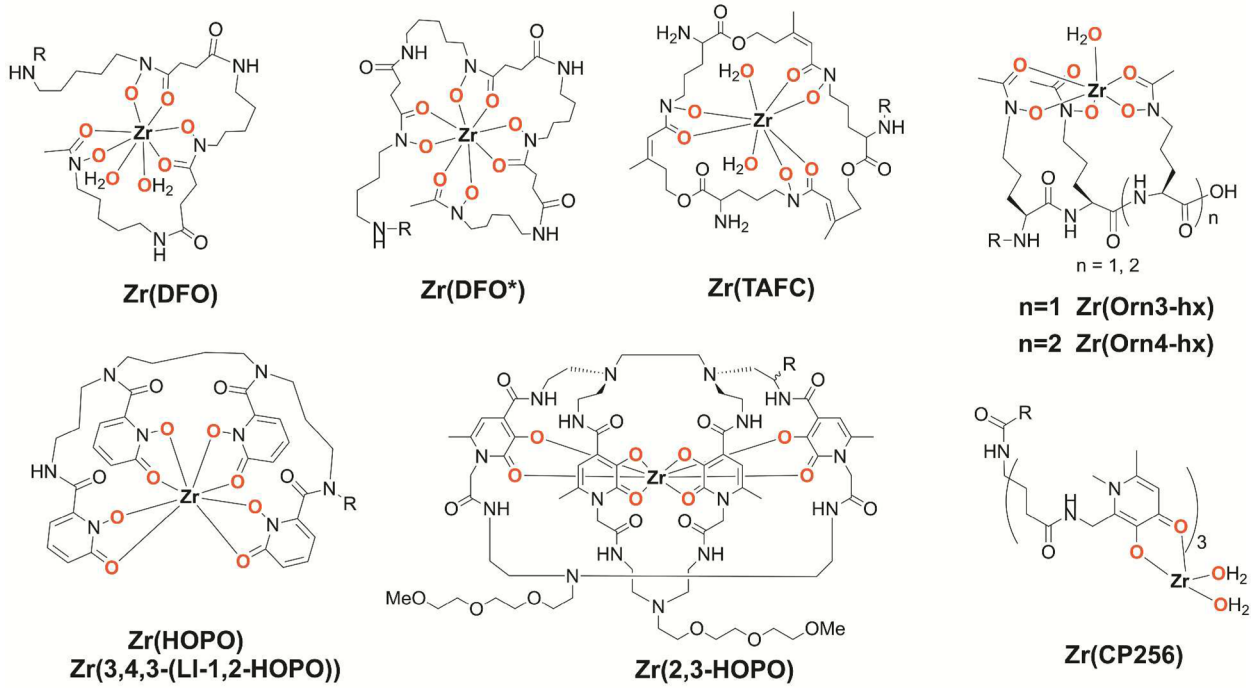

Figure 7. Polyhydroxamate and polypyridinone Zr chelates evaluated for targeted imaging with antibodies.

pancreas, but that glucose induced no changes in Zn secretion. One caveat to this study is that, although the investigators injected ^{62}Zn-EDDA, it is unlikely that this complex survived in vivo given the high lability of Zn(II).[117]

DeGrado et al. recently reported the evaluation of ^{63}Zn-citrate as a biomarker for zinc in a mouse model.[115] In this study, B6.SJL mice were injected with 1.8−3.6 MBq (49−98 μCi) of ^{63}Zn-citrate via the tail vein, and the biodistribution was measured 1 h postinjection. In addition, one of the mice was imaged for 1 h after injection of the tracer. This biodistribution study showed, not surprisingly, that the highest ^{63}Zn uptake was in the pancreas (8.8 ± 3.2% ID/g) with somewhat lower uptake in the liver, kidney, and upper intestine (6.0 ± 1.9% ID/g, 4.2 ± 1.3% ID/g, and 4.7 ± 2.2% ID/g, respectively). The small-animal PET imaging results were consistent with the biodistribution data.

Building on these results, these investigators carried out a first-in-human study with ^{63}Zn-citrate.[118] In this study, they evaluated the distribution of ^{63}Zn in 6 healthy elderly individuals and 6 patients with clinically confirmed Alzheimer's disease (AD). As with the earlier study in mice, the highest tracer uptake was observed in the pancreas, liver, and kidney. Brain uptake was moderate with no significant differences between the healthy subjects and the AD patients. There was, however, a difference in the clearance rate between the two groups with slower clearance observed in the regions of high plaque burden in AD patients, a difference that was attributed to the previously demonstrated affinity of amyloid plaques for Zn.[119]

9. ZIRCONIUM

9.1. Common Radionuclides and Their Properties

Zirconium, an early second-row transition metal primarily explored in the context of ceramics and organometallic catalysts of polymerization reactions, has recently gained considerable traction in the context of nuclear medicine. Several Zr isotopes can be cyclotron produced: ^{86}Zr ($t_{1/2}$ = 17 h, E_γ = 243 keV (96%), ^{88}Zr ($t_{1/2}$ = 83 days, E_γ = 393 keV (97%)), and ^{89}Zr ($t_{1/2}$ = 78.4 h, $E_{\beta+}$ = 396 keV (23%), EC (100%), E_γ = 909 keV (99%)). Of these radionuclides, ^{89}Zr is widely considered to have the greatest potential for clinical applications due to its low-energy positron emission, a half-life well matched to the typical circulation times of monoclonal antibodies, and the fact that it can be produced on biomedical cyclotrons by proton irradiation of natural ^{89}Y targets (100% abundance). The half-life also enables shipping over long distances to sites without on-site cyclotrons.[120]

9.2. Radionuclide Production

Zirconium-89 can be produced using the ^{89}Y(p,n)^{89}Zr and ^{89}Y(d,2n)^{89}Zr nuclear reactions, with a strong preference for the proton reaction, because it can be carried out on most biomedical cyclotrons. The proton energy must be kept below 13 MeV to minimize synthesis of significant amounts of long-lived ^{88}Zr as a side product.[121] The 100% natural abundance of the ^{89}Y target decreases side reactions and minimizes production cost. Using ^{89}Y metal targets, typical yields range from 12 to 61 MBq (0.32−1.6 mCi)/μAh.[122] More recently, pressed yttrium oxide powder targets as well as targets containing a solution of $^{89}Y(NO_3)_3$ have been assessed as alternatives to solid targets and provided promising alternative routes to the synthesis of isotopically pure ^{89}Zr. One advantage of a pressed salt or solution target is elimination or simplification of the target dissolution step after irradiation. Purification and isolation of ^{89}Zr after irradiation is typically carried out by target dissolution in 6 M HCl, followed by immobilization of $^{89}Zr^{4+}$ on a hydroxamate resin from which the Y^{3+} target material is eluted using dilute HCl and water. The ^{89}Zr is then eluted in 1 M oxalic acid with $^{89}Zr^{4+}$ putatively forming an octadentate tetra-oxalate complex.[123]

9.3. Chemistry

Only the 4+ oxidation state of zirconium is stable under physiological conditions and relevant for aqueous coordination

DOI: 10.1021/acs.chemrev.8b00281
Chem. Rev. 2019, 119, 870−901

chemistry. The high charge density of the metal results in a small ionic radius, high Lewis acidity, and high chemical hardness. Zirconium(IV) has a pronounced preference for hard oxygen donors, which enables facile separation from the softer Y^{3+} during target purification using oxygen-rich hydroxamate resins. However, this also presents a formidable challenge for the stabilization of ^{89}Zr complexes suitable for in vivo applications. Above pH 8.5, Zr^{4+} forms hydroxide and oxide species, which are not suitable as starting materials for complex formation. Thus, complexation needs to occur at pH < 8. Despite the small size (80 pm Pauling radius) of the tetravalent cation, Zr^{4+} has a pronounced preference for 7−8 donor atoms.

With the increased interest in ^{89}Zr, the optimization of aqueous Zr^{4+} coordination chemistry under physiological conditions has received extensive attention. The bacterial iron siderophore DFO, FDA-approved for iron-overload disease, has been considered the gold standard chelator over the past decade.[124] DFO provides three hydroxamate donors, and while no crystal structure of the $[Zr(DFO)(OH_2)_2]^+$ complex has been published to date, density functional theory (DFT) calculations indicate that the Zr-DFO exists as a ternary complex with one or two Zr-bound water molecules. While very stable in in vitro ligand and metal challenge experiments, in vivo experiments in mice show elevated uptake of ^{89}Zr in the bone several days postinjection, indicating loss of the isotope from the chelator over time. This observation has prompted efforts to design alternative ^{89}Zr bifunctional chelators (Figure 7).

The primary classes of novel chelators evaluated for ^{89}Zr can be broken down into polyhydroxamates and polyhydroxypyridinones (Figure 7). Design of the ideal Zr-chelator requires a delicate balance of often orthogonal chemical properties: rapid complexation kinetics, high complex inertness, and a minimal log *D* (to minimize disruption of the pharmacokinetics of the vector).

Polyhydroxamates have been investigated more extensively than other Zr-ligand classes. Gasser, Mindt, and co-workers enhanced the DFO structure by adding an additional hydroxamate donor, forming the octadentate DFO* chelator.[125] While somewhat less water-soluble then its hexadentate version, ^{89}Zr-DFO*-mAb conjugates have shown improved retention of ^{89}Zr as indicated by less bone uptake in mice even after extended circulation times (72 and 144 h).[126] Smith and co-workers pursued a conceptually similar approach by functionalizing the N-terminus of DFO with 1-hydroxy-2-pyridinone to afford DFO-1-hydroxy-2-pyridone (DFO-HOPO).[127] The nonfunctionalized ^{89}Zr-DFO-HOPO complex exhibited excellent stability in vivo; however, data on a functionalized, mAb-conjugated version is not yet available. Donnelly and co-workers employed a related strategy that unites functionalization and incorporation of additional donors by conjugation of DFO with O-functionalized squarate.[128] The corresponding immunoconjugate exhibits favorable in vitro and in vivo properties. Other hydroxamate-bearing scaffolds have been based on naturally occurring siderophores. Decristoforo and co-workers evaluated the fungal siderophore fusarinine C (FSC) as a functionalizable macrocyclic tris-hydroxamate chelator for both Ga and Zr isotopes.[129,130] The preorganized nature of fusarinine imparts additional inertness to the corresponding radiochemical complexes, providing enhanced kinetic inertness in vivo. Fusarinine derivatives are prepared using a semisynthetic approach: *Aspergillus fumigatus* secretes Fusarinine-C (TAFC) under iron-limiting conditions. Subsequently, TAFC is functionalized via its accessible N-terminus and demetalated to give the functionalized conjugate. Multimodal, peptide-functionalized versions of FSC have been explored and show excellent short-term stability.[129] Boros and co-workers explored desferrichrome-type chelators (DFCs) derived from ferrichrome and albomycin-like structures produced by various bacterial strains. In contrast to TAFC, DFC-like structures can be chemically synthesized and provide multiple avenues for functionalization and introduction of additional ligand denticity. The corresponding hexa- and octadentate DFC-like mAb-conjugated derivatives show similar in vivo behavior to DFO. The added denticity of the octadentate DFC-like chelate appears not to significantly improve in vivo stability. DFT calculations indicate extensive distortion of the complex environment when compared to an optimized zirconium tetrahydoxamate structure, which may explain why the in vivo stability is not increased.[131]

The second, growing class of Zr-chelators are the polyhydroxypiridinones. The pioneering work on polyhydroxipyridinone-based ligands by Datta and Raymond has been exploited extensively in the context of strong Lewis-acid lanthanides and actinides.[132] Brechbiel and co-workers carried out a detailed study of the complexation of Zr using various positional hydroxypiridinone (HOPO) isomers that identified 1,2-HOPO as the optimal HOPO donor type to generate the most inert complexes.[133] This result is in accordance with results obtained with trastuzumab-conjugated 3,4,3-(LI-1,2-HOPO) by Francesconi and co-workers.[134] The corresponding ^{89}Zr-immunoconjugate releases less ^{89}Zr in vivo, exemplified by a significant decrease in bone uptake, even 144 h post injection.[135] Two 3,4-HOPO derivatives have been evaluated in the context of ^{89}Zr chelation: Blower and co-workers evaluated CP256 and its bifunctional version, YM103,[136] and Häfeli and co-workers evaluated the octadentate 3,4-HOPO derivative (THPN).[137] Contrary to expectations, the ^{89}Zr-labeled YM103-trastuzumab conjugate exhibits pronounced ^{89}Zr release in vivo, whereas no data on the long-term in vivo stability of the ^{89}Zr-THPN derivative is available. To date, two octadentate 3,2-HOPO-derived chelators have been synthesized and evaluated in the context of ^{89}Zr. These caged systems form multiple ^{89}Zr species (possibly variations of in- and out-of-cage complexes) and exhibit release of ^{89}Zr over extended in vivo circulation times that exceed ^{89}Zr release from DFO conjugates.[138]

In summary, the enthusiasm for nuclear medicine applications of ^{89}Zr has invigorated interest in exploring the thus far little-known aqueous coordination chemistry of Zr^{4+}, with a focus on improving long-term kinetic inertness. It is important to note that imaging studies using ^{89}Zr-linked antibodies in human subjects do not show bone uptake of ^{89}Zr that would indicate ^{89}Zr release from the DFO chelator. This somewhat obviates the need for structurally novel bifunctional chelators, compounds that, in contrast to DFO, would require toxicological studies and FDA approval prior to human use. Thus, a focus on alternative applications of ^{89}Zr in addition to immunoPET may be of greater interest.

9.4. Applications

The 78 h half-life of ^{89}Zr is well-matched to typical pharmacokinetics of antibodies, and thus, most targeted applications of ^{89}Zr have utilized antibodies or antibody fragments. Applications of ^{89}Zr-labeled antibodies have been extensively reviewed elsewhere in recent years;[139] therefore, we will focus more on general trends. Currently, more than 20 clinical studies with ^{89}Zr are recruiting patients or are underway. The primary goal of ^{89}Zr-labeled antibodies is to correlate

DOI: 10.1021/acs.chemrev.8b00281
Chem. Rev. 2019, 119, 870−901

sequential FDG-PET/CT and ^{89}Zr immunoPET/CT of patients to gain a better understanding of cell surface receptor expression levels in various cancers. The two-step imaging procedure can inform the further course of treatment and stratify patients for suitable therapeutic intervention. Zirconium-89-labeled antibodies that are involved in active clinical trials include pertuzumab and trastuzumab (HER2+, breast and ovarian cancer),[140] huJ591 (LNCaP, prostate cancer),[141] cetuximab (EGFR, colorectal cancer),[142] and pembrolizumab (PD-L1, nonsmall cell lung cancer).[143]

The success of the ZEPHYR trial (2012−2015) provided the basis for an increasing number of antibodies moving toward clinical translation.[144] The ZEPHYR trial was carried out on breast cancer patients with varying HER2+ expression levels and resistance to conventional trastuzumab therapy. FDG PET/CT was followed by ^{89}Zr-trastuzumab PET/CT preceding treatment with the antibody−drug conjugate (ADC) Kadcyla (trastuzumab emtansine, Genentech). The imaging data were successfully used to predict response to HER2-targeted ADC therapy. Besides monoclonal antibodies, ^{89}Zr-labeled antibody fragments such as F(ab)'s, F(ab)$_2$'s, and minibodies are also increasingly used to visualize target expression. Specifically, monitoring of tumor infiltration by T-cells targeted by ^{89}Zr-labeled CD4 and CD8 targeting antibody fragments can provide a way to noninvasively monitor the success of T-cell therapy.[145] Similarly, tumor-associated macrophages can be monitored using ^{89}Zr-labeled high-density lipoprotein nanoparticles.[146]

^{89}Zr-labeling of nanoparticles has also been explored and can also provide an avenue to paramagnetic multimodal PET/MR tracers (^{89}Zr-labeled feraheme or nanoliposomes). Small defects on the surface of inorganic nanoparticles can enable the chelate-free incorporation of ^{89}Zr, which has been exploited by Holland and co-workers[147] and Cai and co-workers.[148] Another unconventional application of ^{89}Zr is use of the concomitant Cerenkov emission for direct and indirect fluorescence imaging, which could enable guidance for tumor resection following image-mediated diagnosis. In conclusion, the accessibility and ease of production of this isotope has led to a surge in interest over the past decade, with many more clinically translatable tracers and novel applications to come.

10. NIOBIUM

10.1. Common Radionuclides and Their Properties

Niobium is a second-row transition metal with only one stable isotope (^{93}Nb). Niobium radionuclides suitable for nuclear medicine applications include ^{90}Nb and, to a lesser extent, ^{95}Nb.[149] The decay properties of ^{90}Nb ($t_{1/2}$ = 14.6 h, $E_{\beta+}$ = 660 keV (51%), E_γ = 1.13 MeV (92.8%)) make it suitable for PET imaging with antibodies and antibody fragments. Furthermore, the radionuclide can be produced in high yield using natural Zr targets in biomedical cyclotrons, and the intermediate half-life allows shipping over long distances to sites without cyclotron access. Niobium-95 ($t_{1/2}$ = 35 d, $E_{\beta-}$ = 43.4 keV (100%), E_γ = 766 keV (99.8%)) provides a long-lived analogue to ^{90}Nb and can be produced by neutron irradiation of ^{95}Zr. While less suitable for imaging, ^{95}Nb can serve as a surrogate for ^{90}Nb to establish the thus far underexplored chelation chemistry of aqueous Nb(V) at the tracer level.[150]

10.2. Radionuclide Production

^{90}Nb can be produced using various nuclear reactions on a ^{nat}Zr (^{90}Zr, 51.45%; ^{91}Zr, 11.22%; ^{92}Zr, 17.15%; ^{94}Zr, 17.38%; ^{96}Zr, 2.80%) target: ^{90}Zr(p,n)^{90}Nb, ^{91}Zr(p,2n)^{90}Nb, and ^{92}Zr-(p,3n)^{90}Nb. Alternatively, a ^{nat}Y target may be used (^{89}Y-(α,3n)^{90}Nb), but this requires high-energy α irradiation, which is less available. Among the nuclear reactions using Zr targets, the ^{90}Zr(p,n)^{90}Nb nuclear reaction may be most favored as it requires the lowest proton energy (20 MeV) and ^{90}Zr is the most abundant stable Zr isotope. Radchenko et al. reported a yield of 720 ± 52 MBq (19.5 ± 1.4 mCi) for three 1 h irradiations at 5 μA; the high production yield makes this isotope amenable for large-scale production and distribution.

Niobium-95 is produced by what may be best described as a generator method.[150] Natural Zr-granule targets are irradiated by a neutron source to produce ^{95}Zr (β^-, $t_{1/2}$ = 64 days) through the ^{94}Zr(n,γ)^{95}Zr reaction. Subsequently, ^{95}Zr decays to ^{95}Nb. Isolation of both ^{95}Nb and ^{90}Nb requires dissolution of the irradiated Zr targets in 48% HF solutions, 10 M HCl, and boronic acid. Target dissolution is followed by formation of a Nb complex with *N*-benzoyl-*N*-phenylhydroxylamine (NBNP), which can be separated by solvent extraction into $CHCl_3$; dechelation with aqua regia and subsequent ion-exchange chromatography provides the desired Nb isotopes in a mixture of 6 M HCl and 0.01 M oxalic acid.[150]

10.3. Chemistry

Niobium complexes have been reported with oxidation states ranging from Nb^{2+} to Nb^{5+} with a strong tendency of low-valent Nb complexes to act as reductants while being oxidized to d^0 Nb^{5+}. Niobium(V) has high chemical hardness, exemplified by the strong oxophilicity of the metal ion. Literature on niobium coordination complexes in the context of biological applications is limited and has focused primarily on niobocene complexes with Nb^{4+}: niobocene dichloride (Cp_2NbCl_2) has shown in vivo efficacy in the treatment of cancer in preclinical models.[151] The primary limitation of niobocenes in vivo is the oxidation of Nb^{4+} to Nb^{5+}, which results in dissociation of the cyclopentadiene ligands and binding to Fe^{3+} binding sites in proteins as reported by Lynch and co-workers.[152] The propensity of Nb^{5+} to associate with Fe^{3+} binding sites in vivo is exemplary of the high chemical hardness and oxophilicity of Nb^{5+}. Consequently, siderophores have been explored as bifunctional chelators for the coordination of Nb radionuclides. Radchenko et al. report satisfactory complexation properties with DFO and DFO conjugates[153] and only moderate inertness of the corresponding Nb complex, indicating that chelators other than DFO may be required to provide sufficiently high inertness for multiday immunoPET studies.[154]

10.4. Applications

To date, the only in vivo study using Nb radionuclides is a report of DFO-bevacizumab radiolabeled with ^{95}Nb and ^{90}Nb.[154] This study showed poor tumor-to-background ratios and elevated liver and spleen uptake, suggesting metal dissociation and aggregate formation. This underscores the need for a better understanding of aqueous niobium coordination chemistry and the development of novel chelators capable of forming highly inert Nb^{5+} complexes for in vivo applications.

11. TECHNETIUM

11.1. Common Radionuclides and Their Properties

Technetium is the only transition metal with no stable isotopes. Technetium-99 ($t_{1/2}$ = 2.13 × 10^5 years) can be found in uranium-containing pitchblende ore as a natural fission product of ^{238}U. Other long-lived Tc isotopes include ^{97}Tc ($t_{1/2}$ = 4.21 × 10^6 years) and ^{98}Tc ($t_{1/2}$ = 4.20 × 10^6 years), which are reactor

DOI: 10.1021/acs.chemrev.8b00281
Chem. Rev. 2019, 119, 870−901

produced.[155] These long-lived isotopes are not of particular relevance for nuclear medicine applications except ^{99}Tc, which is used as a long-lived congener to study Tc chemistry on a macroscopic level. For nuclear medicine applications, ^{99m}Tc ($t_{1/2}$ = 6 h, E_γ = 141 keV (89%)) is used extensively for single-photon imaging, and >85% of all nuclear medicine studies are carried out using ^{99m}Tc radiopharmaceuticals. Besides attractive emission properties, ^{99m}Tc can be readily obtained from the ^{99}Mo ($t_{1/2}$ = 66 h)/^{99m}Tc generator; ^{99m}Tc generators are a staple of clinical radiopharmacies across the globe.[156] Recently, problems with aging reactor facilities in Canada and elsewhere led to a worldwide ^{99}Mo shortage, prompting interest in alternative production methods for both ^{99}Mo and ^{99m}Tc, as well as interest in other technetium radionuclides. For example, ^{94m}Tc ($t_{1/2}$ = 52 min, $E_{\beta+}$ = 1.07 MeV (70.2%)) is considered a possible PET alternative to ^{99m}Tc, although its positron energy and half-life are both less than ideal.[157]

11.2. Radionuclide Production

Traditionally, ^{99m}Tc has been obtained from the ^{99}Mo/^{99m}Tc generator with the parent ^{99}Mo produced by fission of highly enriched ^{235}U. The ^{99}Mo is isolated as $^{99}MoO_4^{2-}$, which is then immobilized on an alumina column. The ^{99m}Tc is obtained as $^{99m}TcO_4^-$ by elution of the generator with 0.9% (isotonic) saline solution.[158] Alternatively, ^{99}Mo can be produced by neutron irradiation using the ^{98}Mo(n,γ)^{99} Mo reaction. However, neutron irradiation of ^{98}Mo targets results in a very low-specific-activity product.[159] Alternative routes include proton irradiation of an isotopically enriched ^{100}Mo target to produce ^{99}Mo via the ^{100}Mo(p,pn)^{99}Mo reaction, and ^{99m}Tc can be produced directly from the ^{100}Mo(p,2n)^{99m}Tc route.[160] Selivanova and co-workers utilized 2−6 h irradiations with 20−24 MeV protons to produce 620−746 MBq (16.7−20.1 mCi) of high-purity ^{99m}Tc.[160,161] A limitation of this route is that 20−24 MeV proton beams are not available on typical biomedical cyclotrons, limiting the applicability of this approach. However, Schaffer and co-workers produced 7.7 GBq (208 mCi) of ^{99m}Tc after a 1.5 h irradiation using an 18 MeV proton beam, demonstrating that clinically useful quantities of ^{99m}Tc can be produced using a biomedical cyclotron.[162]

Technetium-94m is produced by the ^{94}Mo(p,n)^{94m}Tc reaction using an enriched ^{94}Mo target and 11−12 MeV protons.[157] Early work by Welch and co-workers focused on the use of solid MoO_3 targets, which present considerable difficulties for rapid target processing and subsequent preparation of the radiopharmaceutical of interest within the short time frame that the 52 min half-life provides.[157] More recently, solution targets containing various basic Mo species (e.g., MoO_4^{2-}), nonisotopically enriched and containing only 9.25% ^{94}Mo, have been irradiated using <13 MeV protons. The irradiated target solution containing $^{94m}TcO_4^-$ is purified using a basic aqueous biphasic extraction chromatography resin, which affords $^{94m}TcO_4^-$, and other minor isotopic impurities ($^{94g}TcO_4^-$, $^{96m}TcO_4^-$, and $^{96g}TcO_4^-$) in distilled water. Irradiation times of 60 min produce ∼110 MBq (3 mCi), which is not sufficient to support clinical production but is scalable with isotope-enriched target material and longer irradiation times, within the constraints imposed by the 52 min half-life.

11.3. Chemistry

Technetium belongs to the manganese triad; however, because of the absence of stable isotopes, the chemistry is much less explored than that of Mn and Re. A wide range of oxidation states, from +7 to −1, are known and stabilized using various ligands and coordination environments. Generator and cyclotron production produces $^{99m}TcO_4^-$, with Tc^{7+} in d^0 configuration. However, $^{94m}TcO_4^-$ is a less-than-optimal starting material for the synthesis of lower-oxidation-state coordination compounds, and it must be reduced to a lower oxidation state in order to prepare ^{99m}Tc radiopharmaceuticals. In fact, the development of ^{99m}Tc radiopharmaceuticals languished for >10 years after the development of ^{99}Mo/^{99m}Tc generator because of the challenge of preparing clinically useful ^{99m}Tc radiopharmaceuticals from $^{99m}TcO_4^-$. This changed in 1971 with the development of the first ^{99m}Tc "instant kit" by Eckelman and Richards.[163] A ^{99m}Tc kit typically contains a reducing agent, most often $SnCl_2$, the ligand (e.g., DTPA), and often a bulking agent or buffer. The ^{99m}Tc complex is prepared by simply injecting the $^{99m}TcO_4^-$ solution in saline into the vial, and the desired radiopharmaceutical is formed in >95% yield, usually in a matter of minutes at room temperature. In other scenarios, the reduction step is carried out first and stabilized using a weakly coordinating ligand such as gluconate to transiently stabilize the coordination sphere; in a subsequent step, the chelator-functionalized targeting vector is introduced to form the desired product. The d^2 (Tc^V) and d^6 (Tc^I) configurations are among the most extensively studied.[164,165] Reduction of $^{99m}TcO_4^-$ with $SnCl_2$ typically produces Tc(V)-oxo or -dioxo (d^2) complexes forming square-pyramidal or octahedral complexes, respectively, with tetradentate, acyclic ligands of the softer $N_{4-x}S_x$ type.[166] Coordination of asymmetric $N_{4-x}S_x$ type ligands produces syn and anti isomers, which can exhibit different in vivo behaviors.[167,168] Other Tc(V) coordination environments employ coordination of a [TcN]-L_{4-5}-nitrido[169] and the Tc (hydroxynicotinic acid)L_5 (Tc-HYNIC) coordination environments, favoring square-pyramidal or distorted octahedral geometries with the formation of ternary complexes (Table 3).[170]

Table 3. Most Commonly Utilized ^{99m}Tc Coordination Complex Types, d-Electron Configurations, Reducing Agents Required for Synthesis from TcO_4^-, and Corresponding Ligands

Tc core	d electron configuration	reducing agent used	ligands
TcO_3^+	d^0	SSP-PR_3, reoxidation	N_3
$Tc{=}O^{3+}$, $Tc(O)_2^+$	d^2	$SnCl_2 2H_2O$ glucoheptonate	$N_{4-x}S_x$
$Tc{\equiv}N^{2+}$	d^2	$SnCl_2 2H_2O$, succinic dihydrazide	N, O, S, P
$Tc{=}N{=}N{-}R^{3+}$	d^2	$SnCl_2 2H_2O$ glucoheptonate	HYNIC, $N_{5-x}O$ (or P)$_x$
$Tc(CO)_3^+$	d^6	$K_2(H_3BCO_2)$	$N_{3-x}O_x$, S_3, $(PO)_3^-$

The Tc(I) low-spin d^6 configuration was first exploited by Abrams et al. with the development of the first successful ^{99m}Tc myocardial perfusion agent, $^{99m}Tc(MIBI)_6^+$.[171−173] More recently, the chemistry of Tc(I) has been more extensively explored since Alberto and co-workers developed a one-pot kit to prepare *fac*-$[^{99m}Tc(CO)_3(H_2O)_3]^+$.[174,175] The aquo ligands are labile and can be readily exchanged for mono-, di-, or

DOI: 10.1021/acs.chemrev.8b00281
Chem. Rev. 2019, 119, 870−901

tridentate ligands. Since the introduction of this kit, a wide range of ligands have been explored ranging from nido-carboranes[176] to cyclopentadienyl,[177] triazacyclononane,[178] various single amino acids, or isothiocyanates. To date, however, this has not resulted in the development of any commercially available radiopharmaceuticals. One reason for this is that clinical translation of *fac*-^{99m}Tc(CO)$_3$-based complexes has been hampered by the lipophilicity of the Tc(CO)$_3$ moiety, which increases hepatic uptake in vivo. To decrease lipophilicity and produce more oxidatively resilient complexes, the Alberto group developed the similarly coordinatively flexible Tc(O)$_3$L$_3$ complex (d^0).[179,180] Tc(O)$_3$L$_3$ is also reactive with olefins, capable of carrying out [3 + 2] cycloadditions with two of the three oxo ligands. Further reading on the formation, structure, and reactivity can be found in a recent review by Hahn, Casini, and Kühn.[181]

11.4. Applications

^{99m}Tc-based compounds were first considered to have potential for nuclear medicine applications in 1960 after the ^{99}Mo/^{99m}Tc generator was developed at Brookhaven National Laboratories (BNL) under the leadership of Richards.[182] The demand increased rapidly in the 1960s, which necessitated the development of other generator production sites. The first clinical studies made use of the fact that ^{99m}TcO$_4^-$, like ^{131}I, accumulates in the thyroid and gastric mucosa.[183] The development of new ^{99m}Tc-based imaging agents in the 1960s was, however, limited to poorly defined compounds such as ^{99m}Tc-MAA (MAA = macroagregated albumin) for pulmonary perfusion imaging and ^{99m}Tc-sulfur colloid for liver imaging because of the technical challenge of preparing well-defined ^{99m}Tc compounds from ^{99m}TcO$_4^-$. As described earlier, this changed dramatically in 1971 when Eckelman et al. published the first paper on the development of the ^{99m}Tc "instant kit" for the preparation of ^{99m}Tc-DTPA for renal imaging.[184] This development ushered in a new era for the development of ^{99m}Tc radiopharmaceuticals, and many new agents were introduced in the following years. In general, however, the first generation of kit-based radiopharmaceuticals was not well-characterized, as least in terms of their coordination chemistry, and many are mixtures of several different ^{99m}Tc species. This changed in the late 1970s and early 1980s when Deutsch,[185] Davison, and Jones,[186,187] among others, instituted a new era of well-defined, chemically characterized ^{99m}Tc radiopharmaceuticals. Among the first of these to enter clinical use was ^{99m}Tc-MIBI, the hexakis Tc(I) isonitrile complex myocardial perfusion agent mentioned previously.[171,172] This compound is particularly interesting from a coordination chemistry point of view because it is an unusual example of the synthesis of a Tc(I) complex in an aqueous environment. This was soon followed by other agents for imaging myocardial perfusion (tetrofosmin), cerebral blood (ECD, HMPAO), hepatobiliary function (HIDA), and renal tubular function (MAG3).[188]

The robustness and chemical versatility of the ^{99m}Tc-MAG3 core led to the development of the first bifunctional tracers for targeted imaging applications. However, there are drawbacks to radiolabeling with MAG3 conjugates including the use of stannous chloride as a reducing agent and the need for elevated pH that may lead to aggregation of proteins, as well as nonquantitative radiolabeling yields. A more recently developed alternative is the HYNIC ligand system, which forms ternary complexes with ^{99m}Tc and has found extensive use for targeted applications involving small molecules, peptides, and proteins, with an annexin V and RGD-functionalized derivative under assessment in clinical trials.[189] The conditions required to prepare *fac*-^{99m}Tc(CO)$_3$ are more amenable to the radiolabeling of aggregation- and pH-sensitive entities such as proteins. However, the comparatively slow ligand-exchange kinetics often necessitate elevated temperatures to obtain quantitative radiolabeling yields, which can offset these advantages. Targeted applications with the *fac*-^{99m}Tc(CO)$_3$ core up to 2014 were reviewed by Bartholomä et al.[190] as well as Kühn and co-workers;[191] thus, we will focus on more recent advances and applications. Technetium-99m–protein conjugates of particular interest include the prostate-specific membrane antigen targeted compounds ^{99m}Tc-MIP1427 and ^{99m}Tc-MIP1404, which have demonstrated diagnostic potential in patients, with phase 3 clinical trials complete.[192] There is also rekindled interest in Re(CO)$_3$-based complexes as antineoplastic agents with an intrinsic fluorescence and IR spectroscopic handle as well as the ability to release CO triggered by photoexcitation (photo-CORMs). This has, in turn, led to synthesis of the corresponding ^{99m}Tc(CO)$_3$ analogues to provide information about the in vivo behavior and distribution of the Re complexes.[193] Valliant and co-workers explored [2 + 1] Re(I)/Tc(I) complexes derived from bipyridine and imidazole as possible dual-modality nuclear and optical probes.[194] The [2 + 1] ligand-substitution strategy provides a modular approach to introduction of various targeting vectors or fluorescence sensitizers. This theragnostic approach was also recently explored by Wilson and co-workers, where a Re(CO)$_3$ dimethylphenanthroline complex with potent antiproliferative activity and favorable properties for in vitro fluorescence imaging and its ^{99m}Tc analogue were evaluated for their in vitro and in vivo behavior.[195]

Similarly, Alberto and co-workers functionalized Re(CO)$_3$ with doxorubicin to potentiate its anticancer effects and observed organelle selectivity.[196,197] The corresponding ^{99m}Tc analogue takes advantage of the emission of Auger electrons to impart additional cytotoxic activity (Figure 8). Other Re/Tc-based small molecules developed for targeted applications include β-amyloid targeted small molecules by the groups of Donnelly and Pelecanou.[198,199] While the rhenium complex

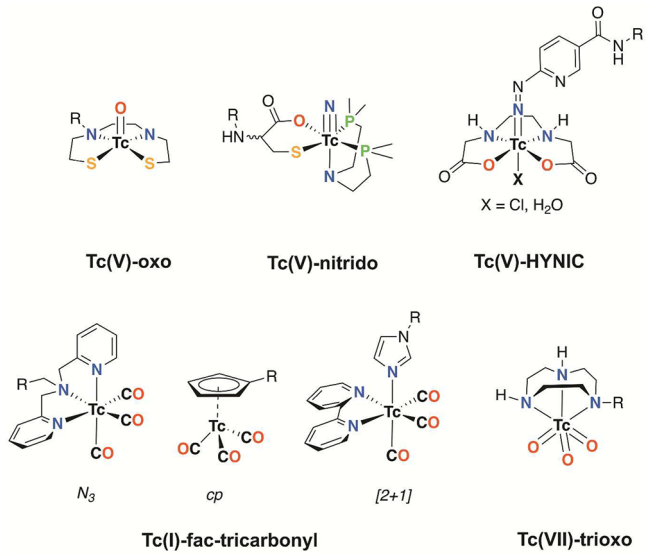

Figure 8. Structures of most commonly used Tc-coordination environments for targeted imaging applications.

DOI: 10.1021/acs.chemrev.8b00281
Chem. Rev. 2019, 119, 870–901

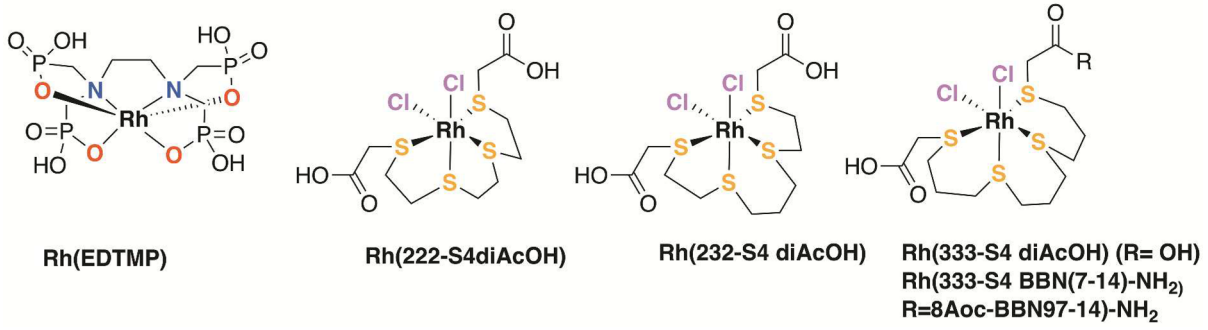

Figure 9. Rh coordination complexes utilized for palliative bone treatment and targeted applications.

visualizes plaques in brain slices by fluorescence imaging, the corresponding ^{99m}Tc complex has the potential to act as an in vivo SPECT tracer, although it exhibited only moderate brain uptake in rodents. The viability of [2 + 1] rhenium and technetium complexes relies on comparatively slow ligand exchange on a low-spin d^6 center. Slow ligand-exchange kinetics can provide an avenue to high complex inertness in vivo even for mono- and bidentate ligand systems. Arano and co-workers explored introduction of peptidic, $\alpha_v\beta_3$ targeting vectors by a monodentate isonitrile donor. The monodentate nature of the targeting vector allows for attachment of three peptide vectors onto the $^{99m}Tc(CO)_3$ core, providing an elegant approach to enhanced targeting ability and multivalency.[200,201] The corresponding complexes are stable in vivo and exhibit enhanced accumulation in target tissues when compared with monovalent analogues using a polydentate chelator to attach the peptide to the metal center.

In conclusion, while the versatile chemistry of Tc has been extensively explored over the past 4 decades, novel applications continue to emerge and add value to the most frequently utilized radioisotope of nuclear medicine.

12. RHODIUM

12.1. Common Radionuclides and Their Properties

The radiochemistry of rhodium has been the subject of multiple reviews, most recently by Feng et al. in 2017.[7] Accordingly, the focus of this discussion will be on an overview of rhodium radiochemistry as well as recent developments. The primary rhodium radionuclide of interest in nuclear medicine is ^{105}Rh ($t_{1/2}$ = 35.4 h). Rhodium-105 is a potential theragnostic radionuclide because it decays with the emission of three β^- particles (179 keV (75.0%), 74 keV (5.2%), and 70 keV (19.7%)) and two low-abundance γ rays (319 keV (20%) and 306 keV (5%)).

12.2. Radionuclide Production

Rhodium-105 can be produced by several different routes. The most common is by neutron irradiation of enriched ^{104}Ru to produce ^{105}Ru, which has a 4.4 h half-life and decays to ^{105}Rh.[202] The irradiated Ru metal target is dissolved in sodium hypochlorite (NaOCl), which oxidizes the ruthenium to RuO_4, which is then separated from the ^{105}Rh by distillation and recovered for reuse.[7,203] The ^{105}Rh solution that remains in the distillation vessel is neutralized with HCl to produce a mixture of rhodium(III)-chloro complexes including $^{105}RhCl_3(OH_2)_3$, $[^{105}RhCl_4(OH_2)_2]^-$, $[^{105}RhCl_5(OH_2)]^{2-}$, and $[^{105}RhCl_6]^{3-}$.[7,204] Because it is relatively simple to separate rhodium from ruthenium, the specific activity of this product is relatively high. However, the apparent specific activity is somewhat lower because the final product is contaminated with the ^{105}Ru that remains in the reaction vessel after distillation.[202]

Other methods used to produce ^{105}Rh include neutron irradiation of ^{103}Rh, which produces low-specific-activity ^{105}Rh by double-neutron capture, and irradiation of ^{nat}Pd with 42 MeV protons, which produces ^{105}Rh by several routes including ^{105}Pd(p,n)^{105}Rh.[205] This study also suggested that ^{105}Rh could be produced using low-energy protons (<20 MeV) via the ^{108}Pd(p,α)^{105}Rh route using an enriched ^{108}Pd target. Rhodium-105 is also a fission product (^{235}U(n,f)^{105}Rh), but this presents a challenging separation problem both in terms of isolating the desired radionuclide from myriad other fission products and in terms of dealing with the radioactive waste products.

12.3. Chemistry

From a chemistry point of view, the primary attraction of ^{105}Rh is that Rh(III) complexes, being low-spin d^6, are extremely kinetically inert, an important consideration for a therapeutic radionuclide. Unfortunately, this kinetic inertness is also a liability in that it is very difficult to prepare Rh(III) complexes without heating them at relatively high temperatures for relatively long times, which limits its utility as a protein label.

The first studies of ^{105}Rh complexes were carried out by Troutner et al., who investigated the complexation of low-specific-activity ^{105}Rh with a variety of nitrogen donor ligands including functionalized tridentate amines,[206,207] a Schiff base ligand[208] and hematoporphyrin IX[209] for labeling gamma globulin, and a cysteine complex for labeling HSA.[210] All of these complexation reactions required heating moderately basic (pH 9) solutions of the ligand and ^{105}Rh at reflux for ∼1 h, and all except the cysteine complex included ethanol. The ethanol in these reactions is thought to act as a reducing agent, reducing the Rh(III) to more labile Rh(I), which then reoxidizes to Rh(III) in the presence of air.

Venkatesh et al. evaluated macrocyclic 16-member S_4 thioether ligands and found that the ^{105}Rh complexes could be prepared in high yield (>99%) by heating the ^{105}Rh-chloro complex with the ligand at pH 3−4 at 80 °C in 15% ethanol for 1 h.[204] Other investigators subsequently evaluated a series of 14-member macrocyclic ligands containing varying numbers of thioethers and found that higher labeling yield (>90%) was obtained when the ligand contained more thiols.[211]

A series of acyclic S_4 ligands were evaluated by Goswami et al., who found that these ligands could be labeled in >90% yield by heating at 85 °C at pH 4−5 for 60 min.[212,213] As is the case with other ^{105}Rh labeling reactions, ethanol is an essential component of the reaction mixture, presumably reducing the Rh(III) starting material to more labile Rh(I). Akgun et al. subsequently

DOI: 10.1021/acs.chemrev.8b00281
Chem. Rev. 2019, 119, 870−901

investigated a series of acyclic amine-thioether ligands and found that the complexation yields were lower than with the tetrathioethers (45−60% vs >90%), presumably because the lower labeling pH was suboptimal for the amine moieties.[214] An additional complication with this class of ligands is the formation of conformers (Figure 9).

In later studies, the amine-thioether ligands were supplanted by diaminediphosphine and dithiodiphosphines, which facilitate complexation at lower temperatures and lower ethanol concentrations because the phosphines act as reductants.[215] This advantage is, however, offset by the requirement for higher ligand concentrations (1 mM), which lowers the effective specific activity of the resulting bioconjugate, because the unlabeled ligand−protein conjugate competes with the labeled complex for the binding site.

The most recent class of ligands to be considered are the acyclic tetrathioethers previously reported by Goswami et al.,[212,213] except that in this case one of the free carboxylate groups was conjugated to bombesin (BBN) for targeting prostate cancer. The nonradioactive [RhCl(333-S4-BBN(7−14)NH2)]$^+$ complex shows low nanomolar affinity for the bombesin subtype 2 receptor (BB2r), but the yield of the ^{105}Rh labeling reaction is <10% (vs >90% for the free ligand).[7] In addition, although these ligands facilitate complex formation at lower temperatures (80−85 °C) and lower ethanol concentrations (5%) than other classes of ligands, these reaction conditions introduced an additional complication: the formation of multiple species in solution due to the esterification of the carboxylate moiety on the ligand in the presence of ethanol at low pH.[7]

One approach to protein labeling that does not seem to have been evaluated with ^{105}Rh is the use of "click chemistry" between a preformed ^{105}Rh complex and a click-functionalized protein. This approach would allow the ^{105}Rh complex to be prepared under relatively rigorous synthetic conditions without concern about damage to the protein vector. The preformed complex could then be attached to the protein using a click reaction.

12.4. Applications

While there are several reports of the evaluation of the in vivo stability of ^{105}Rh complexes with various ligands (e.g., refs 213, 216, and 217), there are few in vivo studies of ^{105}Rh complexes with biologically relevant ligands. In one example, Brooks et al. prepared a ^{105}Rh complex with bleomycin (BLM), a glycoprotein antibiotic that is known to form metal complexes that localize in tumors.[218] The complex was prepared using a method similar to that used to prepare the amine complexes, i.e., heating an aqueous solution of the ligand and ^{105}Rh at 90 °C in the presence of ethanol for 20 min. This reaction produced multiple Rh-BLM species that were found to be stable in plasma. In vivo studies in tumor-bearing rats showed higher uptake in the tumor than in the contralateral muscle, but they also revealed high uptake in the kidneys, and the authors suggested that there was no evidence of preferential uptake in the tumor.

Venkatesh et al. compared the biodistribution of the B72.3 antibody labeled with ^{105}Rh using a preformed amine-oxime complex with that of the ^{131}I-labeled antibody.[219] They found that the biodistribution of the two antibodies was similar, suggesting that the ^{105}Rh was not lost from the antibody in vivo and that the presence of the ^{105}Rh-amine-oxime complex did not significantly alter the biodistribution.

Ando et al. reported the preparation of a ^{105}Rh-EDTMP (EDTMP = ethylenediamine tetra(methylene phosphonic acid)) complex as a potential palliative treatment for bone pain due to tumor metastases.[220] The complex was prepared by simply heating the ^{105}Rh-chloro complex with EDTMP in boiling water for 30 min to produce a ^{105}Rh-EDTMP complex in >99% yield (Figure 9). The complex showed high in vitro stability, and in vivo studies showed rapid blood clearance and high uptake in the bone. Given the challenges that have been encountered in the preparation of ^{105}Rh complexes with bifunctional chelators, this study suggests that perhaps further investigation of small-molecule ^{105}Rh complexes is warranted.

13. PALLADIUM

13.1. Common Radionuclides and Their Properties

Two palladium radionuclides have found medical applications, ^{103}Pd ($t_{1/2}$ = 17.0 days) and ^{109}Pd ($t_{1/2}$ = 13.7 h). Palladium-103 decays by electron capture (100%) with the emission of Auger and conversion electrons and multiple low-abundance γ rays (<1%). Palladium-109 decays by β^- emission (100%) with the emission of Auger and conversion electrons and a large number of γ rays with <1% abundance, as well as one with >1% abundance (88.0 keV, 3.67%). Palladium-109 is also the parent radionuclide in the ^{109}Pd/^{109}Ag generator.[221]

13.2. Radionuclide Production

Palladium-103 is produced in large quantities using the ^{103}Rh-(p,n)^{103}Pd reaction with low-energy (10 MeV) protons.[222] An alternative is ^{107}Ag(p,2p3n)^{103}Pd or ^{103}Rh(d,2n)^{103}Pd, but both of these reactions require higher particle energies than are typically available on biomedical cyclotrons.[222] Palladium-109 is produced by neutron irradiation of an enriched ^{108}Pd metal target, which results in a product with much lower specific activity (~1.85 Bq (50 μCi)/mg).[223,224]

13.3. Chemistry

The irradiated palladium metal target is dissolved in aqua regia with heating. The solution is evaporated to dryness, and the nitric acid is removed by repeated heating to dryness with 12 N HCl to form H_2PdCl_4. Silver-111, which is also formed during the irradiation, is removed by coprecipitation with a small amount of $AgNO_3$. The supernatant containing the ^{109}Pd is removed, evaporated to dryness, and dissolved in dimethylsulfoxide (DMSO) to produce [^{109}Pd]Pd(DMSO)$_2$Cl$_2$, which is used in subsequent syntheses.[225,226]

13.4. Applications

Palladium-103 is widely used for brachytherapy for the treatment of prostate cancer, typically as metal seeds. As described earlier, it decays by electron capture (100%) with the emission of Auger and conversion electrons as well as several low-intensity γ rays (<0.1%).

Palladium-109 was originally proposed for labeling antibodies for antitumor therapy,[227] but more recently investigators have focused on ^{109}Pd-porphyrin complexes because of the use of porphyrins as photosensitizing agents for photodynamic therapy for treating cancer.[228−230] These studies typically show accumulation of the ^{109}Pd-porphyrin complex in the tumor at a concentration of 3−5%.[223,225,226,231] However, a caveat to the purported tumor selectivity of porphyrins is that porphyrins tend to aggregate at concentrations higher than ~1 μM,[232] and the ^{109}Pd-porphyrin complexes were injected at relatively high concentrations because of the low specific activity of the ^{109}Pd (~1.85 GBq (50 mCi)/mg). Therefore, the ^{109}Pd-porphyrin complexes may be accumulating in the tumor as aggregates, through EPR (enhanced permeability and retention).[233] Tumor

DOI: 10.1021/acs.chemrev.8b00281
Chem. Rev. 2019, 119, 870−901

selectivity could be validated by carrying out the biodistribution experiments using higher-specific-activity ^{109}Pd (or ^{103}Pd) to determine if the concentration of the injectate affects the biodistribution.

An important consideration with respect to the use of radiometalated porphyrins is that it is somewhat difficult to insert the metal into the porphyrin core, typically requiring, at a minimum, heating at 80 °C for 1 h. In contrast, the radiometal can be more easily inserted into the porphyrin core by using an *N*-methyl porphyrin as the ligand (Figure 10).[234]

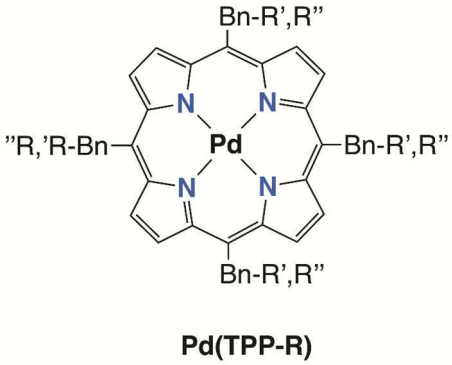

Figure 10. Structure of the Pd-tetraphenylporphyrin (TPP) core.

Although the focus of Pd radiochemistry has been on ^{109}Pd-porphyrins for tumor therapy, several other radiopalladium complexes have also been evaluated for tumor therapy. These include a ^{103}Pd-thiosemicarbazone complex[235,236] and a ^{103}Pd-bleomycin complex.[237] Finally, Doi et al. evaluated the use of ^{109}Pd-hematoporphyrin for lymph node ablation.[234]

14. TANTALUM

14.1. Common Radionuclides and Their Properties

Tantalum-178 ($t_{1/2}$ = 9.3 min) was the subject of considerable interest until approximately 2000, but interest has declined since then. Its primary application was in first-pass radionuclide angiography, where it was principally used in combination with the multiwire proportional counter (MWPC),[238−240] which is well-matched to the low-energy X-ray emissions (54−65 keV) of ^{178}Ta and capable of handling higher count rates than Anger cameras, although it was also used with standard Anger cameras.[241]

14.2. Radionuclide Production

Tantalum-178 is produced by the ^{178}W/^{178}Ta radionuclide generator. This generator was first reported by Neirinckx et al. in 1978,[242] and the most recent version of the generator was reported in 1991.[243] Tungsten-178 ($t_{1/2}$ = 21.7 days) can be produced by several routes, but the route most frequently used for generator production was the ^{181}Ta(p,4n)^{178}W reaction using 40 MeV protons.[244,245] The relatively high proton energy required for this reaction limits the number of facilities where it can be prepared, but the 22 day half-life provides adequate time for shipping and target processing.

In the most recent version of the generator, ^{178}Ta is eluted from the generator with a solution of 0.03 N HCl and 0.1% H_2O_2 and buffered with a solution of 0.13 N Na_2HPO_4 prior to injection.[243] The elution yield is 40−60%, and the breakthrough of the parent ^{178}W is <0.01%.[243]

14.3. Chemistry and Applications

Given the constraints of the 10 min half-life, ^{178}Ta was primarily used simply as the buffered generator eluate to measure the left ventricular ejection fraction,[240] although there were some early efforts to develop simple particulate radiopharmaceuticals such as a lung agent based on labeled albumin microspheres and a liver agent based on "minimicrospheres" (0.5−2 μM).[246]

In the longer term, however, the low energy of the ^{178}Ta emissions, which are highly attenuated by tissue, the challenge of developing radiopharmaceuticals that make optimal use of the 10 min half-life, and the need for a different type of imaging device (the MWPC), with which to optimally image the low-energy emissions of ^{178}Ta, combined to make ^{178}Ta a less-than-optimal choice in comparison to ^{99m}Tc, and there has been little recent interest in this system.

15. RHENIUM

15.1. Common Radionuclides and Their Properties

There are two rhenium radionuclides of clinical interest, ^{186}Re ($t_{1/2}$ = 3.72 days) and ^{188}Re ($t_{1/2}$ = 17.0 h), both of which are primarily of interest for targeted radiotherapy. Rhenium-186 undergoes β^- decay (92.5%) with the emission of two β^- particles (306.1 keV, 21.54%; 359.2 keV, 70.99%) and a low-abundance γ ray (137.2 keV, 9.5%) that can used to verify delivery of the tracer to the target and for dosiometry calculations. Rhenium-188 also undergoes β^- decay (100%), also with the emission of two primary β^- particles (728.9 keV, 26.3%; 795.4 keV, 70.00%) and a low-abundance γ ray (155.0 keV, 15.6%). Other than the half-lives, the primary difference between the two radionuclides is the much higher β^- energy of ^{188}Re, which results in significantly higher tissue penetration (10.5 vs 4.8 mm), and the higher abundance of the ^{188}Re γ ray (15.6% vs 9.5%), which facilitates imaging.[7]

One of the attractions of $^{186/188}$Re is its possible use as a therapeutic analogue of ^{99m}Tc. However, the differences in redox behavior between the two elements and the fact that both rhenium radionuclides emit imagable photons at least partially obviate this application.

15.2. Radionuclide Production

Rhenium-186 can be produced by neutron irradiation of ^{185}Re, but this produces low-specific-activity material. A high-specific-activity product can be produced by the ^{186}W(p,n)^{186}Re reaction using 10 Mev protons[247−249] or by the ^{186}W(d,2n)^{186}Re reaction using 22 meV deuterons;[250] however, this route significantly limits the number of sites at which it can be prepared.

Rhenium-188 is obtained from the ^{188}W/^{188}Re generator.[251−253] The parent ^{188}W ($t_{1/2}$ = 69.8 days) is produced by a double-neutron capture reaction: ^{186}W(n,γ)^{187}W(n,γ)^{188}W.[6,7] The ^{188}Re daughter is eluted from the generator with saline as perrhenate, analogous to the production of ^{99m}Tc using the ^{99}Mo/^{99m}Tc generator. One difference between the two generators is that the specific activity of ^{188}W is much lower than the specific activity of ^{99}Mo, so a larger column is required, which means the elution volume is somewhat larger.

15.3. Chemistry

The radiopharmaceutical chemistry of $^{186/188}$Re has been the subject of several reviews,[6,7,254,255] including a comprehensive discussion in 2017.[256] Accordingly, this discussion will focus on an overview of $^{186/188}$Re radiochemistry rather than an in-depth discussion.

DOI: 10.1021/acs.chemrev.8b00281
Chem. Rev. 2019, 119, 870−901

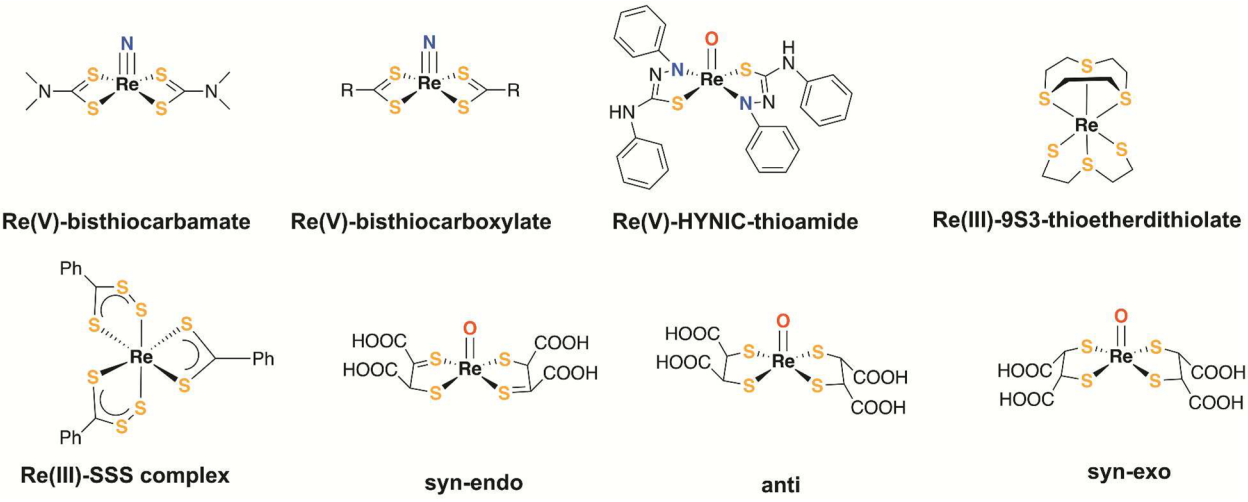

Figure 11. Nitrido and thio-/thiolato complexes of rhenium.

As with ^{99m}Tc, the radiochemistry of $^{186/188}$Re starts with the perrhenate anion, $^{186/188}ReO_4^-$. When ^{188}Re is produced using the $^{188}W/^{188}$Re generator, it is eluted as $^{188}ReO_4^-$. When ^{186}Re is produced via the $^{186}W(p,n)^{186}$Re reaction, the tungsten target is dissolved in 30% H_2O_2, which also results in the production of $^{186}ReO_4^-$. Generally, the chemistry of rhenium is similar to that of its Group 7 congener Tc, so much so that nonradioactive Re is often used as a surrogate for ^{99}Tc ($t_{1/2}$ = 220 000 years) in the characterization of ^{99m}Tc compounds. One important difference between the chemistry of the two elements is that Re(VII) is harder to reduce than Tc(VII). Similarly, lower oxidation states of Re are more easily oxidized than lower oxidation states of Tc, particularly at the very low concentrations encountered in radiochemistry. As a result, it is sometimes necessary to use different donor atoms to improve the redox stability of Re complexes in lower oxidation states. This difference in redox stability also means that Re is sensitive to trace amounts of oxidizing agents that may be present as contaminants in reaction mixtures. For example, in the direct production of ^{186}Re, HNO_3 is used to elute $^{186}ReO_4^-$ from the anion-exchange column used in the separation process, and the small amounts of HNO_3 that are carried through the process can interfere with subsequent efforts to produce ^{186}Re complexes in lower oxidation states.[257] This problem is exacerbated by the fact that the decay of ^{186}Re and ^{188}Re produces greater amounts of radiolytic byproducts than the decay of ^{99m}Tc, and these byproducts can also oxidize Re compounds in lower oxidation states.

In parallel with ^{99m}Tc, much of the early radiochemistry of Re was characterized by poorly defined compounds prepared by mixing together a reducing agent such as $SnCl_2$, a ligand such as DTPA, and perrhenate to prepare "Re-DTPA". However, again in parallel with developments in Tc chemistry, since the 1980s the radiochemistry of rhenium has been characterized by well-defined compounds of known chemical composition.

Rhenium(V) complexes are primarily square-pyramidal with an oxo group at the apex and a mixture of amine and sulfur donor atoms forming the base of the pyramid with the S donors included to improve the stability of the 5+ oxidation state.[258−260]

As with Tc(V), the Re(V) nitride core is also the subject of significant interest. The nitride is typically prepared by reduction of perrhenate in the presence of a hydrazide derivative such as *N*-methyl-*S*-ethyldithiocarbamate. The resulting complexes are typically square-pyramidal with pairs of bidentate ligands such as dithiocarbamates or dithiocarboxylates (Figure 11).[261−265]

There is interest in preparing Re(V)-HYNIC derivatives, analogous to the corresponding Tc(V)-HYNIC complexes, but this is an example of where the differences in redox chemistry between technetium and rhenium complicate the preparation of the rhenium analogues. One example of the use of a Re(V)-HYNIC derivative to label a protein was its use to label trastuzumab from a Re(V)-gluocoheptanoate complex.[266] An alternative approach that circumvents the limitations of the HYNIC moiety with Re(V) is the use of a thioamide rather than hydrazinonicotinomido chelator.[267,268]

One particularly interesting example of creative ^{188}Re(V)═oxo complex is its use as a bridge in octreotide,[269] an application that builds on the previous use of ^{99m}Tc as a bridge in α-MSH (Figure 12).[270]

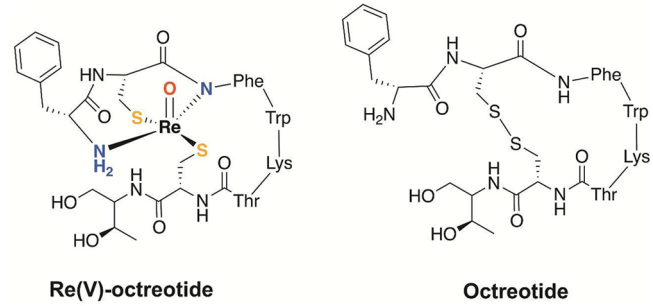

Figure 12. Octreotide and its Re(V)-oxo bridged analogue.

There are a few examples of $^{186/188}$Re(III) complexes, which primarily make use of thiol donors to stabilize the lower oxidation state. In one example, Garin and co-workers used a Re(III)-SSS complex as an alternative to ^{131}I to label lipiodol for the treatment of hepatocellular carcinoma.[271] A Re(III) complex containing a somewhat different S_6 donor set was prepared by Mullen et al.[272] In this case the ligand set is composed of one linear and one cyclic S_3 ligand (9S3), with the linear ligand resulting from the attempted reduction of $[Re^{II}(9S3)_2][BF_4]_2$ to form $Re^{I}(9S3)_2$, which instead led to the oxidation of the metal to Re^{III} and the cleavage a C−S bond to produce the linear form of the ligand.

DOI: 10.1021/acs.chemrev.8b00281
Chem. Rev. 2019, 119, 870−901

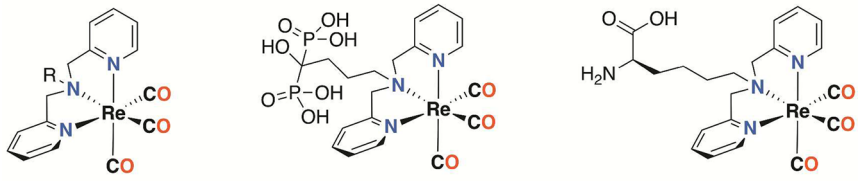

Figure 13. Re(I) tricarbonyl structures discussed in section 14.3.

For Re(I), the $[^{188}Re(CO)_3]^+$ core has attracted significant attention, as it has with ^{99m}Tc. In contrast to ^{99m}Tc, $[^{188}Re(CO)_3(H_2O)_3]^+$ cannot be produced using a simple kit. More robust conditions are required: $BH_3{\cdot}NH_3$ in a CO atmosphere.[273] Also, because the yield of this reaction is lower, with "ReO_2" and unreduced ReO_4^- present in the product mixture, an additional purification step is required.[274]

As with the $[^{99m}Tc(CO)_3(H_2O)_3]^+$ core, the primary use of $[^{188}Re(CO)_3(H_2O)_3]^+$ is as a label for biomolecules (Figure 13). One approach has been to use histidine, cysteine, or methionine residues that are either already present in the protein structure or added to the protein to improve binding.[275−277] A more targeted approach is to use a tridentate bifunctional chelator such as dipyridyl amine.[274,278,279] Other chelating groups that have been used for this application include aliphatic amines and carboxylates.[280] Inclusion of a reactive "R" group allows for conjugation to protein vectors.[281]

15.4. Applications

The parallels between ^{99m}Tc and $^{186/188}Re$ extend, in many cases, to their biological properties. Perhaps the most obvious example is the perrhenate anion, which like $^{99m}TcO_4^-$ is a substrate for the NaI symporter (NIS) and localizes in the thyroid, salivary glands, and gastric mucosa.[282] Zuckier and co-workers reported that the uptake of $^{188}ReO_4^-$ was similar to that of $^{99m}TcO_4^-$ and $^{125}I^-$, suggesting that $^{188}ReO_4^-$ may be an effective radiotherapeutic replacement for $^{131}I^-$.[282] These investigators also demonstrated in a breast cancer model that $^{188}ReO_4^-$ delivered a radiation dose to the tumor that is ∼4.5 times higher than that delivered by $^{131}I^-$ on a per mCi basis.[283] This high therapeutic potential has led to the suggestion that transfection the NIS to tumors might be a way to increase the selective delivery of ^{188}Re to tumors.[284]

The distinctive uptake pattern of $^{186/188}ReO_4^-$ by the thyroid, salivary glands, and gastric mucosa provides a convenient marker for in vivo decomposition of $^{186/188}Re$ radiopharmaceuticals in lower oxidation states. In the therapeutic use of $^{186/188}Re$ in lower oxidation states, uptake in these tissues arising from in vivo decomposition can be blocked by sodium perchlorate or potassium iodide, as is the case with radioiodinated compounds.

The less-than-well-defined chemical compositions of Re and Tc radiopharmaceuticals developed in the 1980s can be seen in one of the first therapeutic Re radiopharmaceuticals, ^{188}Re-HEDP, which was developed for pain palliation arising from bone metastases.[285]

As mentioned previously, one of the more interesting biological applications of rhenium is as a bridge in peptides such as α-MSH and octreotide.[269,270] While chemically interesting, in vitro studies revealed that insertion of the Re(V) atom into the peptide significantly reduced binding to the somatostatin receptor due to a structural perturbation to the binding domain induced by the presence of the rhenium atom.

Another example of a $^{186/188}Re(V)$ complex in clinical use is "pentavalent DMSA" (DMSA = dimercaptosuccinic acid), the ^{188}Re analogue of $[^{99m}Tc(V)O(DMSA)_2]^-$. In a study in prostate cancer patients with bone metastases, Blower et al. found that there was high correlation between the distribution of $[^{99m}Tc(V)O(DMSA)_2]^-$ and $[^{188}Re(V)O(DMSA)_2]^-$ but that the tumor uptake of $[^{188}Re(V)O(DMSA)_2]^-$ was ∼20% lower than that of $[^{99m}Tc(V)O(DMSA)_2]^-$.[286,287] There was no evidence of thyroid uptake, suggesting that the complex is stable in vivo. This early success prompted the development of a kit formulation.[288]

The DMSA ligand exists as two isomers, racemic and meso, and the biological properties of the ^{188}Re (and ^{99m}Tc) complexes of the two isomers are somewhat different. Although initial human studies were carried out with the meso isomer, more recent preclinical studies suggest that the tumor uptake of the ^{188}Re complexes of the rac isomer is higher with lower uptake in normal bone.[289] These investigators also found that the synthesis conditions required to obtain optimal yield were somewhat different for the two isomers with a higher concentration of sodium metabisulfite and ligand and a higher pH required to prepare the Re(V) complex of the rac isomer.

Rhenium(I) tricarbonyl ($[Re(CO)_3]^+$) is proving to be a rich source of biologically interesting $^{186/188}Re$ complexes. Martin de Rosales and co-workers exploited this core to prepare a ^{188}Re-alendronate derivative for bone pain palliation.[274] In contrast to "^{188}Re-HEDP", $^{188}Re(CO)_3$-DPA-alendronate is a discrete, well-characterized Re complex. Biologically, it shows higher bone uptake than ^{188}Re-HEDP at 48 h postinjection (21.2 ± 6.6% ID/g vs 13.4 ± 0.2% ID/g) and higher stability with respect to oxidation to $^{188}ReO_4^-$.

Valliant and co-workers exploited the dipyridylamine (dpa) chelator and the $[Re(CO)_3]^+$ core as the basis for a series of compounds using a concept that they call "single amino-acid chelators" (SAACs), where the carboxylate moiety on the dpa ligand can serve as a linker to a wide range of biological vectors including peptides, nucleosides, and carbohydrates.[278] The dpa chelator was also used by Xia et al. to label IgG via an amide bond between the carboxylate moiety of the dpa and a free amine on the IgG.[279] These investigators reported that the $^{188}Re(CO)_3$-dpa-IgG conjugate was more stable in vitro than directly labeled $^{188}Re(CO)_3$-dpa-IgG, with >90% of the activity retained after 48 h incubation in calf serum at 37 °C compared to ∼60% retention for the directly labeled conjugate.

DOI: 10.1021/acs.chemrev.8b00281
Chem. Rev. 2019, 119, 870−901

16. PLATINUM

16.1. Common Radionuclides and Their Properties

The platinum radionuclide that has received the most attention with respect to nuclear medicine is ^{195m}Pt, although there are also several studies using ^{191}Pt ($t_{1/2}$ = 2.8 days)[290] and ^{193m}Pt ($t_{1/2}$ = 4.3 days).[291,292] Platinum-195m has a half-life of 4 days and decays to stable ^{195}Pt with the emission of several low-to-medium energy γ rays that are suitable for single-photon imaging.

16.2. Radionuclide Production

Platinum-195m is easily prepared by the neutron irradiation of isotopically enriched ^{194}Pt. Aalbersberg et al. recently reported that irradiation of >96% isotopically enriched ^{194}Pt at the Petten High Flux Reactor produced ^{195m}Pt with a specific activity of 33 MBq (890 μCi)/mg (6.4 GBq (170 mCi)/mmol).[293] Several radionuclides other than ^{195m}Pt are also produced during the production of ^{195m}Pt including ^{197}Pt, ^{191}Pt, ^{192}Ir, ^{194}Ir, ^{198}Au, and ^{199}Au, with ^{195m}Pt only comprising 62% of the radioactivity at the end of irradiation. The half-lives of ^{197}Pt and ^{194}Ir are relatively short, so allowing 2 days of decay postirradiation increases ^{195m}Pt to 77% of the total radioactivity. Higher-specific-activity ^{195m}Pt can be prepared by the ^{192}Os(α,n)^{195m}Pt reaction using 18−24 MeV α particles or by the ^{197}Au(γ,np)^{195m}Pt reaction.[294] The comparatively low specific activity is not a limiting factor for biological studies of Pt-based chemotherapeutics because the administered doses of these drugs are typically on the order of tens to hundreds of mg.

16.3. Chemistry

The irradiated Pt metal target is dissolved in aqua regia with heating to form H_2PtCl_6 and then extracted with methyl isobutyl ketone (MIBK) to remove ^{199}Au.[295] The first step in the synthesis of ^{195m}Pt-labeled cisplatin from H_2PtCl_6 is reduction of the Pt(IV) hexachloro complex to the tetrachloro Pt(II) complex with hydroxylamine hydrochloride.[295] This is a somewhat exacting process because it requires a precise stoichiometric amount of hydroxylamine hydrochloride. Excess reductant will reduce the Pt(IV) to Pt(0), and insufficient reductant will leave it as Pt(IV). The tetrachloro complex is converted to the tetraiodo complex with excess KI and treated with a small excess of NH_4OH to form the diaminodiodo complex (*cis*-[^{195m}Pt]Pt(NH_3)$_2$I$_2$), which is then converted to the diaminodiaquo complex by treatment of the solution with $AgNO_3$. The *cis*-chloro complex is obtained by treating the aquo complex with 12 M HCl and heating.[295] This is obviously not a simple process, especially in the context of working with a significant quantity of ^{195m}Pt. Zeevaart et al. recently published a variation on this procedure in which the starting material for the synthesis is irradiated ^{195m}PtCl$_2$.[296] While this approach does avoid the stoichiometric reduction of Pt(IV) to Pt(II), it is still a multistep process. Suwa et al. reported the synthesis of carboplatin labeled with a mixture of platinum radionuclides using a method similar to that described by Hoeschele for the synthesis of [^{195m}Pt]cisplatin.[297]

16.4. Applications

The principal focus of biological studies with ^{195m}Pt-labeled cisplatin has been to measure their biodistribution in order to better define the toxicity profile of the nonradioactive chemotherapeutics. The human biodistribution of ^{195m}Pt-labeled cisplatin was reported by Smith and Taylor,[298] who found that 25−30% of the injected dose is excreted in the urine within the first 24 h but that subsequent clearance is much slower with a liver clearance half-time of 8 d. There was no evidence of accumulation of the compound in the tumor. More recently, Sathekge et al. obtained similar results in a dosimetry study in normal volunteers.[299]

17. MERCURY

17.1. Common Radionuclides and Their Properties

Mercury-197 decays by electron capture with the emission of a γ ray (77 keV, 19%) and several X-rays (67−78 keV, 70%).[300] In contrast, ^{203}Hg decays with the emission of a high-abundance (82%) 279 keV γ ray. However, the combination of low photon abundance and low energy of the ^{197}Hg emissions, suboptimal photon energy for ^{203}Hg, and concern about mercury toxicity because of the low specific activity of the radionuclides led to the replacement of these mercury radiopharmaceuticals with ^{99m}Tc-based agents.

17.2. Radionuclide Production

Recently there has been some interest in reviving mercury for use as a theragnostic radionuclide.[301,302] Walther et al. recently reported the production of high-purity $^{197m/197}$Hg by irradiation of a gold foil with a 10 MeV proton beam.[302] This route is less expensive than previous approaches that used enriched Hg targets because ^{197}Au is 100% abundant. This route also adds an additional decay path, from ^{197m}Hg to ^{197}Hg ($t_{1/2}$ = 23.8 h) and additional γ ray (133.98 keV, 33.5%). The specific activity is very high (~500 GBq (~14 Ci)/μmol) compared to ~2 GBq (50 mCi)/μmol when ^{197}Hg is produced using the ^{196}Hg(n,γ)^{197}Hg reaction, obviating concerns about mercury toxicity. The authors suggest that $^{197m/197}$Hg could be used for a combined diagnostic/therapeutic radionuclide, because, in addition to the low-abundance photons, which can be imaged, it also produces a large number of Auger and conversion electrons that can be used for therapy. Therefore, $^{197m/197}$Hg may find application in theragnostics if suitable radiopharmaceuticals are developed.

17.3. Chemistry and Applications

Historically, both ^{197}Hg ($t_{1/2}$ = 64.1 h) and ^{203}Hg ($t_{1/2}$ = 46.6 days) have important roles in nuclear medicine. In fact, some of the very earliest nuclear medicine images were acquired with ^{203}Hg-labeled Neohydrin (chlormerodin) as a brain scanning agent (Figure 14).[303]

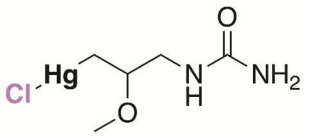

Chloromerodin

Figure 14. Structure of Neohydrin (chlormerodin).

18. CONCLUSIONS

There is an interesting cycle to the use of different radionuclides for imaging and therapy. During the early growth phase of nuclear medicine, in the 1960s, many different radionuclides were using for imaging, including many radiometals such as ^{51}Cr, ^{57}Co, $^{197/203}$Hg, ^{198}Au, and ^{59}Fe.[304] With the development of the

DOI: 10.1021/acs.chemrev.8b00281
Chem. Rev. 2019, 119, 870−901

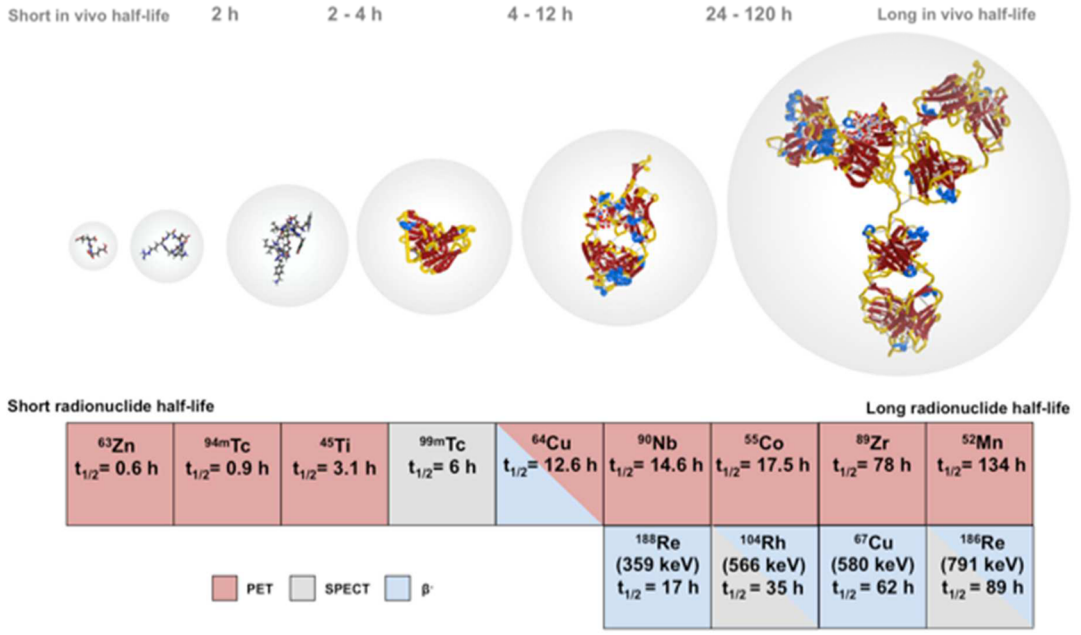

Figure 15. Isotopes of current and emerging interest for imaging and therapy applications ordered from short to long half-life, matching the in vivo half-life of small molecules, peptides, proteins, and monoclonal antibodies.

^{99}Mo/^{99m}Tc generator in the late 1950s and the subsequent development of the ^{99m}Tc instant kit in 1971,[163] these were almost completely replaced by ^{99m}Tc-based radiopharmaceuticals.

Similarly, the early years of PET imaging (the 1970s) were dominated by the standard PET radionuclides, ^{18}F, ^{15}O, ^{13}N, and ^{11}C. There are, however, inherent restrictions to using only these four radionuclides for PET imaging, the most obvious of which is their half-lives. The longest-lived standard PET radionuclide, ^{18}F, has a physical half-life of only 110 min, which effectively limits its use to imaging biological processes with half-lives of, at most, 6−8 h, corresponding to 3−4 half-lives. A second limitation is the relatively rigorous labeling conditions, typically requiring heating at temperatures greater than 100 °C for 15−30 min in anhydrous organic solvents, conditions that restrict their use to robust precursors. In the 1990s, there was a major shift in PET chemistry as investigators became interested in using nonstandard positron-emitting radionuclides, principally radiometals. Among the first nonstandard PET radionuclides was ^{64}Cu, but it was quickly followed by many others, including ^{68}Ga and ^{89}Zr. In contrast to standard PET radionuclides, radiometals offer several advantages, including a wide range of half-lives, to better match the biological process of interest, and relatively mild labeling conditions, facilitating their use with more fragile proteins, such as antibodies (Figure 15). Recent developments in production now provide access to novel radiometals such as ^{63}Zn, ^{45}Ti, ^{52} Mn, ^{55}Co, ^{90}Nb, and ^{104}Rh and open new opportunities for targeted imaging. Short-lived ^{63}Zn allows the study of Zn^{2+} metabolism in the context of neurodegenerative disease, diabetes, and prostate cancer. Titanium-45 and ^{90}Nb can serve as shorter-lived congeners to the already widely used ^{89}Zr. Cobalt-55 exhibits an intermediate half-life, suitable for targeted imaging with larger peptides, rapidly clearing antibodies, and antibody fragments. The long-lived PET radionuclide ^{52}Mn can enhance MR images obtained with ^{nat}Mn-based contrast agents and add value to the growing PET-MR scanner base.

In the realm of targeted radiotherapy, radiometals offer these same advantages as well as the ability to optimize the therapeutic emission properties of the agent by choosing a radiometal with the optimal β^- energy for the therapeutic target or by using an α-emitting radionuclide that imparts maximal damage to the target within a very short-range. Indeed, the radiopharmaceuticals that have been approved by the FDA recently are almost exclusively based on radiometals, from ^{223}Ra (Xofigo) for treating bone pain due to cancer metastases to ^{68}Ga-dotatate (NetSpot) for imaging somatostatin-receptor-positive neuroendocrine tumors and ^{177}Lu-labeled dotatate (Lutathera) for treating somatostatin receptor positive gastroenteropancreatic neuroendocrine tumors. Radiotherapeutics incorporating $^{186/188}$Re, ^{67}Cu, and ^{104}Rh will be able to further enhance treatment options with β^- emitting radionuclide. There are many more radiometal-based diagnostics and therapeutics in the approval pipeline, and it is our responsibility as radiochemists to continue to develop new agents with which to more effectively diagnose and treat disease.

AUTHOR INFORMATION

Corresponding Authors

*E-mail: eszter.boros@stonybrook.edu.
*E-mail: alan.packard@childrens.harvard.edu.

ORCID

Eszter Boros: 0000-0002-4186-6586
Alan B. Packard: 0000-0003-0906-1021

Notes

The authors declare no competing financial interest.

Biographies

Eszter Boros is a native of Zurich, Switzerland. She received a B.Sc. (2006) and an M.Sc. (2007) in Chemistry from the University of Zurich, where she was a three-time Alfred Werner Fellowship recipient.

DOI: 10.1021/acs.chemrev.8b00281
Chem. Rev. 2019, 119, 870−901

At the University of Zurich, she conducted research on ^{99m}Tc-based intercalators under the mentorship of Prof. Roger Alberto. From 2007 to 2011, she pursued a Ph.D. in Chemistry at the University of British Columbia with a UBC Graduate Scholarship in the groups of Chris Orvig and Michael J. Adam, where she worked on bifunctional chelators for ^{68}Ga, ^{111}In, and ^{64}Cu. In 2011, Eszter joined the group of Peter Caravan in the Department of Radiology at Massachusetts General Hospital and Harvard Medical School to work on MRI contrast agent development and preclinical imaging as a Mobility Swiss National Science Foundation fellow. In 2015, she was promoted to instructor at Harvard Medical School after receipt of an NIH K99 Pathway to Independence Award. In September 2017, she joined the Department of Chemistry at Stony Brook University as an Assistant Professor with a cross-appointment in Radiology at Stony Brook Medicine. Her current research interest spans from basic aqueous coordination chemistry, structure−activity relationships of metal-based drugs, to preclinical imaging and therapy with metal-based tracers and therapeutics for cancer and infection.

Alan Packard received his Bachelor's Degree in chemistry from the University of New Hampshire (1970), where he spent most of his time analyzing trace nutrients in seawater, and his Ph.D. in inorganic chemistry from Colorado State University (1974), where he studied Jahn−Teller distortions in copper complexes. This was followed by a postdoctoral fellowship at the University of Cincinnati, where he was introduced to technetium chemistry, and two years as an assistant scientist at Brookhaven National Laboratory, where he continued his investigation into new technetium complexes. In 1982, he moved to Boston, where he is now Associate Professor of Radiology at Harvard Medical School and a Sr. Research Associate in Nuclear Medicine and Director of Radiopharmaceutical Research at Boston Children's Hospital. His research interests still include radiometals but have shifted over the years from technetium to copper and zirconium and, most recently, to ^{18}F.

ACKNOWLEDGMENTS

E.B. acknowledges funding sources, specifically the NIH for a pathway to independence award (R00HL125728-03), a REACH award (U01HL127522-18150031), and Stony Brook University for startup funds. Devondra Pitt is acknowledged for her help with collection of references for sections 2−6 and 8−10. A.B.P. acknowledges support from the NIH (5 R01 HL108107) and the Children's Hospital Radiology Foundation.

REFERENCES

(1) Palmer, M. R.; Zhu, X.; Parker, J. A. Modeling and simulation of positron range effects for high resolution PET imaging. *IEEE Trans. Nucl. Sci.* **2005**, *52*, 1391−1395.
(2) Palmer, M. R.; Brownell, G. L. Annihilation density distribution calculations for medically important positron emitters. *IEEE Trans. Med. Imaging* **1992**, *11*, 373−378.
(3) Bunka, M.; Müller, C.; Vermeulen, C.; Haller, S.; Türler, A.; Schibli, R.; van der Meulen, N. P. Imaging quality of ^{44}Sc in comparison with five other PET radionuclides using Derenzo phantoms and preclinical PET. *Appl. Radiat. Isot.* **2016**, *110*, 129−133.
(4) McQuade, P.; McCarthy, D. W.; Welch, M. J. In *Positron Emission Tomography: Basic Science and Clinical Practice*; Valk, P. E., Bailey, D. L., Townsend, D. W., Maisey, M. N., Eds.; Springer-Verlag: London, 2003.
(5) Wadas, T. J.; Wong, E. H.; Weisman, G. R.; Anderson, C. J. Coordinating radiometals of copper, gallium, indium, yttrium, and zirconium for PET and SPECT imaging of disease. *Chem. Rev.* **2010**, *110*, 2858−2902.
(6) Cutler, C. S.; Hennkens, H. M.; Sisay, N.; Huclier-Markai, S.; Jurisson, S. S. Radiometals for combined imaging and therapy. *Chem. Rev.* **2013**, *113*, 858−883.
(7) Feng, Y.; Phelps, T. E.; Carroll, V.; Gallazzi, F.; Sieckman, G.; Hoffman, T. J.; Barnes, C. L.; Ketring, A. R.; Hennkens, H. M.; Jurisson, S. S. Chemistry and radiochemistry of As, Re and Rh isotopes relevant to radiopharmaceutical applications: high specific activity radionuclides for imaging and treatment. *Dalton Trans.* **2017**, *46*, 14677−14690.
(8) Kostelnik, T. I.; Orvig, C. *Chem. Rev.* **2018**, in press.
(9) Hoffman, T. J.; Seger, R. M.; Mckenzie, E. H.; Volkert, W. A.; Holmes, R. A.; Pettit, R. P.; Canning, L.; Cumming, S. A.; Nechvatal, G. 1st pass cerebral extraction studies with Tc-99m propylene amine oxime complexes. *J. Nucl. Med.* **1985**, *26*, P129−P130.
(10) Hevesy, G. The absorption and translocation of lead by plants: A contribution to the application of the method of radioactive indicators in the investigation of the change of substance in plants. *Biochem. J.* **1923**, *17*, 439−445.
(11) Szelecsényi, F.; Kovács, Z.; Nagatsu, K.; Zhang, M.-R.; Suzuki, K. Production cross sections of radioisotopes from ^{3}He-particle induced nuclear reactions on natural titanium. *Appl. Radiat. Isot.* **2017**, *119*, 94−100.
(12) Radchenko, V.; Meyer, C. A. L.; Engle, J. W.; Naranjo, C. M.; Unc, G. A.; Mastren, T.; Brugh, M.; Birnbaum, E. R.; John, K. D.; Nortier, F. M.; et al. Separation of ^{44}Ti from proton irradiated scandium by using solid-phase extraction chromatography and design of ^{44}Ti/^{44}Sc generator system. *J. Chromatogr. A* **2016**, *1477*, 39−46.
(13) van der Meulen, N. P.; Bunka, M.; Domnanich, K. A.; Müller, C.; Haller, S.; Vermeulen, C.; Türler, A.; Schibli, R. Cyclotron production of ^{44}Sc: from bench to bedside. *Nucl. Med. Biol.* **2015**, *42*, 745−751.
(14) Fazaeli, Y.; Aboudzadeh, M.; Aardaneh, K.; Kakavand, T.; Bayat, F.; Yousefi, K. A new approach to targetry and cyclotron production of ^{45}Ti by proton irradiation of ^{45}Sc. *Nucl. Technol. Radiat. Prot.* **2014**, *29*, 28−33.
(15) Severin, G. W.; Nielsen, C. H.; Jensen, A. I.; Fonslet, J.; Kjær, A.; Zhuravlev, F. Bringing radiotracing to titanium-based antineoplastics: Solid phase radiosynthesis, PET and ex vivo evaluation of antitumor agent [^{45}Ti](salan)Ti(dipic). *J. Med. Chem.* **2015**, *58*, 7591−7595.
(16) Cini, M.; Bradshaw, T. D.; Woodward, S. Using titanium complexes to defeat cancer: The view from the shoulders of titans. *Chem. Soc. Rev.* **2017**, *46*, 1040−1051.
(17) Tshuva, E. Y.; Miller, M. In *Metallo-Drugs: Development and Action of Anticancer Agents: Development and Action of Anticancer Agents*; Sigel, A., Sigel, H., Freisinger, E., Sigel, R. K. O., Eds.; Walter de Gruyter GmbH: Berlin, 2018.
(18) Jones, K. E.; Batchler, K. L.; Zalouk, C. l.; Valentine, A. M. Ti(IV) and the siderophore desferrioxamine B: A tight complex has biological and environmental implications. *Inorg. Chem.* **2017**, *56*, 1264−1272.
(19) Price, R.; Sheil, R.; Scharli, R.; Chan, S.; Gibbons, P.; Jeffery, C.; Morandeau, L. SNMMI Annual Meeting, Vancouver, BC, Canada, 2013.
(20) Chen, F.; Valdovinos, H. F.; Hernandez, R.; Goel, S.; Barnhart, T. E.; Cai, W. Intrinsic radiolabeling of titanium-45 using mesoporous silica nanoparticles. *Acta Pharmacol. Sin.* **2017**, *38*, 907−913.
(21) Tse, C. W.; Mundy, J. N.; McFall, W. D. Half-lives of ^{51}Cr, ^{48}Cr, and ^{48}V. *Phys. Rev. C: Nucl. Phys.* **1974**, *10*, 838−839.
(22) Bartholomew, G.; Earle, E.; Gunye, M. Neutron-Capture γ-ray studies in ^{50}Cr (n, γ) ^{51}Cr. *Can. J. Phys.* **1966**, *44*, 2111−2130.
(23) Kassis, A. I.; Sastry, K. S. R.; Adelstein, S. J. Intracellular distribution and radiotoxicity of chromium-51 in mammalian cells: Auger-electron dosimetry. *J. Nucl. Med.* **1985**, *26*, 59−67.
(24) Stacy, B.; Thorburn, G. Chromium-51 ethylenediaminetetraacetate for estimation of glomerular filtration rate. *Science* **1966**, *152*, 1076−1077.
(25) Kerr, R. M.; Du Bois, J. J.; Holt, P. R. Use of ^{125}I-and ^{51}Cr-labeled albumin for the measurement of gastrointestinal and total albumin catabolism. *J. Clin. Invest.* **1967**, *46*, 2064−2082.
(26) Krawczykowa, Z.; Liniecki, J.; Pertyński, T.; Stepień, J.; Durski, K.; Surma, M. Evaluation of pigmentary intraocular tumors and the extent of the neoplastic process using Cr-51-and Co-57-labeled bleomycin. *Klin. Oczna* **1983**, *85*, 245−247.
(27) Troughton, J. S.; Greenfield, M. T.; Greenwood, J. M.; Dumas, S.; Wiethoff, A. J.; Wang, J.; Spiller, M.; McMurry, T. J.; Caravan, P.

DOI: 10.1021/acs.chemrev.8b00281
Chem. Rev. 2019, 119, 870−901

Synthesis and evaluation of a high relaxivity manganese(II)-based MRI contrast agent. *Inorg. Chem.* **2004**, *43*, 6313−6323.
(28) Caravan, P.; Farrar, C. T.; Frullano, L.; Uppal, R. Influence of molecular parameters and increasing magnetic field strength on relaxivity of gadolinium- and manganese-based T1 contrast agents. *Contrast Media Mol. Imaging* **2009**, *4*, 89−100.
(29) Fonslet, J.; Tietze, S.; Jensen, A. I.; Graves, S. A.; Severin, G. W. Optimized procedures for manganese-52: production, separation and radiolabeling. *Appl. Radiat. Isot.* **2017**, *121*, 38−43.
(30) Lewis, C. M.; Graves, S. A.; Hernandez, R.; Valdovinos, H. F.; Barnhart, T. E.; Cai, W.; Meyerand, M. E.; Nickles, R. J.; Suzuki, M. ^{52}Mn production for PET/MRI tracking of human stem cells expressing divalent metal transporter 1 (DMT1). *Theranostics* **2015**, *5*, 227.
(31) Klein, A. T. J.; Rösch, F.; Qaim, S. M. Investigation of ^{50}Cr(d, n)^{51}Mn and ^{nat}Cr(p, x)^{51}Mn processes with respect to the production of the positron emitter ^{51}Mn. *Radiochim. Acta* **2000**, *88*, 253−264.
(32) Graves, S.; Valdovinos, H.; Barnhart, T.; Nickles, R. Novel ^{51}Mn production methods for calcium channel transport based applications. *J. Nucl. Med.* **2016**, *57*, 380−380.
(33) Graves, S. A.; Hernandez, R.; Valdovinos, H. F.; Ellison, P. A.; Engle, J. W.; Barnhart, T. E.; Cai, W.; Nickles, R. J. Preparation and in vivo characterization of $^{51}MnCl_2$ as PET tracer of Ca^{2+} channel-mediated transport. *Sci. Rep.* **2017**, *7*, 3033.
(34) Wooten, A. L.; Lewis, B. C.; Lapi, S. E. Cross-sections for (p, x) reactions on natural chromium for the production of ^{52,52m,54}Mn radioisotopes. *Appl. Radiat. Isot.* **2015**, *96*, 154−161.
(35) Phukan, B.; Mukherjee, C.; Goswami, U.; Sarmah, A.; Mukherjee, S.; Sahoo, S. K.; Moi, S. C. A new bis (aquated) high relaxivity Mn(II) complex as an alternative to Gd(III)-based MRI contrast agent. *Inorg. Chem.* **2018**, *57*, 2631−2638.
(36) Artali, R.; Baranyai, Z.; Botta, M.; Giovenzana, G. B.; Maspero, A.; Negri, R.; Palmisano, G.; Sisti, M.; Tollari, S. Solution thermodynamics, computational and relaxometric studies of ditopic DO3A-based Mn(II) complexes. *New J. Chem.* **2015**, *39*, 539−547.
(37) Gale, E. M.; Atanasova, I. P.; Blasi, F.; Ay, I.; Caravan, P. A manganese alternative to gadolinium for MRI contrast. *J. Am. Chem. Soc.* **2015**, *137*, 15548−15557.
(38) Vanasschen, C.; Brandt, M.; Ermert, J.; Coenen, H. H. Radiolabelling with isotopic mixtures of ^{52g}/^{55}Mn(II) as a straight route to stable manganese complexes for bimodal PET/MR imaging. *Dalton Trans.* **2016**, *45*, 1315−1321.
(39) Graves, S. A.; Hernandez, R.; Fonslet, J.; England, C. G.; Valdovinos, H. F.; Ellison, P. A.; Barnhart, T. E.; Elema, D. R.; Theuer, C. P.; Cai, W.; et al. Novel preparation methods of ^{52}Mn for immunoPET imaging. *Bioconjugate Chem.* **2015**, *26*, 2118−2124.
(40) Jensen, A. I.; Severin, G. W.; Hansen, A. E.; Fliedner, F. P.; Eliasen, R.; Parhamifar, L.; Kjær, A.; Andresen, T. L.; Henriksen, J. R. Remote-loading of liposomes with manganese-52 and in vivo evaluation of the stabilities of ^{52}Mn-DOTA and ^{64}Cu-DOTA using radiolabelled liposomes and PET imaging. *J. Controlled Release* **2018**, *269*, 100−109.
(41) Khandaker, M. U.; Ali, S. K.; Kassim, H. A.; Yusof, N. Evaluated cross-sections of ^{55}Co radionuclide, a non-standard positron emitter for clinical applications. *Radiat. Phys. Chem.* **2017**, *140*, 511−520.
(42) Amjed, N.; Hussain, M.; Aslam, M.; Tárkányi, F.; Qaim, S. Evaluation of nuclear reaction cross sections for optimization of production of the emerging diagnostic radionuclide ^{55}Co. *Appl. Radiat. Isot.* **2016**, *108*, 38−48.
(43) Valdovinos, H.; Hernandez, R.; Graves, S.; Ellison, P.; Barnhart, T.; Theuer, C.; Engle, J.; Cai, W.; Nickles, R. Cyclotron production and radiochemical separation of ^{55}Co and ^{58m}Co from ^{54}Fe, ^{58}Ni and ^{57}Fe targets. *Appl. Radiat. Isot.* **2017**, *130*, 90−101.
(44) Mitran, B.; Thisgaard, H.; Rosenström, U.; Dam, J. H.; Larhed, M.; Tolmachev, V.; Orlova, A. High contrast PET imaging of GRPR expression in prostate cancer using cobalt-labeled bombesin antagonist RM26. *Contrast Media Mol. Imaging* **2017**, *2017*, 1−10.
(45) Mastren, T.; Marquez, B. V.; Sultan, D. E.; Bollinger, E.; Eisenbeis, P.; Voller, T.; Lapi, S. E. Cyclotron production of high−specific activity ^{55}Co and in vivo evaluation of the stability of ^{55}Co metal-chelate-peptide complexes. *Mol. Imaging* **2015**, *14*, 526−533.
(46) Thisgaard, H.; Olesen, M. L.; Dam, J. H. Radiosynthesis of ^{55}Co- and ^{58m}Co-labelled DOTATOC for positron emission tomography imaging and targeted radionuclide therapy. *J. Labelled Compd. Radiopharm.* **2011**, *54*, 758−762.
(47) Spingler, B.; Scanavy-Grigorieff, M.; Werner, A.; Berke, H.; Lippard, S. J. Crystal structure determination of a (μ-amido)(μ-hydroxo)(μ-superoxo) dicobalt(III) complex from the werner collection. *Inorg. Chem.* **2001**, *40*, 1065−1066.
(48) Bosnich, B.; Poon, C. K.; Tobe, M. Complexes of cobalt(III) with a cyclic tetradentate secondary amine. *Inorg. Chem.* **1965**, *4*, 1102−1108.
(49) Cotton, F. A.; Goodgame, D.; Goodgame, M. The electronic structures of tetrahedral cobalt(II) complexes. *J. Am. Chem. Soc.* **1961**, *83*, 4690−4699.
(50) Heffern, M. C.; Yamamoto, N.; Holbrook, R. J.; Eckermann, A. L.; Meade, T. J. Cobalt derivatives as promising therapeutic agents. *Curr. Opin. Chem. Biol.* **2013**, *17*, 189−196.
(51) Munteanu, C. R.; Suntharalingam, K. Advances in cobalt complexes as anticancer agents. *Dalton Trans.* **2015**, *44*, 13796−13808.
(52) Antunes, P.; Ginj, M.; Zhang, H.; Waser, B.; Baum, R.; Reubi, J.-C.; Maecke, H. Are radiogallium-labelled DOTA-conjugated somatostatin analogues superior to those labelled with other radiometals? *Eur. J. Nucl. Med. Mol. Imaging* **2007**, *34*, 982−993.
(53) Heppeler, A.; André, J. P.; Buschmann, I.; Wang, X.; Reubi, J. C.; Hennig, M.; Kaden, T. A.; Maecke, H. R. Metal-ion-dependent biological properties of a chelator-derived somatostatin analogue for tumour targeting. *Chem. - Eur. J.* **2008**, *14*, 3026−3034.
(54) Simonsen, L. O.; Harbak, H.; Bennekou, P. Cobalt metabolism and toxicology—a brief update. *Sci. Total Environ.* **2012**, *432*, 210−215.
(55) Gramsbergen, J.; Duin, L.; Loopuijt, L.; Paans, A.; Vaalburg, W.; Korf, J. Imaging of the degeneration of neurons and their processes in rat or cat brain by $^{45}CaCl_2$ autoradiography or $^{55}CoCl_2$ positron emission tomography. *J. Neurochem.* **1988**, *50*, 1798−1807.
(56) Stevens, H.; Jansen, H. M.; De Reuck, J.; Lemmerling, M.; Strijckmans, K.; Goethals, P.; Lemahieu, I.; De Jong, B. M.; Willemsen, A. T.; Korf, J. Co-55-PET in stroke: relation to bloodflow, oxygen metabolism and gadolinium-MRI. *Acta Neurol. Belg.* **1997**, *97*, 172−177.
(57) Goethals, P.; Volkaert, A.; Vandewielle, C.; Dierckx, R.; Lameire, N. ^{55}Co-EDTA for renal imaging using positron emission tomography (PET): a feasibility study. *Nucl. Med. Biol.* **2000**, *27*, 77−81.
(58) Brandt, L. J.; Bernstein, L. H.; Abdul, W. Production of vitamin B12 analogues in patients with small-bowel bacterial overgrowth. *Ann. Intern. Med.* **1977**, *87*, 546−551.
(59) Woolfenden, J. M.; Alberts, D. S.; Hall, J. N.; Patton, D. D. Cobalt-57 bleomycin for imaging head and neck tumors. *Cancer* **1979**, *43*, 1652−1657.
(60) Dabrowiak, J.; Tsukayama, M. Cobalt(III) complex of pseudotetrapeptide A of bleomycin. *J. Am. Chem. Soc.* **1981**, *103*, 7543−7550.
(61) Wu, W.; Vanderwall, D. E.; Turner, C. J.; Kozarich, J. W.; Stubbe, J. Solution structure of Co-bleomycin A2 green complexed with d(CCAGGCCTGG). *J. Am. Chem. Soc.* **1996**, *118*, 1281−1294.
(62) Nieweg, O.; Beekhuis, H.; Paans, A.; Piers, D.; Vaalburg, W.; Welleweerd, J.; Wiegman, I.; Woldring, M. Detection of lung cancer with ^{55}Co-bleomycin using a positron camera. A comparison with ^{57}Co-bleomycin and ^{55}Co-bleomycin single photon scintigraphy. *Eur. J. Nucl. Med.* **1982**, *7*, 104−107.
(63) Ferreira, C. L.; Lapi, S.; Steele, J.; Green, D. E.; Ruth, T. J.; Adam, M. J.; Orvig, C. ^{55}Cobalt complexes with pendant carbohydrates as potential PET imaging agents. *Appl. Radiat. Isot.* **2007**, *65*, 1303−1308.
(64) Garousi, J.; Andersson, K. G.; Dam, J. H.; Olsen, B. B.; Mitran, B.; Orlova, A.; Buijs, J.; Ståhl, S.; Löfblom, J.; Thisgaard, H.; et al. The use of radiocobalt as a label improves imaging of EGFR using DOTA-conjugated Affibody molecule. *Sci. Rep.* **2017**, *7*, 5961.

DOI: 10.1021/acs.chemrev.8b00281
Chem. Rev. 2019, 119, 870−901

(65) Dam, J. H.; Olsen, B. B.; Baun, C.; Høilund-Carlsen, P. F.; Thisgaard, H. A PSMA ligand labeled with cobalt-55 for PET imaging of prostate cancer. *Mol. Imaging Biol.* **2017**, *19*, 915−922.
(66) Dam, J. H.; Olsen, B. B.; Baun, C.; Høilund-Carlsen, P.-F.; Thisgaard, H. In vivo evaluation of a bombesin analogue labeled with Ga-68 and Co-55/57. *Mol. Imaging Biol.* **2016**, *18*, 368−376.
(67) Williams, H. A.; Robinson, S.; Julyan, P.; Zweit, J.; Hastings, D. A comparison of PET imaging characteristics of various copper radioisotopes. *Eur. J. Nucl. Med. Mol. Imaging* **2005**, *32*, 1473−1480.
(68) Fujibayashi, Y.; Matsumoto, K.; Yonekura, Y.; Konishi, J.; Yokoyama, A. A new zinc-62/copper-62 generator as a copper-62 source for PET radiopharmaceuticals. *J. Nucl. Med.* **1989**, *30*, 1838−1842.
(69) Smith, S. V. Molecular imaging with copper-64. *J. Inorg. Biochem.* **2004**, *98*, 1874−1901.
(70) McCarthy, D. W.; Bass, L. A.; Cutler, P. D.; Shefer, R. E.; Klinkowstein, R. E.; Herrero, P.; Lewis, J. S.; Cutler, C. S.; Anderson, C. J.; Welch, M. J. High purity production and potential applications of copper-60 and copper-61. *Nucl. Med. Biol.* **1999**, *26*, 351−358.
(71) Okazawa, H.; Yonekura, Y.; Fujibayashi, Y.; Nishizawa, S.; Magata, Y.; Ishizu, K.; Tanaka, F.; Tsuchida, T.; Tamaki, N.; Konishi, J. Clinical application and quantitative evaluation of generator-produced copper-62-PTSM as a brain perfusion tracer for PET. *J. Nucl. Med.* **1994**, *35*, 1910−1915.
(72) Green, M. A.; Mathias, C. J.; Willis, L. R.; Handa, R. K.; Lacy, J. L.; Miller, M. A.; Hutchins, G. D. Assessment of Cu-ETS as a PET radiopharmaceutical for evaluation of regional renal perfusion. *Nucl. Med. Biol.* **2007**, *34*, 247−255.
(73) McCarthy, D. W.; Shefer, R. E.; Klinkowstein, R. E.; Bass, L. A.; Margeneau, W. H.; Cutler, C. S.; Anderson, C. J.; Welch, M. J. Efficient production of high specific activity ^{64}Cu using a biomedical cyclotron. *Nucl. Med. Biol.* **1997**, *24*, 35−43.
(74) Alves, F.; Alves, V.; Do Carmo, S.; Neves, A.; Silva, M.; Abrunhosa, A. Production of copper-64 and gallium-68 with a medical cyclotron using liquid targets. *Mod. Phys. Lett. A* **2017**, *32*, 1740013.
(75) Novak-Hofer, I.; Schubiger, A. P. Copper-67 as a therapeutic nuclide for radioimmunotherapy. *Eur. J. Nucl. Med. Mol. Imaging* **2002**, *29*, 821−830.
(76) Marceau, N.; Kruck, T.; McConnell, D.; Aspin, N. The production of copper-67 from natural zinc using a linear accelerator. *Int. J. Appl. Radiat. Isot.* **1970**, *21*, 667−669.
(77) Smith, N. A.; Bowers, D. L.; Ehst, D. A. The production, separation, and use of ^{67}Cu for radioimmunotherapy: A review. *Appl. Radiat. Isot.* **2012**, *70*, 2377−2383.
(78) Schwarzbach, R.; Zimmermann, K.; Bläuenstein, P.; Smith, A.; Schubiger, P. A. Development of a simple and selective separation of ^{67}Cu from irradiated zinc for use in antibody labelling: A comparison of methods. *Appl. Radiat. Isot.* **1995**, *46*, 329−336.
(79) Solomon, E. I.; Heppner, D. E.; Johnston, E. M.; Ginsbach, J. W.; Cirera, J.; Qayyum, M.; Kieber-Emmons, M. T.; Kjaergaard, C. H.; Hadt, R. G.; Tian, L. Copper active sites in biology. *Chem. Rev.* **2014**, *114*, 3659−3853.
(80) Holm, R. H.; Kennepohl, P.; Solomon, E. I. Structural and functional aspects of metal sites in biology. *Chem. Rev.* **1996**, *96*, 2239−2314.
(81) Nomura, M.; Yamaguchi, T. Concentration dependence of EXAFS and XANES of copper(II) perchlorate aqueous solution: comparison of solute structure in liquid and glassy states. *J. Phys. Chem.* **1988**, *92*, 6157−6160.
(82) Martell, A.; Chaberek, S., Jr.; Courtney, R.; Westerback, S.; Hyytiainen, H. Hydrolytic tendencies of metal chelate compounds. I. Cu(II) chelates. *J. Am. Chem. Soc.* **1957**, *79*, 3036−3041.
(83) Zeng, L.; Miller, E. W.; Pralle, A.; Isacoff, E. Y.; Chang, C. J. A selective turn-on fluorescent sensor for imaging copper in living cells. *J. Am. Chem. Soc.* **2006**, *128*, 10−11.
(84) Rodriguez-Granillo, A.; Wittung-Stafshede, P. Structure and dynamics of Cu(I) binding in copper chaperones Atox1 and CopZ: a computer simulation study. *J. Phys. Chem. B* **2008**, *112*, 4583−4593.
(85) Blower, P. J.; Lewis, J. S.; Zweit, J. Copper radionuclides and radiopharmaceuticals in nuclear medicine. *Nucl. Med. Biol.* **1996**, *23*, 957−980.
(86) Ballinger, J. R. Imaging hypoxia in tumors. *Semin. Nucl. Med.* **2001**, *31*, 321−329.
(87) Vāvere, A. L.; Lewis, J. S. Cu−ATSM: A radiopharmaceutical for the PET imaging of hypoxia. *Dalton Trans.* **2007**, 4893−4902.
(88) Tamura, K.; Kurihara, H.; Yonemori, K.; Tsuda, H.; Suzuki, J.; Kono, Y.; Honda, N.; Kodaira, M.; Yamamoto, H.; Yunokawa, M.; et al. ^{64}Cu-DOTA-trastuzumab PET imaging in patients with HER2-positive breast cancer. *J. Nucl. Med.* **2013**, *54*, 1869−1875.
(89) Zeng, D.; Guo, Y.; White, A. G.; Cai, Z.; Modi, J.; Ferdani, R.; Anderson, C. J. Comparison of conjugation strategies of cross-bridged macrocyclic chelators with cetuximab for copper-64 radiolabeling and PET Imaging of EGFR in colorectal tumor-bearing mice. *Mol. Pharmaceutics* **2014**, *11*, 3980−3987.
(90) Hancock, R. D.; Martell, A. E. Ligand design for selective complexation of metal ions in aqueous solution. *Chem. Rev.* **1989**, *89*, 1875−1914.
(91) Anderson, C. J.; Connett, J. M.; Schwarz, S. W.; Rocque, P. a.; Guo, L. W.; Philpott, G. W.; Zinn, K. R.; Meares, C. F.; Welch, M. J. Copper-64-labeled antibodies for PET imaging. *J. Nucl. Med.* **1992**, *33*, 1685−1691.
(92) Kukis, D. L.; Li, M.; Meares, C. F. Selectivity of antibody-chelate conjugates for binding copper in the presence of competing metals. *Inorg. Chem.* **1993**, *32*, 3981−3982.
(93) Mirick, G. R.; O'Donnell, R. T.; Denardo, S. J.; Shen, S.; Meares, C. F.; Denardo, G. L. Transfer of copper from a chelated ^{67}Cu-antibody conjugate to ceruloplasmin in lymphoma patients. *Nucl. Med. Biol.* **1999**, *26*, 841−845.
(94) Wong, E. H.; Weisman, G. R.; Hill, D. C.; Reed, D. P.; Rogers, M. E.; Condon, J. P.; Fagan, M. A.; Calabrese, J. C.; Lam, K.-C.; Guzei, I. A.; et al. Cross-bridged cyclams and pendant arm derivatives. *J. Am. Chem. Soc.* **2000**, *122*, 10561.
(95) Ferdani, R.; Stigers, D. J.; Fiamengo, A. L.; Wei, L.; Li, B. T. Y.; Golen, J. A.; Rheingold, A. L.; Weisman, G. R.; Wong, E. H.; Anderson, C. J. Synthesis, Cu(II) complexation, ^{64}Cu-labeling and biological evaluation of cross-bridged cyclam chelators with phosphonate pendant arms. *Dalton Trans.* **2012**, *41*, 1938−1950.
(96) Sun, X.; Wuest, M.; Weisman, G. R.; Wong, E. H.; Reed, D. P.; Boswell, C. A.; Motekaitis, R.; Martell, A. E.; Welch, M. J.; Anderson, C. J. Radiolabeling and In Vivo Behavior of Copper-64-Labeled Cross-Bridged Cyclam Ligands. *J. Med. Chem.* **2002**, *45*, 469−477.
(97) Juran, S.; Walther, M.; Stephan, H.; Bergmann, R.; Steinbach, J.; Kraus, W.; Emmerling, F.; Comba, P. Hexadentate bispidine derivatives as versatile bifunctional chelate agents for copper (II) radioisotopes. *Bioconjugate Chem.* **2009**, *20*, 347−359.
(98) Lima, L. M. P.; Esteban-Gómez, D.; Delgado, R.; Platas-Iglesias, C.; Tripier, R. Monopicolinate cyclen and cyclam derivatives for stable copper(II) complexation. *Inorg. Chem.* **2012**, *51*, 6916−6927.
(99) Boros, E.; Rybak-Akimova, E.; Holland, J. P.; Rietz, T.; Rotile, N.; Blasi, F.; Day, H.; Latifi, R.; Caravan, P. Pycup: A bifunctional, cage-like ligand for ^{64}Cu radiolabeling. *Mol. Pharmaceutics* **2014**, *11*, 617−629.
(100) Bernhardt, P. V.; Harrowfield, J. M.; Hockless, D. C. R.; Sargeson, A. M. N-Methylated macrobicyclic hexaamines of copper(II) and nickel(II): large steric effects. *Inorg. Chem.* **1994**, *33*, 5659−5670.
(101) Dearling, J. L.; Voss, S. D.; Dunning, P.; Snay, E.; Fahey, F.; Smith, S. V.; Huston, J. S.; Meares, C. F.; Treves, S. T.; Packard, A. B. Imaging cancer using PET—the effect of the bifunctional chelator on the biodistribution of a ^{64}Cu-labeled antibody. *Nucl. Med. Biol.* **2011**, *38*, 29−38.
(102) Maheshwari, V.; Dearling, J. L. J.; Treves, S. T.; Packard, A. B. Measurement of the rate of copper(II) exchange for ^{64}Cu complexes of bifunctional chelators. *Inorg. Chim. Acta* **2012**, *393*, 318−323.
(103) Ma, M. T.; Cooper, M. S.; Paul, R. L.; Shaw, K. P.; Karas, J. A.; Scanlon, D.; White, J. M.; Blower, P. J.; Donnelly, P. S. Macrobicyclic cage amine ligands for copper radiopharmaceuticals: A single bivalent cage amine containing two lys3-bombesin targeting peptides. *Inorg. Chem.* **2011**, *50*, 6701−6710.

DOI: 10.1021/acs.chemrev.8b00281
Chem. Rev. 2019, 119, 870−901

(104) De Silva, R. A.; Jain, S.; Lears, K. A.; Chong, H.-S.; Kang, C. S.; Sun, X.; Rogers, B. E. Copper-64 radiolabeling and biological evaluation of bifunctional chelators for radiopharmaceutical development. *Nucl. Med. Biol.* **2012**, *39*, 1099−1104.
(105) Wadas, T.; Wong, E.; Weisman, G.; Anderson, C. Copper chelation chemistry and its role in copper radiopharmaceuticals. *Curr. Pharm. Des.* **2007**, *13*, 3−16.
(106) Copper Cu-64-ATSM and PET/CT scan in predicting disease progression in patients with newly-diagnosed stage IB, stage II, stage III, or stage IVA cervical cancer who are undergoing radiation therapy and cisplatin treatment. ClinicalTrials.gov, NCI, April 12, 2011.
(107) Fujibayashi, Y.; Taniuchi, H.; Yonekura, Y.; Ohtani, H.; Konishi, J.; Yokoyama, A. Copper-62-ATSM: a new hypoxia imaging agent with high membrane permeability and low redox potential. *J. Nucl. Med.* **1997**, *38*, 1155−1160.
(108) Lewis, M. R.; Boswell, C. a.; Laforest, R.; Buettner, T. L.; Ye, D.; Connett, J. M.; Anderson, C. J. Conjugation of monoclonal antibodies with TETA using activated esters: biological comparison of ^{64}Cu-TETA-1A3 with ^{64}Cu-BAT-2IT-1A3. *Cancer Biother.Radiopharm.* **2001**, *16*, 483−494.
(109) DeNardo, S. J.; DeNardo, G. L.; Kukis, D. L.; Shen, S.; Kroger, L. A.; DeNardo, D. A.; Goldstein, D. S.; Mirick, G. R.; Salako, Q.; Mausner, L. F.; et al. ^{67}Cu-2IT-BAT-Lym-1 pharmacokinetics, radiation dosimetry, toxicity and tumor regression in patients with lymphoma. *J. Nucl. Med.* **1999**, *40*, 302−310.
(110) Prasanphanich, A. F.; Nanda, P. K.; Rold, T. L.; Ma, L.; Lewis, M. R.; Garrison, J. C.; Hoffman, T. J.; Sieckman, G. L.; Figueroa, S. D.; Smith, C. J. [^{64}Cu-NOTA-8-Aoc-BBN(7−14)NH2] targeting vector for positron-emission tomography imaging of gastrin-releasing peptide receptor-expressing tissues. *Proc. Natl. Acad. Sci. U. S. A.* **2007**, *104*, 12462−12467.
(111) Sarkar, S.; Bhatt, N.; Ha, Y. S.; Huynh, P. T.; Soni, N.; Lee, W.; Lee, Y. J.; Kim, J. Y.; Pandya, D. N.; An, G. I.; et al. High in vivo stability of ^{64}Cu-labeled cross-bridged chelators is a crucial factor in improved tumor imaging of RGD peptide conjugates. *J. Med. Chem.* **2018**, *61*, 385−395.
(112) Haynes, N. G.; Lacy, J. L.; Nayak, N.; Martin, C. S.; Dai, D.; Mathias, C. J.; Green, M. A. Performance of a ^{62}Zn/^{62}Cu generator in clinical trials of PET perfusion agent ^{62}Cu-PTSM. *J. Nucl. Med.* **2000**, *41*, 309−314.
(113) Lyster, D. M.; Noujaim, A. A. Unit dose preparation of zinc-63 EDTA for use in nuclear medicine. *Int. J. Nucl. Med. Biol.* **1974**, *1*, 220−223.
(114) Guerra Gómez, F. L.; Takada, Y.; Hosoi, R.; Momosaki, S.; Yanamoto, K.; Nagatsu, K.; Suzuki, H.; Zhang, M.-R.; Inoue, O.; Arano, Y.; et al. Production and purification of the positron emitter zinc-63. *J. Labelled Compd. Radiopharm.* **2012**, *55*, 5−9.
(115) DeGrado, T. R.; Pandey, M. K.; Byrne, J. F.; Engelbrecht, H. P.; Jiang, H.; Packard, A. B.; Thomas, K. A.; Jacobson, M. S.; Curran, G. L.; Lowe, V. J. Preparation and preliminary evaluation of ^{63}Zn-zinc citrate as a novel PET imaging biomarker for zinc. *J. Nucl. Med.* **2014**, *55*, 1348−1354.
(116) Fujibayashi, Y.; Saji, H.; Yomoda, I.; Kawai, K.; Horiuchi, K.; Adachi, H.; Torizuka, K.; Yokoyama, A. ^{62}Zn-EDDA: A radiopharmaceutical for pancreatic functional diagnosis. *Int. J. Nucl. Med. Biol.* **1986**, *12*, 439−446.
(117) Blindauer, C. A.; Harvey, I.; Bunyan, K. E.; Stewart, A. J.; Sleep, D.; Harrison, D. J.; Berezenko, S.; Sadler, P. J. Structure, properties, and engineering of the major zinc binding site on human albumin. *J. Biol. Chem.* **2009**, *284*, 23116−23124.
(118) DeGrado, T. R.; Kemp, B. J.; Pandey, M. K.; Jiang, H.; Gunderson, T. M.; Linscheid, L. R.; Woodwick, A. R.; McConnell, D. M.; Fletcher, J. G.; JOhnson, G. B.; et al. First PET imaging studies with ^{63}Zn-zinc citrate in healthy human participants and patients with Alzheimer disease. *Mol. Imaging* **2016**, *15*, 153601211667379.
(119) Craddock, T. J. A.; Tuszynski, J. A.; Chopra, D.; Casey, N.; Goldstein, L. E.; Hameroff, S. R.; Tanzi, R. E. The zinc dyshomeostasis hypothesis of Alzheimer's disease. *PLoS One* **2012**, *7*, No. e33552.
(120) Holland, J. P.; Williamson, M. J.; Lewis, J. S. Unconventional Nuclides for Radiopharmaceuticals. *Mol. Imaging* **2010**, *9*, 7290.2010.00008.
(121) Dabkowski, A.; Paisey, S.; Talboys, M.; Marshall, C. Optimization of cyclotron production for Radiometal of zirconium-89. *Acta Phys. Pol., A* **2015**, *127*, 1479−1482.
(122) Link, J. M.; Krohn, K. A.; O'Hara, M. J. A simple thick target for production of ^{89}Zr using an 11 MeV cyclotron. *Appl. Radiat. Isot.* **2017**, *122*, 211−214.
(123) Dias, G. M.; Ramogida, C. F.; Rousseau, J.; Zacchia, N. A.; Hoehr, C.; Schaffer, P.; Lin, K.-S.; Bénard, F. ^{89}Zr for antibody labeling and in vivo studies−a comparison between liquid and solid target production. *Nucl. Med. Biol.* **2018**, *58*, 1−7.
(124) Meijs, W. E.; Herscheid, J. D.; Haisma, H. J.; Pinedo, H. M. Evaluation of desferal as a bifunctional chelating agent for labeling antibodies with Zr-89. *J. Labelled Comp. Radiopharm.* **1992**, *43*, 1443−1447.
(125) Patra, M.; Bauman, A.; Mari, C.; Fischer, C. A.; Blacque, O.; Häussinger, D.; Gasser, G.; Mindt, T. L. An octadentate bifunctional chelating agent for the development of stable zirconium-89 based molecular imaging probes. *Chem. Commun.* **2014**, *50*, 11523−11525.
(126) Vugts, D. J.; Klaver, C.; Sewing, C.; Poot, A. J.; Adamzek, K.; Huegli, S.; Mari, C.; Visser, G. W. M.; Valverde, I. E.; Gasser, G.; et al. Comparison of the octadentate bifunctional chelator DFO*-pPhe-NCS and the clinically used hexadentate bifunctional chelator DFO-pPhe-NCS for ^{89}Zr-immuno-PET. *Eur. J. Nucl. Med. Mol. Imaging* **2017**, *44*, 286−295.
(127) Allott, L.; Da Pieve, C.; Meyers, J.; Spinks, T.; Ciobota, D.; Kramer-Marek, G.; Smith, G. Evaluation of DFO-HOPO as an octadentate chelator for zirconium-89. *Chem. Commun.* **2017**, *53*, 8529−8532.
(128) Rudd, S. E.; Roselt, P.; Cullinane, C.; Hicks, R. J.; Donnelly, P. S. A desferrioxamine B squaramide ester for the incorporation of zirconium-89 into antibodies. *Chem. Commun.* **2016**, *52*, 11889−11892.
(129) Zhai, C.; Summer, D.; Rangger, C.; Franssen, G. M.; Laverman, P.; Haas, H.; Petrik, M.; Haubner, R.; Decristoforo, C. A novel bifunctional cyclic chelator for ^{89}Zr labeling−radiolabeling and targeting properties of RGD conjugates. *Mol. Pharmaceutics* **2015**, *12*, 2142−2150.
(130) Petrik, M.; Zhai, C.; Novy, Z.; Urbanek, L.; Haas, H.; Decristoforo, C. In vitro and in vivo comparison of selected Ga-68 and Zr-89 labelled siderophores. *Mol. Imaging Biol.* **2016**, *18*, 344−352.
(131) Adams, C. J.; Wilson, J. J.; Boros, E. Multifunctional desferrichrome analogues as versatile ^{89}Zr(IV) chelators for immuno-PET probe development. *Mol. Pharmaceutics* **2017**, *14*, 2831−2842.
(132) Datta, A.; Raymond, K. N. Gd−Hydroxypyridinone (HOPO)-Based High-Relaxivity Magnetic Resonance Imaging (MRI) Contrast Agents. *Acc. Chem. Res.* **2009**, *42*, 938−947.
(133) Guerard, F.; Beyler, M.; Lee, Y. S.; Tripier, R.; Gestin, J. F.; Brechbiel, M. W. Investigation of the complexation of ^{nat}Zr(IV) and ^{89}Zr(IV) by hydroxypyridinones for the development of chelators for PET imaging applications. *Dalton Trans.* **2017**, *46*, 4749−4758.
(134) Deri, M. A.; Ponnala, S.; Zeglis, B. M.; Pohl, G.; Dannenberg, J. J.; Lewis, J. S.; Francesconi, L. C. Alternative chelator for ^{89}Zr radiopharmaceuticals: Radiolabeling and evaluation of 3,4,3-(LI-1,2-HOPO). *J. Med. Chem.* **2014**, *57*, 4849−4860.
(135) Deri, M.; Ponnala, S.; Kozlowski, P.; Burton-Pye, B. P.; Cicek, H.; Hu, C.; Lewis, J. S.; Francesconi, L. C. p-SCN-Bn-HOPO: A superior bifunctional chelator for ^{89}Zr immunoPET. *Bioconjugate Chem.* **2015**, *26*, 2579−2259.
(136) Ma, M. T.; Meszaros, L. K.; Paterson, B. M.; Berry, D. J.; Cooper, M. S.; Ma, Y.; Hider, R. C.; Blower, P. J. Tripodal tris(hydroxypyridinone) ligands for immunoconjugate PET imaging with ^{89}Zr^{4+}: comparison with desferrioxamine-B. *Dalton Trans.* **2015**, *44*, 4884−4900.
(137) Buchwalder, C.; Rodríguez-Rodríguez, C.; Schaffer, P.; Karagiozov, S. K.; Saatchi, K.; Häfeli, U. O. A new tetrapodal 3-hydroxy-4-pyridinone ligand for complexation of ^{89}zirconium for

DOI: 10.1021/acs.chemrev.8b00281
Chem. Rev. 2019, 119, 870−901

positron emission tomography (PET) imaging. *Dalton Trans.* **2017**, *46*, 9654−9663.
(138) Tinianow, J. N.; Pandya, D. N.; Pailloux, S. L.; Ogasawara, A.; Vanderbilt, A. N.; Gill, H. S.; Williams, S. P.; Wadas, T. J.; Magda, D.; Marik, J. Evaluation of a 3-hydroxypyridin-2-one (2,3-HOPO) based macrocyclic chelator for $^{89}Zr^{4+}$ and its use for immunoPET imaging of HER2 positive model of ovarian carcinoma in mice. *Theranostics* **2016**, *6*, 511−521.
(139) Boros, E.; Holland, J. P. Chemical aspects of metal ion chelation in the synthesis and application antibody-based radiotracers. *J. Labelled Compd. Radiopharm.* **2018**, *61*, 652−671.
(140) Marquez, B. V.; Ikotun, O. F.; Zheleznyak, A.; Wright, B.; Hari-Raj, A.; Pierce, R. A.; Lapi, S. E. Evaluation of ^{89}Zr-pertuzumab in breast cancer xenografts. *Mol. Pharmaceutics* **2014**, *11*, 3988−3995.
(141) Pandit-Taskar, N.; O'Donoghue, J. A.; Durack, J. C.; Lyashchenko, S. K.; Cheal, S. M.; Beylergil, V.; Lefkowitz, R. A.; Carrasquillo, J. A.; Martinez, D. F.; Fung, A. M.; et al. A phase I/II study for analytic validation of ^{89}Zr-J591 immunoPET as a molecular imaging agent for metastatic prostate cancer. *Clin. Cancer Res.* **2015**, *21*, 5277−5285.
(142) Sihver, W.; Pietzsch, J.; Krause, M.; Baumann, M.; Steinbach, J.; Pietzsch, H.-J. Radiolabeled cetuximab conjugates for EGFR targeted cancer diagnostics and therapy. *Pharmaceuticals* **2014**, *7*, 311−338.
(143) McKnight, B. N.; Viola-Villegas, N. T. ^{89}Zr-ImmunoPET companion diagnostics and their impact in clinical drug development. *J. Labelled Compd. Radiopharm.* **2018**, *61*, 727−738.
(144) Gebhart, G.; Lamberts, L.; Wimana, Z.; Garcia, C.; Emonts, P.; Ameye, L.; Stroobants, S.; Huizing, M.; Aftimos, P.; Tol, J.; et al. Molecular imaging as a tool to investigate heterogeneity of advanced HER2-positive breast cancer and to predict patient outcome under trastuzumab emtansine (T-DM1): the ZEPHIR trial. *Ann. Oncol.* **2016**, *27*, 619−624.
(145) Freise, A. C.; Zettlitz, K. A.; Salazar, F. B.; Lu, X.; Tavaré, R.; Wu, A. M. ImmunoPET imaging of murine CD4+ T cells using anti-CD4 Cys-diabody: Effects of protein dose on T cell function and imaging. *Mol. Imaging Biol.* **2017**, *19*, 599−609.
(146) Edmonds, S.; Volpe, A.; Shmeeda, H.; Parente-Pereira, A. C.; Radia, R.; Baguña-Torres, J.; Szanda, I.; Severin, G. W.; Livieratos, L.; Blower, P. J.; et al. Exploiting the metal-chelating properties of the drug cargo for in vivo positron emission tomography imaging of liposomal nanomedicines. *ACS Nano* **2016**, *10*, 10294−10307.
(147) Boros, E.; Bowen, A. M.; Josephson, L.; Vasdev, N.; Holland, J. P. Chelate-free metal ion binding and heat-induced radiolabeling of iron oxide nanoparticles. *Chem. Sci.* **2015**, *6*, 225−236.
(148) Goel, S.; Chen, F.; Luan, S.; Valdovinos, H. F.; Shi, S.; Graves, S. A.; Ai, F.; Barnhart, T. E.; Theuer, C. P.; Cai, W. Engineering intrinsically zirconium-89 radiolabeled self-destructing mesoporous silica nanostructures for in vivo biodistribution and tumor targeting studies. *Adv. Sci.* **2016**, *3*, 1600122.
(149) Kim, J. S. Combination radioimmunotherapy approaches and quantification of immuno-PET. *Nucl. Med. Mol. Imaging* **2016**, *50*, 104−111.
(150) Radchenko, V.; Filosofov, D.; Bochko, O.; Lebedev, N.; Rakhimov, A.; Hauser, H.; Eisenhut, M.; Aksenov, N.; Bozhikov, G.; Ponsard, B.; et al. Separation of ^{90}Nb from zirconium target for application in immuno-PET. *Radiochim. Acta* **2014**, *102*, 433−442.
(151) Parks, T. B.; Cruz, Y. M.; Tinoco, A. D. Applying the Fe(III) binding property of a chemical transferrin mimetic to Ti(IV) anticancer drug design. *Inorg. Chem.* **2014**, *53*, 1743−1749.
(152) Harding, M. M.; Prodigalidad, M.; Lynch, M. J. Organometallic anticancer agents. 2. Aqueous chemistry and interaction of niobocene dichloride with nucleic acid constituents and amino acids. *J. Med. Chem.* **1996**, *39*, 5012−5016.
(153) Radchenko, V.; Busse, S.; Roesch, F. Desferrioxamine as an appropriate chelator for ^{90}Nb: Comparison of its complexation properties for M-Df-Octreotide (M= Nb, Fe, Ga, Zr). *Nucl. Med. Biol.* **2014**, *41*, 721−727.
(154) Radchenko, V.; Bouziotis, P.; Tsotakos, T.; Paravatou-Petsotas, M.; de la Fuente, A.; Loudos, G.; Harris, A. L.; Xanthopoulos, S.; Filosofov, D.; Hauser, H.; et al. Labeling and preliminary in vivo assessment of niobium-labeled radioactive species: A proof-of-concept study. *Nucl. Med. Biol.* **2016**, *43*, 280−287.
(155) Cohen, I.; Robles, A.; Mendoza, P.; Airas, R.; Montoya, E. Experimental evidences of ^{95m}Tc production in a nuclear reactor. *Appl. Radiat. Isot.* **2018**, *135*, 207−211.
(156) Boyd, R. E. Molybdenum-99: technetium-99m generator. *Radiochim. Acta* **1982**, *30*, 123−145.
(157) Bigott, H. M.; Laforest, R.; Liu, X.; Ruangma, A.; Wuest, F.; Welch, M. J. Advances in the production, processing and microPET image quality of technetium-94m. *Nucl. Med. Biol.* **2006**, *33*, 923−933.
(158) Ali, S. A.; Ache, H. J. Production techniques of fission molybdenum-99. *Radiochim. Acta* **1987**, *41*, 65−72.
(159) Chattopadhyay, S.; Das, S. S.; Das, M. K.; Goomer, N. C. Recovery of ^{99m}Tc from $Na_2[^{99}Mo]MoO_4$ solution obtained from reactor-produced (n, γ) ^{99}Mo using a tiny Dowex-1 column in tandem with a small alumina column. *Appl. Radiat. Isot.* **2008**, *66*, 1814−1817.
(160) Selivanova, S. V.; Lavallee, E.; Senta, H.; Caouette, L.; Sader, J. A.; van Lier, E. J.; Zyuzin, A.; van Lier, J. E.; Guerin, B.; Turcotte, E.; Lecomte, R. Radioisotopic Purity of Sodium Pertechnetate ^{99m}Tc Produced with a Medium-Energy Cyclotron: Implications for Internal Radiation Dose, Image Quality, and Release Specifications. *J. Nucl. Med.* **2015**, *56*, 1600.
(161) Andersson, J. D.; Thomas, B.; Selivanova, S. V.; Berthelette, E.; Wilson, J. S.; McEwan, A. J. B.; Gagnon, K. Robust high-yield ∼1TBq production of cyclotron based sodium [^{99m}Tc]pertechnetate. *Nucl. M3ed. Biol.* **2018**, *60*, 63.
(162) Bénard, F.; Buckley, K. R.; Ruth, T. J.; Zeisler, S. K.; Klug, J.; Hanemaayer, V.; Vuckovic, M.; Hou, X.; Celler, A.; Appiah, J.-P.; et al. Implementation of multi-curie production of ^{99m}Tc by conventional medical cyclotrons. *J. Nucl. Med.* **2014**, *55*, 1017−1022.
(163) Eckelman, W. C.; Richards, P. Instant ^{99m}Tc compounds. *Nuklearmedizin* **1971**, *10*, 245−251.
(164) Alberto, R. From oxo to carbonyl and arene complexes; A journey through technetium chemistry. *J. Organomet. Chem.* **2018**, *869*, 264−269.
(165) Johannsen, B.; Scheunemann, M.; Spies, H.; Brust, P.; Wober, J.; Syhre, R.; Pietzsch, H. J. Technetium(V) and rhenium(V) complexes for 5-HT2A serotonin receptor binding: Structure-affinity considerations. *Nucl. Med. Biol.* **1996**, *23*, 429−438.
(166) Tisato, F.; Refosco, F.; Mazzi, U.; Bandoli, G.; Nicolini, M. Technetium(V) and rhenium(V) complexes with N-(2-mercaptophenyl)-salicylideneiminate - crystal-structure of chloro(oxo)[*N*-(2-sulphidophenyl)-salicylideneiminato-nos]technetium(V). *J. Chem. Soc., Dalton Trans.* **1987**, 1693−1699.
(167) Lipowska, M.; Hansen, L.; Cini, R.; Xu, X. L.; Choi, H.; Taylor, A. T.; Marzilli, L. G. Synthesis of new N_2S_2 ligands and Re(V)O(N_2S_2) analogues of Tc-99m renal imaging agents. Characterization by NMR spectroscopy, molecular mechanics calculations, and X-ray crystallography. *Inorg. Chim. Acta* **2002**, *339*, 327−340.
(168) Wong, E.; Fauconnier, T.; Bennett, S.; Valliant, J.; Nguyen, T.; Lau, F.; Lu, L. F. L.; Pollak, A.; Bell, R. A.; Thornback, J. R. Rhenium(V) and technetium(V) oxo complexes of an $N_2N'S$ peptidic chelator: Evidence of interconversion between the syn and anti conformations. *Inorg. Chem.* **1997**, *36*, 5799−5808.
(169) Baldas, J. The chemistry of technetium nitrido complexes. *Top. Curr. Chem.* **1996**, *176*, 37−76.
(170) von Guggenberg, E.; Behe, M.; Behr, T. M.; Saurer, M.; Seppi, T.; Decristoforo, C. Tc-99m-labeling and in vitro and in vivo evaluation of HYNIC- and (*N*-alpha-His)acetic acid-modified [D-Glu(1)]-minigastrin. *Bioconjugate Chem.* **2004**, *15*, 864−871.
(171) Abrams, M. J.; Davison, A.; Jones, A. G.; Costello, C. E.; Pang, H. Synthesis and characterization of hexakis(alkyl isocyanide) and hexakis(aryl isocyanide) complexes of technetium(I). *Inorg. Chem.* **1983**, *22*, 2798−2800.
(172) Holman, B. L.; Jones, A. G.; Lister-James, J.; Davison, A.; Abrams, M. J.; Kirshenbaum, J. M.; Tumeh, S. S.; English, R. J. A new Tc-99m-labeled myocardial imaging agent, hexakis(t- butylisonitrile)-

DOI: 10.1021/acs.chemrev.8b00281
Chem. Rev. 2019, 119, 870−901

technetium(I) [Tc-99m TBI]: initial experience in the human. *J. Nucl. Med.* **1984**, *25*, 1350−1355.
(173) Jones, A. G.; Abrams, M. J.; Davison, A.; Brodack, J. W.; Toothaker, A. K.; Adelstein, S. J.; Kassis, A. I. Biological studies of a new class of technetium complexes: the hexakis(alkylisonitrile)technetium-(I) cations. *Int. J. Nucl. Med. Biol.* **1984**, *11*, 225−234.
(174) Alberto, R.; Schibli, R.; Egli, A.; Schubiger, P. A.; Herrmann, W. A.; Artus, G.; Abram, U.; Kaden, T. A. Metal carbonyl syntheses XXII. Low pressure carbonylation of $[MOCl_4]^-$ and $[MO_4]^-$: the technetium(I) and rhenium(I) complexes $[NEt_4]_2[MCl_3(CO)_3]$. *J. Organomet. Chem.* **1995**, *493*, 119−127.
(175) Alberto, R.; Schibli, R.; Abram, U.; Huebener, R.; Berke, H.; Kaden, T. A.; Schubiger, P. A. A simple single step synthesis of $(^{99}TcH_3(CO)_{12})$ from $(^{99}TcO_4)^-$ and the X-ray crystal structure. Application to the production of no carrier added $(^{188}Re_3H3(CO)_{12})$. *Chem. Commun.* **1996**, 1291−1292.
(176) Sogbein, O. O.; Merdy, P.; Morel, P.; Valliant, J. F. Preparation of Re(I)- and Tc-99m(I)-metallocarboranes in water under weakly basic reaction conditions. *Inorg. Chem.* **2004**, *43*, 3032−3034.
(177) Knight Castro, H. H.; Meetsma, A.; Teuben, J. H.; Vaalburg, W.; Panek, K.; Ensing, G. Synthesis, reactions and structure of $Cp'Tc(CO)_3$ derivatives. *J. Organomet. Chem.* **1991**, *410*, 63−71.
(178) Braband, H.; Abram, U. Technetium complexes with triazacyclononane. *Inorg. Chem.* **2006**, *45*, 6589−6591.
(179) Braband, H.; Tooyama, Y.; Fox, T.; Alberto, R. Syntheses of high-valent *fac*-$[^{99m}TcO_3]^+$ complexes and [3 + 2] cycloadditions with alkenes in water as a direct labelling strategy. *Chem. - Eur. J.* **2009**, *15*, 633−638.
(180) Braband, H.; Imstepf, S.; Benz, M.; Spingler, B.; Alberto, R. Combining bifunctional chelator with (3 + 2)-cycloaddition approaches: Synthesis of dual-function technetium complexes. *Inorg. Chem.* **2012**, *51*, 4051−4057.
(181) Hahn, E. M.; Casini, A.; Kühn, F. E. Re(VII) and Tc(VII) trioxo complexes stabilized by tridentate ligands and their potential use as radiopharmaceuticals. *Coord. Chem. Rev.* **2014**, *276*, 97−111.
(182) Gottschalk, A. Technetium-99m in clinical nuclear medicine. *Annu. Rev. Med.* **1969**, *20*, 131−139.
(183) Atkins, H. L.; Richards, P. Assessment of thyroid function and anatomy with technetium-99m as pertechnetate. *J. Nucl. Med.* **1968**, *9*, 7−15.
(184) Eckelman, W. C.; Meinken, G.; Richards, P. The chemical state of Tc-99m in biomedical products. II. The chelation of reduced technetium with DTPA. *J. Nucl. Med.* **1972**, *13*, 577−581.
(185) Deutsch, E.; Libson, K.; Vanderheyden, J. L.; Ketring, A. R.; Maxon, H. R. The chemistry of rhenium and technetium as related to the use of isotopes of these elements in therapeutic and diagnostic nuclear medicine. International Journal of Radiation Applications & Instrumentation - Part B. *Nucl. Med. Biol.* **1986**, *13*, 456−477.
(186) Jones, A. G.; Orvig, C.; Trop, H. S.; Davison, A.; Davis, M. A. A Survey of Reducing Agents for the Synthesis of Tetraphenylarsonium Oxotechnetiumbis(ethanedithiolate) from [^{99}Tc] Pertechnetate in Aqueous Solution. *J. Nucl. Med.* **1980**, *21*, 279−281.
(187) Jones, A. G.; Davison, A. The Relevance of Basic Technetium Chemistry to Nuclear Medicine. *J. Nucl. Med.* **1982**, *23*, 1041−1043.
(188) Schwochau, K. *Technetium: chemistry and radiopharmaceutical applications*; Wiley-VCH: New York, 2007.
(189) Tokita, N.; Hasegawa, S.; Maruyama, K.; Izumi, T.; Blankenberg, F. G.; Tait, J. F.; Strauss, H. W.; Nishimura, T. Tc-99m-HYNIC-annexin V imaging to evaluate inflammation and apoptosis in rats with autoimmune myocarditis. *Eur. J. Nucl. Med. Mol. Imaging* **2003**, *30*, 232−238.
(190) Bartholomä, M.; Louie, A.; Valliant, J.; Zubieta, J. Technetium and gallium derived radiopharmaceuticals: Comparing and contrasting the chemistry of two important radiometals for the molecular imaging era. *Chem. Rev.* **2010**, *110*, 2903−2920.
(191) Jürgens, S.; Herrmann, W. A.; Kühn, F. E. Rhenium and technetium based radiopharmaceuticals: Development and recent advances. *J. Organomet. Chem.* **2014**, *751*, 83−89.
(192) Chatalic, K. L.; Heskamp, S.; Konijnenberg, M.; Molkenboer-Kuenen, J. D.; Franssen, G. M.; van Groningen, M. C. C.; Schottelius, M.; Wester, H.-J.; van Weerden, W. M.; Boerman, O. C.; et al. Towards personalized treatment of prostate cancer: PSMA I&T, a promising prostate-specific membrane antigen-targeted theranostic agent. *Theranostics* **2016**, *6*, 849−861.
(193) Kianfar, E.; Schäfer, C.; Lornejad-Schäfer, M. R.; Portenkirchner, E.; Knör, G. New photo-CORMs: Deeply-coloured biocompatible rhenium complexes for the controlled release of carbon monoxide. *Inorg. Chim. Acta* **2015**, *435*, 174−177.
(194) Yazdani, A.; Janzen, N.; Czorny, S.; Valliant, J. F. Technetium-(I) complexes of bathophenanthrolinedisulfonic acid. *Inorg. Chem.* **2017**, *56*, 2958−2965.
(195) Knopf, K. M.; Murphy, B. L.; MacMillan, S. N.; Baskin, J. M.; Barr, M. P.; Boros, E.; Wilson, J. J. In vitro anticancer activity and in vivo biodistribution of rhenium(I) tricarbonyl aqua complexes. *J. Am. Chem. Soc.* **2017**, *139*, 14302−14314.
(196) Imstepf, S.; Pierroz, V.; Rubbiani, R.; Felber, M.; Fox, T.; Gasser, G.; Alberto, R. Organometallic rhenium complexes divert doxorubicin to the mitochondria. *Angew. Chem., Int. Ed.* **2016**, *55*, 2792−2795.
(197) Imstepf, S.; Pierroz, V.; Raposinho, P.; Felber, M.; Fox, T.; Fernandes, C.; Gasser, G.; Santos, I.; Alberto, R. Towards ^{99m}Tc-based imaging agents with effective doxorubicin mimetics: a molecular and cellular study. *Dalton Trans.* **2016**, *45*, 13025−13033.
(198) Hayne, D. J.; Lim, S.; Donnelly, P. S. Metal complexes designed to bind to amyloid-β for the diagnosis and treatment of Alzheimer's disease. *Chem. Soc. Rev.* **2014**, *43*, 6701−6715.
(199) Kiritsis, C.; Mavroidi, B.; Shegani, A.; Palamaris, L.; Loudos, G.; Sagnou, M.; Pirmettis, I.; Papadopoulos, M.; Pelecanou, M. 2-(4′-Aminophenyl) benzothiazole Labeled with ^{99m}Tc-Cyclopentadienyl for Imaging β-Amyloid Plaques. *ACS Med. Chem. Lett.* **2017**, *8*, 1089−1092.
(200) Mizuno, Y.; Uehara, T.; Hanaoka, H.; Endo, Y.; Jen, C.-W.; Arano, Y. Purification-free method for preparing technetium-99m-labeled multivalent probes for enhanced in vivo imaging of saturable systems. *J. Med. Chem.* **2016**, *59*, 3331−3339.
(201) Taira, Y.; Uehara, T.; Tsuchiya, M.; Takemori, H.; Mizuno, Y.; Takahashi, S.; Suzuki, H.; Hanaoka, H.; Akizawa, H.; Arano, Y. Coordination-mediated synthesis of purification-free bivalent ^{99m}Tc-labeled probes for in vivo imaging of saturable systems. *Bioconjugate Chem.* **2018**, *29*, 459−466.
(202) Jia, W.; Ma, D.; Volkert, E. W.; Ketring, A. R.; Ehrhardt, G. J.; Jurisson, S. S. Production of no-carrier-added ^{105}Rh from neutron irradiated ruthenium target. *Platinum Met. Rev.* **2000**, *44*, 50−55.
(203) Grazman, B.; Troutner, D. E. ^{105}Rh as a potential radiotherapeutic agent. *Int. J. Rad. Appl. Instrum. A* **1988**, *39*, 257−260.
(204) Venkatesh, M.; Goswami, N.; Volkert, W. A.; Schlemper, E. O.; Ketring, A. R.; Barnes, C. L.; Jurisson, S. A. Rh-105 complex of tetrathiacyclohexadecane diol with potential for formulating bifunctional chelates. *Nucl. Med. Biol.* **1996**, *23*, 33−40.
(205) Khandaker, M.; Kim, K.; Kim, G. Production parameters of the therapeutic Rh radionuclide using medium energy cyclotron. *Pramana* **2012**, *79*, 243−248.
(206) John, C. S.; Pillai, M. R. A.; Lo, J. M.; Troutner, D. E. Labeling of proteins with ^{105}Rh. *Int. J. Rad. Appl. Instrum. A* **1989**, *40*, 701−705.
(207) Pillai, M. R. A.; Lo, J. M.; John, C. S.; Troutner, D. E. Labeling of proteins using [^{105}Rh]Rh-4-(p-aminobenzyl)-diethylenetriamine. *Int. J. Rad. Appl. Instrum. B* **1990**, *17*, 419−426.
(208) Pillai, M. R. A.; John, C. S.; Troutner, D. E. Labeling of human IgG with rhodium-105 using a new pentadentate bifunctional ligand. *Bioconjugate Chem.* **1990**, *1*, 191−197.
(209) Pillai, M. R. A.; Lo, J. M.; Troutner, D. E. Labeling of hematoporphyrin with ^{105}Rh and binding studies with human gamma globulin. *Int. J. Rad. Appl. Instrum. A* **1990**, *41*, 69−73.
(210) Lo, J. M.; Pillai, M. R. A.; John, C. S.; Troutner, D. E. Labeling of human serum albumin with ^{105}Rh-cysteine complexes. *Int. J. Rad. Appl. Instrum. A* **1990**, *41*, 63−67.

DOI: 10.1021/acs.chemrev.8b00281
Chem. Rev. 2019, 119, 870−901

(211) Li, N.; Barnes, C.; Eberlein, C. M.; Ochrymowycz, L.; Volkert, W. A.; Ketring, A. R. Comparisons of ^{105}Rh(III) Chloride Complexation with [14]aneNS$_3$, [14]aneN$_2$S$_2$ and [14]aneN$_4$ Macrocycles in Aqueous Solution. *Radiochim. Acta* **1996**, *75*, 83−95.
(212) Goswami, N.; Alberto, R.; Barnes, C. L.; Jurisson, S. Rhodium(III) complexes with acyclic tetrathioether ligands. Effects of backbone chain length on the conformation of the Rh(III) complex. *Inorg. Chem.* **1996**, *35*, 7546−7555.
(213) Goswami, N.; Higginbotham, C.; Volkert, W.; Alberto, R.; Nef, W.; Jurisson, S. Rhodium-105 tetrathioether complexes: Radiochemistry and initial biological evaluation. *Nucl. Med. Biol.* **1999**, *26*, 951−957.
(214) Akgun, Z.; Engelbrecht, H.; Fan, K.-H.; Barnes, C. L.; Cutler, C. S.; Jurisson, S. S.; Lever, S. Z. The complexation of rhodium(III) with acyclic diaminedithioether (DADTE) ligands. *Dalton Trans.* **2010**, *39*, 10169−10178.
(215) Cagnolini, A.; Ballard, B.; Engelbrecht, H. P.; Rold, T. L.; Barnes, C.; Cutler, C.; Hoffman, T. J.; Kannan, R.; Katti, K.; Jurisson, S. S. Tetradentate bis-phosphine ligands (P_2N_2 and P_2S_2) and their Rh(III), Ni(II) and ^{105}Rh Complexes: X-ray crystal structures of trans-[RhCl$_2$(L2)]PF$_6$, [Ni(L2)](PF$_6$)$_2$ and μ-O$_2$SO$_2$-[Ni(L5)]$_2$(PF$_6$)$_2$. *Nucl. Med. Biol.* **2011**, *38*, 63−76.
(216) Jurisson, S. S.; Ketring, A. R.; Volkert, W. A. Rhodium-105 complexes as potential radiotherapeutic agents. *Transition Met. Chem.* **1997**, *22*, 315−317.
(217) Li, N.; Struttman, M.; Higginbotham, C.; Grall, A. J.; Skerlj, J. F.; Vollano, J. F.; Bridger, S. A.; Ochrymowycz, L. A.; Ketring, A. R.; Abrams, M. J.; et al. Biodistribution of model ^{105}Rh-labeled tetradentate thiamacrocycles in rats. *Nucl. Med. Biol.* **1997**, *24*, 85−92.
(218) Brooks, R. C.; Carnochan, P.; Vollano, J. F.; Powell, N. A.; Zweit, J.; Sosabowski, J. K.; Martellucci, S.; Darkes, M. C.; Fricker, S. P.; Murrer, B. A. Metal complexes of bleomycin: evaluation of [Rh-105]-bleomycin for use in targeted radiotherapy. *Nucl. Med. Biol.* **1999**, *26*, 421−430.
(219) Venkatesh, M.; Schlempe, E. O.; Jurisson, S. S.; Ketring, A. R.; Volkert, W. A.; Corlija, M. Preparation of ^{105}Rh labeled monoclonal antibody (MAb B72.3) using aminobenzylpropyleneamineoxime as the bifunctional chelating agent; comparison to ^{131}I labeled MAb B72.3. *Radiochim. Acta* **1999**, *85*, 157−163.
(220) Ando, A.; Ando, I.; Tonami, N.; Kinuya, S.; Okamoto, N.; Sugimoto, M.; Fukuda, N.; Matsumoto, S. Production of ^{105}Rh-EDTMP and its bone accumulation. *Appl. Radiat. Isot.* **2000**, *52*, 211−215.
(221) Mansur, M. S.; Mushtaq, A.; Muhammad, A. A ^{109}Pd → ^{109m}Ag generator. *Appl. Radiat. Isot.* **1995**, *46*, 1007−1008.
(222) Hussain, M.; Sudar, S.; Aslam, M. N.; Shah, H. A.; Ahmad, R.; Malik, A. A.; Qaim, S. M. A comprehensive evaluation of charged-particle data for production of the therapeutic radionuclide ^{103}Pd. *Appl. Radiat. Isot.* **2009**, *67*, 1842−1854.
(223) Chakraborty, S.; Das, T.; Sarma, H. D.; Banerjee, S. Effect of lipophilicity on biological properties of ^{109}Pd-porphyrin complexes: a preliminary investigation. *J. Porphyrins Phthalocyanines* **2012**, *16*, 64−71.
(224) Das, T.; Chakraborty, S.; Sarma, H. D.; Banerjee, S. ^{109}Pd labeled 5,10,15,20-tetrakis[4-carboxymethyleneoxyphenyl]porphyrin: a potential agent for targeted tumor therapy. *Curr. Radiopharm.* **2012**, *5*, 340−347.
(225) Chakraborty, S.; Das, T.; Banerjee, S.; Sarma, H. D.; Venkatesh, M. Preparation and preliminary biological evaluation of a novel ^{109}Pd labeled porphyrin derivative for possible use in targeted tumor therapy. *Q. J. Nucl. Med. Mol. Imaging* **2007**, *51*, 16−23.
(226) Das, T.; Chakraborty, S.; Sarma, H. D.; Banerjee, S. A novel [^{109}Pd]palladium labeled porphyrin for possible use in targeted radiotherapy. *Radiochim. Acta* **2008**, *96*, 427−433.
(227) Fawwaz, R. A.; Wang, T. S.; Srivastava, S. C.; Rosen, J. M.; Ferrone, S.; Hardy, M. A.; Alderson, P. O. Potential of palladium-109-labeled antimelanoma monoclonal antibody for tumor therapy. *J. Nucl. Med.* **1984**, *25*, 796−799.
(228) Brown, S. B.; Brown, E. A.; Walker, I. The present and future role of photodynamic therapy in cancer treatment. *Lancet Oncol.* **2004**, *5*, 497−508.
(229) Harrod-Kim, P. Tumor ablation with photodynamic therapy: introduction to mechanism and clinical applications. *J. Vasc. Interv. Radiol.* **2006**, *17*, 1441−1448.
(230) Dougherty, T. J.; Gomer, C. J.; Henderson, B. W.; Jori, G.; Kessel, D.; Korbelik, M.; Moan, J.; Peng, Q. Photodynamic therapy. *J. Natl. Cancer Inst.* **1998**, *90*, 889−905.
(231) Das, T.; Chakraborty, S.; Sarma, H. D.; Banerjee, S. ^{109}Pd labeled 5,10,15,20-tetrakis[4-carboxymethyleneoxyphenyl]porphyrin: a potential agent for targeted tumor therapy. *Curr. Radiopharm.* **2012**, *5*, 340−347.
(232) Pasternack, R. F.; Francesconi, L.; Raff, D.; Spiro, E. Aggregation of nickel(II), copper(II), and zinc(II) derivatives of water-soluble porphyrins. *Inorg. Chem.* **1973**, *12*, 2606−2611.
(233) Prabhakar, U.; Maeda, H.; Jain, R. K.; Sevick-Muraca, E. M.; Zamboni, W.; Farokhzad, O. C.; Barry, S. T.; Gabizon, A.; Grodzinski, P.; Blakey, D. C. Challenges and key considerations of the enhanced permeability and retention effect for nanomedicine drug delivery in oncology. *Cancer Res.* **2013**, *73*, 2412−2417.
(234) Doi, J. D.; Lavallee, D. K.; Srivastava, S. C.; Prach, T.; Richards, P.; Fawwaz, R. A. Preparation of ^{109}Pd-hematoporphyrin for selective lymphatic ablation using N-methylhematoporphyrin. *Int. J. Appl. Radiat. Isot.* **1981**, *32*, 877−880.
(235) Jalilian, A. R.; Sadeghi, M.; Yari Kamrani, Y. Development of [^{103}Pd]-labeled-bis(N4-methylthiosemicarbazone) complexes as possible therapeutic agents. *Radiochim. Acta* **2006**, *94*, 865−869.
(236) Jalilian, A. R.; Sadeghi, M.; Yari-Kamrani, Y.; Ensaf, M. R. Development of [^{103}Pd]-2-acetylpyridine 4N-methyl thiosemicarbazone complex for targeted therapy. *J. Radioanal. Nucl. Chem.* **2006**, *268*, 605−611.
(237) Jalilian, A. R.; Yari-Kamrani, Y.; Sadeghi, M. Production of [^{103}Pd]Bleomycin complex for targeted therapy. *Nukleonika* **2006**, *51*, 119−123.
(238) Zimmerman, R. E. Proc IAEA Symposium, Los Angeles, 1976; pp 121−140.
(239) Perez-Mendez, V.; Kaufman, L.; Lim, C. B.; Price, D. C.; Blumin, L.; Cavalieri, R. Multiwire proportional chambers in nuclear medicine: Present status and perspectives. *Int. J. Nucl. Med. Biol.* **1976**, *3*, 29−33.
(240) Lacy, J. L.; Verani, M. S.; Ball, M. E.; Boyce, T. M.; Gibson, R. W.; Roberts, R. First-pass radionuclide angiography using a multiwire gamma camera and tantalum-178. *J. Nucl. Med.* **1988**, *29*, 293−301.
(241) Holman, B. L.; Zimmerman, R. E.; Bifolck, L. V.; Neirinckx, R. D. Scintigraphic imaging with tantalum-178 and the Anger scintillation camera: concise communication. *J. Nucl. Med.* **1979**, *20*, 538−542.
(242) Neirinckx, R. D.; Jones, A. G.; Davis, M. A.; Harris, G. I.; Holman, B. L. Tantalum-178—a short-lived nuclide for nuclear medicine: development of a potential generator system. *J. Nucl. Med.* **1978**, *19*, 514−519.
(243) Lacy, J. L.; Layne, W. W.; Guidry, G. W.; Verani, M. S.; Roberts, R. Development and clinical performance of an automated, portable tungsten-178/tantalum-178 generator. *J. Nucl. Med.* **1991**, *32*, 2158−2161.
(244) Siddiqi, T. A.; Emery, G. T. Gamma-ray intensities and branchings in ^{178}Hf following decay of ^{178}Ta (9.3 min). *Phys. Rev. C: Nucl. Phys.* **1972**, *6*, 1009−1015.
(245) Holman, B. L.; Harris, G. I.; Neirinckx, R. D.; Jones, A. G.; Idoine, J. Tantalum-178–a short-lived nuclide for nuclear medicine: production of the parent W-178. *J. Nucl. Med.* **1978**, *19*, 510−513.
(246) Neirinckx, R. D.; Holman, B. L.; Davis, M. A.; Zimmerman, R. E. Tantalum-178-labeled agents for lung and liver imaging. *J. Nucl. Med.* **1979**, *20*, 1176−1180.
(247) Shigeta, N.; Matsuoka, H.; Osa, A.; Koizumi, M.; Izumo, M.; Kobayashi, K.; Hashimoto, K.; Sekine, T.; Lambrecht, R. M. Production method of no-carrier-added ^{186}Re. *J. Radioanal. Nucl. Chem.* **1996**, *205*, 85−92.

DOI: 10.1021/acs.chemrev.8b00281
Chem. Rev. 2019, 119, 870−901

(248) Lapi, S.; Mills, W. J.; Wilson, J.; McQuarrie, S.; Publicover, J.; Schueller, M.; Schyler, D.; Ressler, J. J.; Ruth, T. J. Production cross-sections of $^{181-186}$Re isotopes from proton bombardment of natural tungsten. *Appl. Radiat. Isot.* **2007**, *65*, 345−349.
(249) Tárkányi, F.; Hermanne, A.; Takács, S.; Ditrói, F.; Kovalev, F.; Ignatyuk, A. V. New measurement and evaluation of the excitation function of the ^{186}W(p,n) nuclear reaction for production of the therapeutic radioisotope ^{186}Re. *Nucl. Instrum. Methods Phys. Res., Sect. B* **2007**, *264*, 389−394.
(250) Balkin, E. R.; Gagnon, K.; Strong, K. T.; Smith, B. E.; Dorman, E. F.; Emery, R. C.; Pauzauskie, P. J.; Fassbender, M. E.; Cutler, C. S.; Ketring, A. R.; et al. Deuteron irradiation of W and WO_3 for production of high specific activity ^{186}Re: Challenges associated with thick target preparation. *Appl. Radiat. Isot.* **2016**, *115*, 197−207.
(251) Boschi, A.; Uccelli, L.; Pasquali, M.; Duatti, A.; Taibi, A.; Pupillo, G.; Esposito, J. ^{188}W/^{188}Re generator system and its therapeutic applications. *J. Chem.* **2014**, *2014*, 1−14.
(252) Konior, M.; Iller, E. Classic radionuclide ^{188}W/^{188}Re generator (experiments, design and construction). *Mod. Chem. Appl.* **2014**, *2*, 143.
(253) Dash, A.; Knapp Jr, F. F. An overview of radioisotope separation technologies for development of ^{188}W/^{188}Re radionuclide generators providing ^{188}Re to meet future research and clinical demands. *RSC Adv.* **2015**, *5*, 39012−39036.
(254) Donnelly, P. S. The role of coordination chemistry in the development of copper and rhenium radiopharmaceuticals. *Dalton Trans.* **2011**, *40*, 999−1010.
(255) Carroll, V.; Demoin, D. W.; Hoffman, T. J.; Jurisson, S. S. Inorganic chemistry in nuclear imaging and radiotherapy: current and future directions. *Radiochim. Acta* **2012**, *100*, 653−667.
(256) Blower, P. J. Rhenium-188 radiochemistry: challenges and prospects. *Int. J. Nucl. Med. Res.* **2017**, *4*, 39−53.
(257) Demoin, D. W.; Dame, A. N.; Minard, W. D.; Gallazzi, F.; Seickman, G. L.; Rold, T. L.; Bernskoetter, N.; Fassbender, M. E.; Hoffman, T. J.; Deakyne, C. A.; et al. Monooxorhenium(V) complexes with 222-N_2S_2 MAMA ligands for bifunctional chelator agents: Syntheses and preliminary in vivo evaluation. *Nucl. Med. Biol.* **2016**, *43*, 802−811.
(258) Hansen, L.; Cini, R.; Taylor, A.; Marzilli, L. G. Rhenium(V) oxo complexes relevant to technetium renal imaging agents derived from mercaptoacetylglycylglycylaminobenzoic acid isomers. Structural and molecular mechanics studies. *Inorg. Chem.* **1992**, *31*, 2801−2808.
(259) Francesconi, L. C.; Graczyk, G.; Wehrli, S.; Shaikh, S. N.; McClinton, D.; Liu, S.; Zubieta, J.; Kung, H. F. Synthesis and characterization of neutral MVO (M = technetium, rhenium) amine-thiol complexes containing a pendant phenylpiperidine group. *Inorg. Chem.* **1993**, *32*, 3114−3124.
(260) Guhlke, S.; Schaffland, A.; Zamora, P. O.; Sartor, J.; Diekmann, D.; Bender, H.; Knapp, F. F.; Biersack, H. J. ^{188}Re- and ^{99m}Tc-MAG3 as prosthetic groups for labeling amines and peptides: Approaches with pre- and postconjugate labeling. *Nucl. Med. Biol.* **1998**, *25*, 621−631.
(261) Demaimay, F.; Dazord, L.; Roucoux, A.; Noiret, N.; Patin, H.; Moisan, A. Rhenium-188 and technetium-99m nitridobis(N-ethoxy-N-ethyldithiocarbamate) leucocyte labelling radiopharmaceuticals: [^{188}ReN(NOET)$_2$] and [^{99m}TcN(NOET)$_2$], NOET = Et(EtO)NCS$_2$: their in vitro localization and chemical behaviour. *Nucl. Med. Biol.* **1997**, *24*, 701−705.
(262) Demaimay, F.; Roucoux, A.; Dazord, L.; Noiret, N.; Moisan, A.; Patin, H. Studies of technetium-99m nitridobisdithiocarboxylate leucocyte specific radiopharmaceutical: [^{99m}TcN(DTCX)$_2$], DTCX = $CH_3(CH_2)_8CS_2$. The cellular and subcellular distribution in human blood cells, and chemical behaviour. Synthesis of the analogous rhenium-188 radiopharmaceutical. *Nucl. Med. Biol.* **1999**, *26*, 225−231.
(263) Boschi, A.; Bolzati, C.; Uccelli, L.; Duatti, A. High-yield synthesis of the terminal ^{188}Re triple bond N multiple bond from generator-produced [^{188}ReO^4]$^-$. *Nucl. Med. Biol.* **2003**, *30*, 381−387.
(264) Boschi, A.; Massi, A.; Uccelli, L.; Pasquali, M.; Duatti, A. PEGylated N-methyl-S-methyl dithiocarbazate as a new reagent for the high-yield preparation of nitrido Tc-99m and Re-188 radiopharmaceuticals. *Nucl. Med. Biol.* **2010**, *37*, 927−934.
(265) Bordoloi, J. K.; Berry, D.; Khan, I. U.; Sunassee, K.; de Rosales, R. T.; Shanahan, C.; Blower, P. J. Technetium-99m and rhenium-188 complexes with one and two pendant bisphosphonate groups for imaging arterial calcification. *Dalton Trans.* **2015**, *44*, 4963−4975.
(266) Luo, T.-Y.; Cheng, P.-C.; Chiang, P.-F.; Chuang, T.-W.; Yeh, C.-H.; Lin, W.-J. ^{188}Re-HYNIC-trastuzumab enhances the effect of apoptosis induced by trastuzumab in HER2-overexpressing breast cancer cells. *Ann. Nucl. Med.* **2015**, *29*, 52−62.
(267) Clarke, C.; Cowley, A. R.; Dilworth, J. R.; Donnelly, P. S. Pyridylthiocarbazide complexes of rhenium with potential radiopharmaceutical applications. *Dalton Trans.* **2004**, 2402−2403.
(268) North, A. J.; Karas, J. A.; Ma, M. T.; Blower, P. J.; Ackermann, U.; White, J. M.; Donnelly, P. S. Rhenium and technetium-oxo complexes with thioamide derivatives of pyridylhydrazine bifunctional chelators conjugated to the tumour targeting peptides octreotate and cyclic-RGDfK. *Inorg. Chem.* **2017**, *56*, 9725−9741.
(269) Bigott-Hennkens, H. M.; Junnotula, S.; Ma, L.; Gallazzi, F.; Lewis, M. R.; Jurisson, S. S. Synthesis and in vitro evaluation of a rhenium-cyclized somatostatin derivative series. *J. Med. Chem.* **2008**, *51*, 1223−1230.
(270) Giblin, M. F.; Wang, N.; Hoffman, T. J.; Jurisson, S. S.; Quinn, T. P. Design and characterization of α-melanotropin peptide analogs cyclized through rhenium and technetium metal coordination. *Proc. Natl. Acad. Sci. U. S. A.* **1998**, *95*, 12814−12818.
(271) Garin, E.; Noiret, N.; Malbert, C.; Lepareur, N.; Roucoux, A.; Caulet-Maugendre, S.; Moisan, A.; Lecloirec, J.; Herry, J. Y.; Bourguet, P. Development and biodistribution of ^{188}Re-SSS lipiodol following injection into the hepatic artery of healthy pigs. *Eur. J. Nucl. Med. Mol. Imaging* **2004**, *31*, 542−546.
(272) Mullen, G. E. D.; Blower, P. J.; Price, D. J.; Powell, A. K.; Howard, M. J.; Went, M. J. Trithiacyclononane as a Ligand for Potential Technetium and Rhenium Radiopharmaceuticals: Synthesis of [M(9S3)($SC_2H_4SC_2H_4S$)][BF_4] (M = ^{99}Tc, Re, ^{188}Re) via C−S Bond Cleavage. *Inorg. Chem.* **2000**, *39*, 4093−4098.
(273) Schibli, R.; Schwarzbach, R.; Alberto, R.; Ortner, K.; Schmalle, H.; Dumas, C.; Egli, A.; Schubiger, P. A. Steps toward high specific activity labeling of biomolecules for therapeutic application: preparation of precursor [^{188}Re$(H_2O)_3(CO)_3$]$^+$ and synthesis of tailor-made bifunctional ligand systems. *Bioconjugate Chem.* **2002**, *13*, 750−756.
(274) Martin de Rosales, R. T.; Finucane, C.; Foster, J.; Mather, S. J.; Blower, P. J. ^{188}Re(CO)$_3$-dipicolylamine-alendronate: A new bisphosphonate conjugate for the radiotherapy of bone metastases. *Bioconjugate Chem.* **2010**, *21*, 811−815.
(275) Guo, R.; Ma, Y.; Zhang, R.; Liang, S.; Shen, H.; Xu, H.; Li, B. Rhenium-188 labeled recombinant human plasminogen kringle5 (rhk5) and preliminary biodistribution. *Nuklearmedizin* **2011**, *50*, 234−239.
(276) Tavare, R.; Williams, J.; Howland, K.; Blower, P. J.; Mullen, G. E. [Re$(CO)_3$]$^+$ labelling of a novel cysteine/hexahistidine tag: insights into binding mode by liquid chromatography-mass spectrometry. *J. Inorg. Biochem.* **2012**, *114*, 24−27.
(277) Blower, P. J. A nuclear chocolate box: the periodic table of nuclear medicine. *Dalton Trans.* **2015**, *44*, 4819−4844.
(278) Bartholoma, M.; Valliant, J.; Maresca, K. P.; Babich, J.; Zubieta, J. Single amino acid chelates (SAAC): a strategy for the design of technetium and rhenium radiopharmaceuticals. *Chem. Commun.* **2009**, 493−512.
(279) Xia, J.; Long, S.; Yu, J.; Wang, Y.; Cao, Z. Pyridyl derivatives provide new pathways for labeling protein with fac-[^{188}Re$(CO)_3(H_2O)_3$]$^+$. *J. Radioanal. Nucl. Chem.* **2009**, *281*, 493−500.
(280) Alberto, R.; Schibli, R.; Waibel, R.; Abram, U.; Schubiger, A. P. Basic aqueous chemistry of [M$(OH_2)_3(CO)_3$]+ (M = Re, Tc) directed towards radiopharmaceutical application. *Coord. Chem. Rev.* **1999**, *190−192*, 901−919.
(281) Stephenson, K. A.; Zubieta, J.; Banerjee, S. R.; Levadala, M. K.; Taggart, L.; Ryan, L.; McFarlane, N.; Boreham, D. R.; Maresca, K. P.; Babich, J. W.; et al. A new strategy for the preparation of peptide-targeted radiopharmaceuticals based on an FMOC-lysine-derived single amino acid chelate (SAAC). Automated solid-phase synthesis,

DOI: 10.1021/acs.chemrev.8b00281
Chem. Rev. 2019, 119, 870−901

NMR characterization, and in vitro screening of fMLF(SAAC)G and fMLF[(SAAC−Re(CO)$_3$)$^+$]G. *Bioconjugate Chem.* **2004**, *15*, 128−136.
(282) Zuckier, L. S.; Dohan, O.; Li, Y.; Chang, C. J.; Carrasco, N.; Dadachova, E. Kinetics of perrhenate uptake and comparative biodistribution of perrhenate, pertechnetate, and iodide by NaI symporter−expressing tissues in vivo. *J. Nucl. Med.* **2004**, *45*, 500−507.
(283) Dadachova, E.; Bouzahzah, B.; Zuckier, L. S.; Pestell, R. G. Rhenium-188 as an alternative to iodine-131 for treatment of breast tumors expressing the sodium/iodide symporter (NIS). *Nucl. Med. Biol.* **2002**, *29*, 13−18.
(284) Ahn, B.-C. Sodium iodide symporter for nuclear molecular imaging and gene therapy: From bedside to bench and back. *Theranostics* **2012**, *2*, 392−402.
(285) Singh, J.; Reghebi, K.; Lazarus, C. R.; Clarke, S. E.; Callahan, A. P.; Knapp, F. F., Jr.; Blower, P. J. Studies on the preparation and isomeric composition of ^{186}Re- and ^{188}Re-pentavalent rhenium dimercaptosuccinic acid complex. *Nucl. Med. Commun.* **1993**, *14*, 197−203.
(286) Blower, P. J.; Lam, A. S. K.; O'Doherty, M. J.; Kettle, A. G.; Coakley, A. J.; Knapp, F. F., Jr Pentavalent rhenium-188 dimercaptosuccinic acid for targeted radiotherapy: synthesis and preliminary animal and human studies. *Eur. J. Nucl. Med. Mol. Imaging* **1998**, *25*, 613−621.
(287) Blower, P. J.; Kettle, A. G.; O'Doherty, M. J.; Coakley, A. J.; Knapp, F. F., Jr. ^{99m}Tc(V)DMSA quantitatively predicts ^{188}Re(V)-DMSA distribution in patients with prostate cancer metastatic to bone. *Eur. J. Nucl. Med.* **2000**, *27*, 1405−1409.
(288) Pirmettis, I.; Limouris, G. S.; Bouziotis, P.; Papadopoulos, M.; Knapp, F. F., Jr.; Chiotellis, E. Pentavalent rhenium-188 dimercaptosuccinic acid: a new kit formulation and its initial evaluation in mice. *Radiochim. Acta* **2001**, *89*, 115−118.
(289) Park, J.-Y.; Lee, T.-S.; Choi, T.-H.; Cheon, G.-J.; Choi, C.-W.; Awh, O.-D. A comparative study of ^{188}Re(V)-meso-DMSA and ^{188}Re-(V)-rac-DMSA: preparation and in vivo evaluation in nude mice xenografted with a neuroendocrine tumor. *Nucl. Med. Biol.* **2007**, *34*, 1029−1036.
(290) Areberg, J.; Björkman, S.; Einarsson, L.; Frankenberg, B.; Lundqvist, H.; Mattsson, S.; Norrgren, K.; Scheike, O.; Wallin, R. Gamma camera imaging of platinum in tumours and tissues of patients after administration of ^{191}Pt-cisplatin. *Acta Oncol.* **1999**, *38*, 221−228.
(291) Lange, R. C.; Spencer, R. P.; Harder, H. C. Synthesis and distribution of a radiolabeled antitumor agent: cis-diamminedichloroplatinum (II). *J. Nucl. Med.* **1972**, *13*, 328−330.
(292) Lange, R. C.; Spencer, R. P.; Harder, H. C. The antitumor agent cis-Pt(NH$_3$)$_2$Cl$_2$: distribution studies and dose calculations for ^{193m}Pt and ^{195m}Pt. *J. Nucl. Med.* **1973**, *14*, 191−195.
(293) Aalbersberg, E. A.; de Wit-van der Veen, B. J.; Zwaagstra, O.; Codee-van der Schilden, K.; Vegt, E.; Vogel, W. V. Preclinical imaging characteristics and quantification of platinum-195m SPECT. *Eur. J. Nucl. Med. Mol. Imaging* **2017**, *44*, 1347−1354.
(294) Dykiy, M. P.; Dovbnya, A. N.; Lyashko, Y. V.; Medvedeva, E. P.; Medvedev, D. V.; Uvarov, V. L. Photonuclear production of ^{193m,195m}Pt and synthesis of radioactive cisplatin. *J. Labelled Compd. Radiopharm.* **2007**, *50*, 480−482.
(295) Hoeschele, J. D.; Butler, T. A.; Roberts, J. A.; Guyer, C. E. Analysis and refinement of the microscale synthesis of the platinum-195m-labeled antitumor drug, cis-dichlorodiammineplatinum(II), cis-DDP. *Radiochim. Acta* **1982**, *31*, 27−36.
(296) Zeevaart, J. R.; Wagener, J.; Marjanovic-Painter, B.; Sathekge, M.; Soni, N.; Zinn, C.; Perkins, G.; Smith, S. V. Production of high specific activity ^{195m}Pt-cisplatinum at South African Nuclear Energy Corporation for Phase 0 clinical trials in healthy individual subjects. *J. Labelled Compd. Radiopharm.* **2013**, *56*, 495−503.
(297) Suwa, M.; Kogawa, O.; Nowatari, H.; Murase, Y.; Homma, Y.; Hashimoto, Y. A microscale synthesis of a promising radiolabeled antitumor drug: cis-1,1-cyclobutanedicarboxylato-(2R)-2-methyl-1,4-butanediamineplatinum(II), NK121. *J. Labelled Compd. Radiopharm.* **1992**, *31*, 349−354.
(298) Smith, P. H. S.; Taylor, D. M. Distribution and retention of the antitumor agent ^{195m}Pt-cis-dichlorodiammine platinum(II) in man. *J. Nucl. Med.* **1974**, *15*, 349−351.
(299) Sathekge, M.; Wagener, J.; Smith, S. V.; Soni, N.; Marjanovic-Painter, B.; Zinn, C.; Van de Wiele, C.; D'Asseler, Y.; Perkins, G.; Zeevaart, J. R. Biodistribution and dosimetry of ^{195m}Pt-cisplatin in normal volunteers. *Nuklearmedizin* **2013**, *52*, 222−227.
(300) Kocher, D. C. *Radioactive Decay Data Tables*; U.S. Department of Energy: Springfield, VA, 1982.
(301) Sadeghi, M.; Bakhtiari, M.; Bakht, M. K.; Anjomrouz, M.; Mokhtari, L. Overview of mercury radionuclides and nuclear model calculations of ^{195}Hg^{m,g} and ^{197}Hg^{m,g} to evaluate experimental cross section data. *Phys. Rev. C: Nucl. Phys.* **2012**, *85*, No. 034605.
(302) Walther, M.; Preusche, S.; Bartel, S.; Wunderlich, G.; Freudenberg, R.; Steinbach, J.; Pietzsch, H.-J. Theranostic mercury: $^{197(m)}$Hg with high specific activity for imaging and therapy. *Appl. Radiat. Isot.* **2015**, *97*, 177−181.
(303) Blau, M.; Bender, M. A. Radiomercury (Hg 203) labeled neohydrin: A new agent for brain tumor localization. *J. Nucl. Med.* **1962**, *3*, 83−93.
(304) Blahd, W. H. *Nuclear Medicine*, 2nd ed.; McGraw-Hill: New York, 1971.

DOI: 10.1021/acs.chemrev.8b00281
Chem. Rev. 2019, 119, 870−901